

## Topics

Purification techniques  
Elemental analysis  
Thermogravimetric analysis  
Mass spectrometry  
Vibrational spectroscopy  
Electronic spectroscopy  
NMR spectroscopy  
EPR spectroscopy  
Mössbauer spectroscopy  
Diffraction methods  
Photoelectron spectroscopy  
Computational methods

# 4 Experimental techniques



## 4.1 Introduction

Analysing chemical compounds and confirming their identities is a crucial part of practical chemistry. In addition to applications in research laboratories, analysis is a daily part of scientists' work in areas such as the pharmaceutical industry, food and drink quality control, environmental monitoring and forensics. Modern laboratories offer a wide range of analytical techniques, and in this chapter, the theory and applications of some of these methods are detailed. We focus on the techniques used to determine the identity and spectroscopic properties of a compound, and will not be concerned with determining the amounts of trace elements or compounds in, for example, water and air samples.<sup>†</sup>

Analytical methods can be grouped roughly according to their use in:

- compositional analysis and formula determination;
- investigating bonding, connectivity of atoms and oxidation states of elements in a compound;
- determining molecular structure.

Introductions to several techniques (cyclic voltammetry, transmission electron microscopy, magnetism, emission spectroscopy) have been left until later in the book to facilitate association with appropriate theoretical details or specific applications.

The component being analysed in a system is called the *analyte*.

<sup>†</sup> For an introduction to methods of solving analytical problems in environmental, forensic, pharmaceutical and food sciences, see Chapter 36 in C.E. Housecroft and E.C. Constable (2010) *Chemistry*, 4th edn, Prentice Hall, Harlow.

## 4.2 Separation and purification techniques

Before you begin to analyse a compound, it is crucial to ensure its purity. This section introduces routine methods of separation and purification of chemical compounds.

### Gas chromatography (GC)

*Gas chromatography (GC)* is a separation technique in which the mobile phase is a gas; the stationary phase is packed inside a capillary or microbore column.

Gas chromatography (GC) is used to separate *volatile* components of a mixture and depends upon the different interactions of the components in a *mobile phase* (the carrier gas) with a *stationary phase* (e.g. alumina or silica) contained in a chromatography column. The sample is injected into a flow of dried carrier gas which is heated so that the components of the sample are in the vapour phase. The sample is carried into a capillary or microbore chromatography column (Fig. 4.1), the temperature of which is controlled to maintain the vapour state for the samples. The times taken for the components in the mixture to be eluted from the chromatography column are characteristic *retention times* and the data are output as a chromatogram (a plot of relative intensity against time). Components in the sample that interact least well with the stationary phase have the shortest retention times, while more strongly adsorbed components move more slowly through the column. While GC is applied routinely to separate volatile compounds, liquid chromatography (LC) has wider applications in inorganic chemistry.

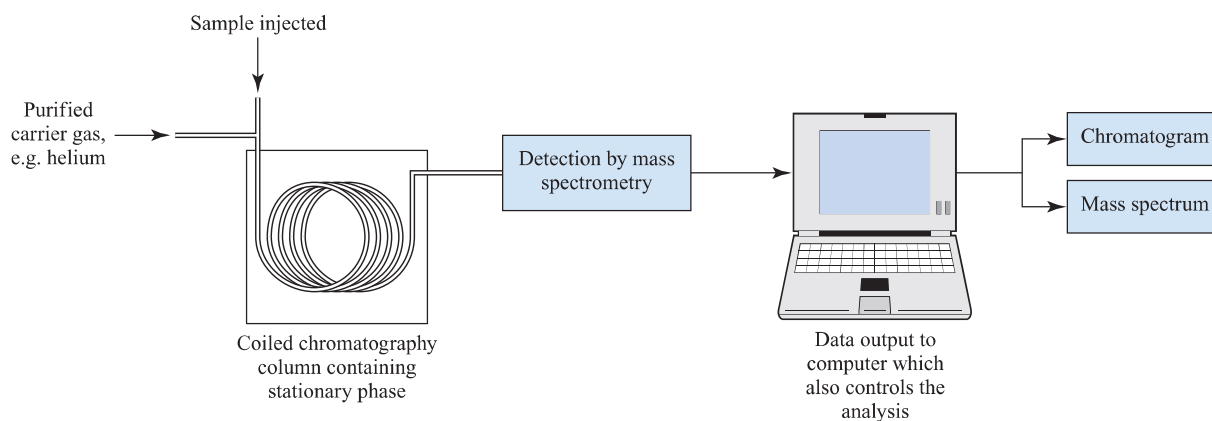


**Fig. 4.1** Schematic diagram showing the components of a computer-controlled gas chromatography-mass spectrometer (GC-MS) instrument.

## Liquid chromatography (LC)

**Liquid chromatography (LC)** is a separation technique in which the mobile phase is a liquid; the stationary phase is either packed inside a column or adhered to a glass plate.

For the purification of a product after synthesis, column liquid chromatography is often used. The crude material is adsorbed onto a *stationary phase* (e.g. alumina or silica with particle diameter  $\approx 20\ \mu\text{m}$ ). The column is eluted with a solvent or solvent mixture (the *mobile phase*) chosen so as to separate the components based on their different solubilities and interactions with the stationary phase. Test separations are first carried out using thin-layer chromatography (TLC). The ratio of the distance travelled by the analyte to that of the solvent front is called the retention

factor ( $R_f$  value). An equilibrium is set up between surface-bound and solution species, and the preference of a given species for the stationary or mobile phase is given by the equilibrium constant  $K$ , where:

$$K = \frac{a_{\text{stationary}}}{a_{\text{mobile}}}$$

At low concentrations, activities,  $a$ , can be approximated to concentrations. As the column is eluted with solvent, some components are removed from the stationary phase more readily than others, and separation of the mixture is achieved. Figure 4.2 shows an open-column set-up. For coloured compounds, separation can be monitored by eye but instrumental methods of detection (e.g. UV absorption spectroscopy or mass spectrometry) can be integrated into the system (Fig. 4.3). In column chromatography, fractions are eluted under gravity flow or under pressure (flash chromatography).

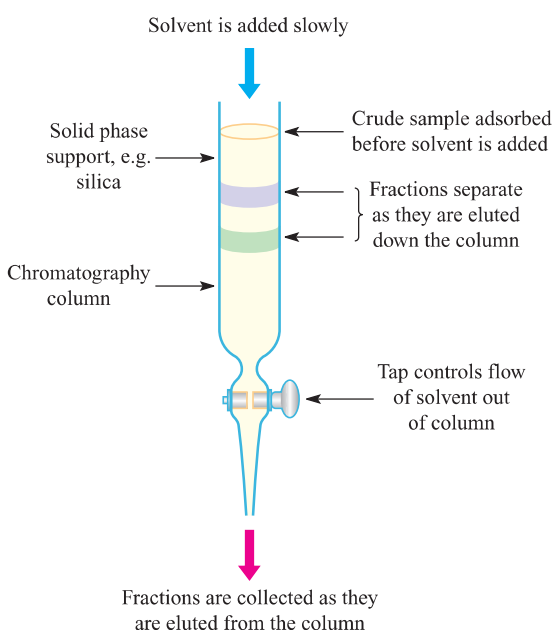


**Fig. 4.2** Schematic representation of an open column chromatography set-up.

## High-performance liquid chromatography (HPLC)

**High-performance liquid chromatography (HPLC)** is a form of liquid chromatography in which the mobile phase is introduced under pressure and the stationary phase consists of very small particles (diameter 3–10  $\mu\text{m}$ ).

The technique of high-performance liquid chromatography (HPLC) is summarized in Fig. 4.4. All parts of the separation process are computer controlled. Solvents are degassed before use, and the rate of flow of each solvent is controlled so that the solvent mixture entering the pump has a pre-determined composition. The pump operates at pressures up to  $\approx 40\ \text{MPa}$ , and the flow-rate delivered by the pump is varied as required. After injection of the sample, the mobile phase enters the chromatography column. The eluted fractions are monitored using a detector (e.g. UV-VIS, fluorescence, IR or circular dichroism spectroscopies or mass spectrometry) and the data are recorded in terms of, for example, absorbance against retention time.

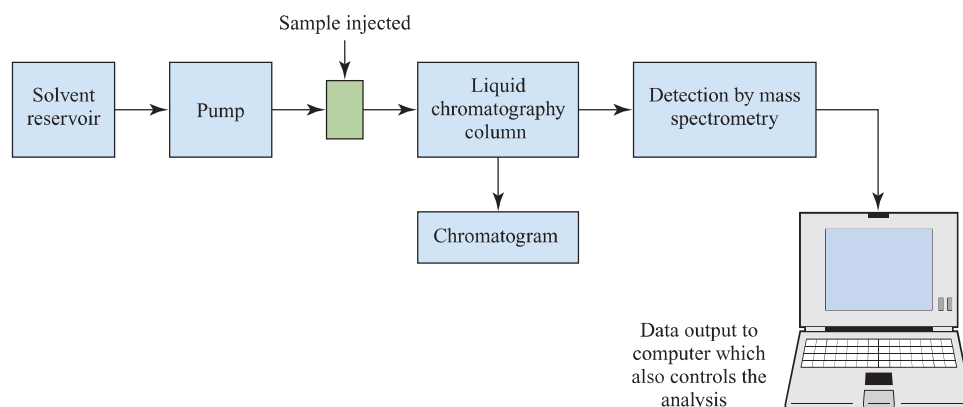
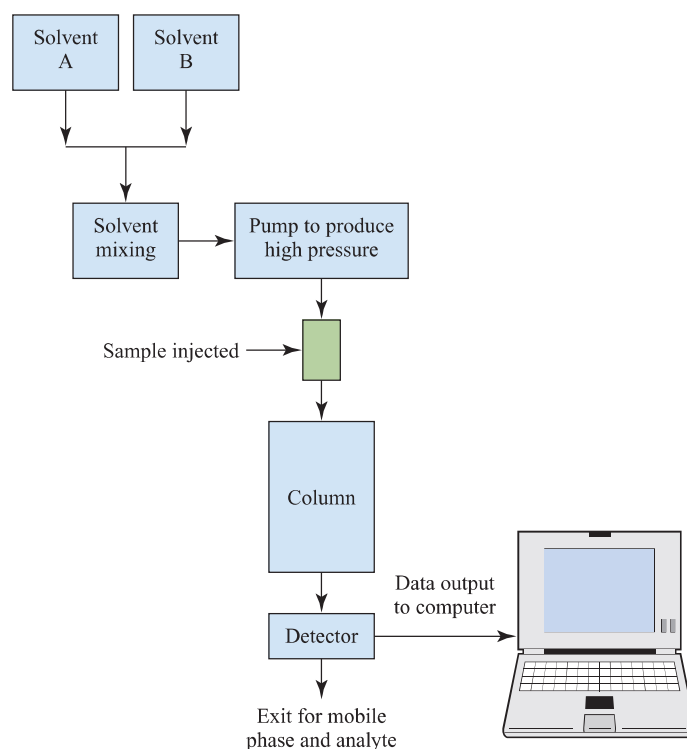


**Fig. 4.3** Schematic diagram showing the components of a computer-controlled liquid chromatography-mass spectrometer (LC-MS) instrument.



(a)



(b)

**Fig. 4.4** (a) An HPLC instrument. The solvents are contained in the bottles at the top. The column is in the chamber with the open door. (b) Schematic diagram illustrating the components of a computer-controlled HPLC instrument.

Analytical HPLC uses columns of length 3–25 cm and width 2–4 mm, and stationary phase particle diameter of 3–10  $\mu\text{m}$ . Preparative HPLC may use up to 1 g of sample, with  $\approx 25$  cm long columns of diameter 10–150 mm. In *normal-phase* HPLC, the stationary phase is a polar adsorbent such as silica (uniform particle diameter  $\approx 10 \mu\text{m}$ ) packed into a column. The solvents are usually non-polar

or of low polarity. Fractions are eluted from the column in order of their polarity, with non-polar components eluting first. The steric properties of substituents in a compound have a significant influence on the rate of elution. In *reversed-phase* HPLC, the surface of the stationary phase is modified so that it is hydrophobic. This is combined with polar solvents, usually water mixed with MeOH,

MeCN or THF, and the fractions are eluted from the column in order of decreasing polarity.

An example of the application of HPLC is the separation of fullerenes (see Section 14.4). Columns packed with stationary phases designed specifically for preparative-scale fullerene separation are commercially available (e.g. Cosmosil™ Buckyprep columns).

## Recrystallization

**Recrystallization** is a purification step involving the dissolution and crystallization of a solid from a solvent or solvent mixture.

After synthesis and chromatographic separation of a solid compound, recrystallization is usually used as the final purification step. Suppose you wish to separate a compound **A** from *minor* impurities. First, it is necessary to find a solvent in which **A** is insoluble at low temperatures, but is very soluble at higher temperatures. Typically, polar or ionic compounds are soluble in polar solvents (e.g. water, acetonitrile, dichloromethane, methanol), while non-polar compounds are soluble in non-polar solvents (e.g. hexanes, toluene). The impurities may also be soluble in the same solvent or solvent mixture but, ideally, a solvent is found in which the impurities are insoluble. For the latter case, after preliminary tests to find a suitable solvent, the solvent is added to crude **A** and the mixture is heated. The insoluble impurities are removed by filtering the hot solution, and the filtrate is allowed to cool either at or below room temperature. As the solution cools, the solubility of **A** decreases and, once the solution has become saturated, **A** begins to crystallize from the solution. If crystallization is relatively rapid, microcrystals form. If both **A** and the impurities are soluble in the same solvent, the crude sample is dissolved in boiling solvent and the solution is allowed to cool slowly. Crystal growth involves the assembly of an ordered crystal lattice (Fig. 4.5 and see Chapter 6) and the aim is to exclude impurities from the lattice.

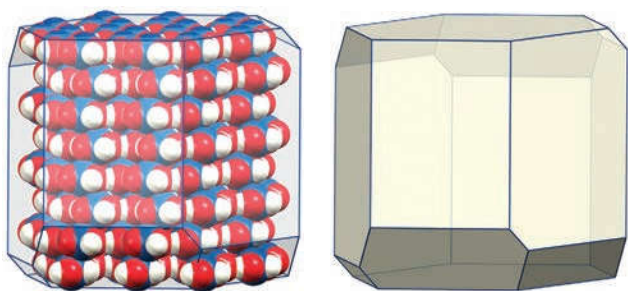


**Fig. 4.5** When boric acid,  $B(OH)_3$ , crystallizes, the molecules pack in layers and this produces crystals of well-defined shape (*morphology*).

## 4.3 Elemental analysis

### CHN analysis by combustion

The quantitative analysis for carbon, hydrogen and/or nitrogen in a compound is carried out simultaneously using a *CHN analyser*. The compound is fully combusted and the amounts of products are measured. An accurately known mass of sample (2–5 mg) is sealed in an aluminium or tin capsule. After the sample has been introduced into the analyser, its combustion and product analysis are fully automated. The sample passes into a pyrolysis tube and is heated at  $\approx 900^\circ\text{C}$  in an atmosphere of pure  $O_2$ . Carbon, hydrogen and nitrogen are oxidized to  $CO_2$ ,  $H_2O$  and nitrogen oxides. A stream of helium carries the gaseous products into a chamber containing heated copper where the oxides of nitrogen are reduced to  $N_2$ , and excess  $O_2$  is removed. The carrier gas then transports the mixture of  $CO_2$ ,  $H_2O$  and  $N_2$  into the analysing chamber where they are separated using a specialized type of gas chromatography (frontal chromatography) which does not require a mobile phase. Detection of the gases uses a thermal conductivity detector. The automated analysis takes about 5 minutes, and C, H and N percentages are recorded to within an accuracy of  $<0.3\%$ .

Modern CHN analysers are also equipped to determine S and O compositions. Sulfur is determined by oxidation to  $SO_2$ , and oxygen by conversion to CO, then to  $CO_2$ .

### Self-study exercises

1. CH analysis of a compound  $[PtCl_2(PR_3)_2]$  gives C 54.65, H 3.83%. Is  $R = Ph$  or  $Bu$ ? Are the experimental data within acceptable limits compared to the calculated values?
2. CHN analysis for a complex  $[TiCl_n(py)_{6-n}]$  gives C 46.03, H 3.85, N 10.72%. What is the value of  $n$ ?

### Atomic absorption spectroscopy (AAS)

The quantitative determination of a metal can be carried out using *atomic absorption spectroscopy (AAS)* by observing the diagnostic absorption spectrum of gaseous atoms of the metal.

The emission spectrum of atomic hydrogen (Section 1.4) consists of a series of sharp lines, each line corresponding to a discrete electronic transition from higher to lower energy levels (Fig. 1.3). Conversely, if atomic hydrogen is irradiated, it will give rise to an *absorption spectrum*. Every element has a characteristic atomic emission and absorption spectrum, and the most common analytical method for quantitative determination of a given metal is *atomic absorption spectroscopy (AAS)*. Usually, radiation

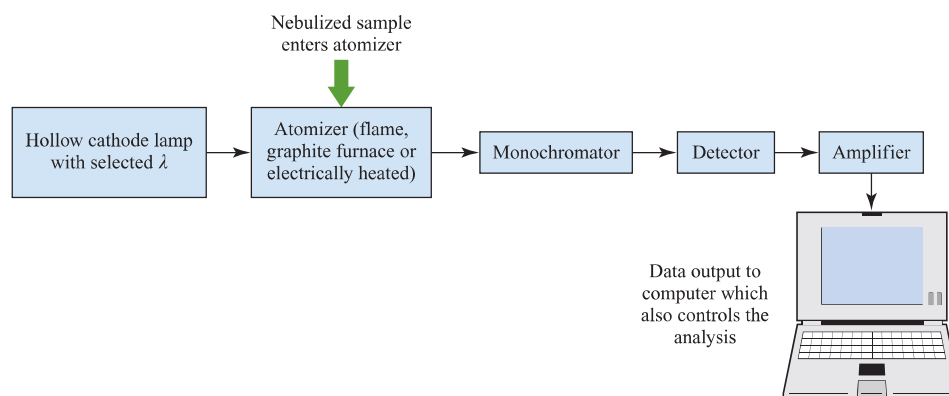


**Fig. 4.6** Schematic diagram showing the components of an atomic absorption spectrometer.

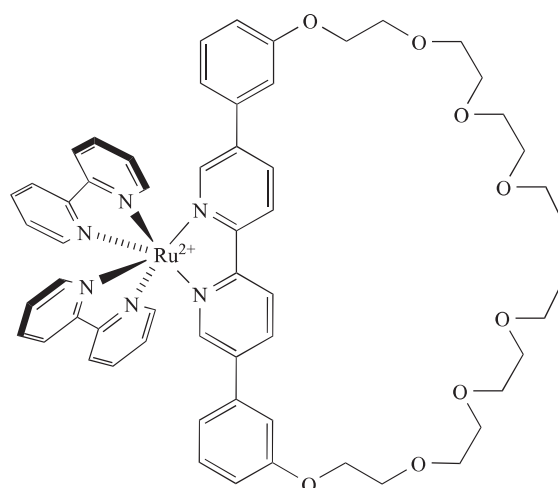
using a wavelength corresponding to one specific transition is selected for the analysis (e.g. 217.0 or 283.3 nm for Pb).

The metal being analysed is not usually in its elemental form, and so the first step is *digestion* (decomposition) of the sample and of a series of standards. The standards contain known concentrations of the metal being analysed and are used to construct a calibration curve (see below). The atomic absorption spectrometer (Fig. 4.6) contains either a flame atomizer, a graphite furnace or an electrically heated atomizer. Each standard for the calibration is initially *aspirated*, i.e. air is sucked through the liquid sample as it passes into a *nebulizing chamber*. The fine spray of liquid that forms is then atomized. Radiation of the appropriate wavelength for the metal being detected is generated in a hollow cathode lamp and passed through the atomized standard or sample. The amount of radiation absorbed is recorded. Modern AAS instruments are computer controlled, and data are automatically recorded and processed. A linear relationship between absorbance and concentration follows from the Beer–Lambert law (see Section 4.7). However, at absorbances greater than  $\approx 0.5$ , deviations from a linear plot occur, and it is therefore necessary to work with suitably dilute solutions. Starting from a stock solution of accurately known concentration, a series of five standard solutions is prepared and used to obtain the calibration curve. The latter must include a blank (i.e. solvent) to account for background effects. Once the calibration curve has been drawn, the process is repeated with the sample of unknown composition, and the measured absorbance is used to determine the concentration of metal in the sample. The AAS technique is extremely sensitive and the limit of detection is of the order of  $\mu\text{g dm}^{-3}$ .

#### Worked example 4.1 Sodium ions trapped in an inorganic complex

The cation,  $[\text{X}]^{2+}$ , drawn below was prepared as the salt  $[\text{X}][\text{PF}_6]_2$ . Elemental analysis showed the compound to be  $[\text{X}][\text{PF}_6]_2 \cdot x\text{Na}[\text{PF}_6]$ . The complex is soluble in

acetonitrile (MeCN), but not in water. The sodium content of the bulk sample was determined by AAS.



A stock solution ( $1.0 \times 10^{-4} \text{ mol dm}^{-3}$ ) of NaCl was prepared. Standards were made by adding 2.0, 3.0, 4.0, 6.0 or  $10.0 \text{ cm}^3$  of the stock solution to a  $100 \text{ cm}^3$  volumetric flask;  $5 \text{ cm}^3$  of MeCN were added to each flask which was then filled to the  $100 \text{ cm}^3$  mark with deionized water. A blank was also prepared. The sample for analysis was prepared by dissolving 8.90 mg of  $[\text{X}][\text{PF}_6]_2 \cdot x\text{Na}[\text{PF}_6]$  in  $2.5 \text{ cm}^3$  of MeCN in a  $50 \text{ cm}^3$  volumetric flask. This was filled to the mark with deionized water. This solution was diluted 10-fold with a 5% (by volume) MeCN/water solution. Using a sodium hollow cathode lamp ( $\lambda = 589 \text{ nm}$ ), AAS was used to determine the absorbance of each standard. Each absorbance reading was corrected for the absorbance of the blank and the data are tabulated below:

$[\text{Na}^+]/\mu\text{mol dm}^{-3}$	2.0	3.0	4.0	6.0	10.0
Corrected absorbance, $A$	0.0223	0.0340	0.0481	0.0650	0.1144

[Data: P. Rösler, Ph.D. Thesis, University of Basel, 2009]

(a) Confirm the concentrations of the standards given in the table. (b) How is the blank prepared? (c) Plot a calibration curve and determine the relationship between  $A$  and  $[\text{Na}^+]$ . (d) The sample of  $[\text{X}][\text{PF}_6]_2 \cdot x\text{Na}[\text{PF}_6]$  gave an absorbance of 0.0507. Determine the concentration of  $\text{Na}^+$  ions in the sample. Hence determine  $x$  in the formula.

(a) For the stock solution:  $[\text{Na}^+] = 1.0 \times 10^{-4} \text{ mol dm}^{-3}$

In  $2.0 \text{ cm}^3$  of this solution:

$$\begin{aligned} \text{Number of moles of } \text{Na}^+ &= \frac{2.0 \times 1.0 \times 10^{-4}}{1000} \\ &= 2.0 \times 10^{-7} \text{ moles} \end{aligned}$$

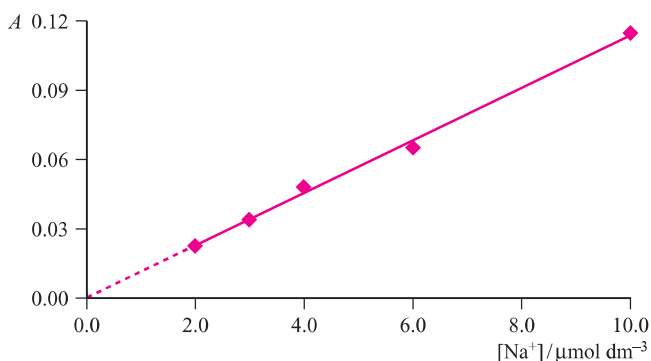
After making up to  $100 \text{ cm}^3$ :

$$\begin{aligned} [\text{Na}^+] &= \frac{2.0 \times 10^{-7} \times 10^3}{100} = 2.0 \times 10^{-6} \text{ mol dm}^{-3} \\ &= 2.0 \mu\text{mol dm}^{-3} \end{aligned}$$

The other concentrations can be similarly confirmed.

(b) The blank must contain the same solvents as the sample, so should be a mixture of deionized water and 5% MeCN by volume.

(c) Using the data given, construct a plot of  $A$  against  $[\text{Na}^+]$ . The linear least squares fit gives a line going through the origin (a result of the correction made using the blank).



The equation for the line is:

$$A = 0.0114 \times [\text{Na}^+]$$

(d) From the above equation, you can determine  $[\text{Na}^+]$  for the sample using the value of  $A = 0.0507$ :

$$[\text{Na}^+] = \frac{0.0507}{0.0114} = 4.45 \mu\text{mol dm}^{-3}$$

Therefore the concentration of  $\text{Na}[\text{PF}_6]$  is  $4.45 \mu\text{mol dm}^{-3} = 4.45 \times 10^{-6} \text{ mol dm}^{-3}$

The solution of the sample used in the analysis comprises  $8.90 \text{ mg } [\text{X}][\text{PF}_6]_2 \cdot x\text{Na}[\text{PF}_6]$  in  $50 \text{ cm}^3$ , diluted 10-fold, i.e.  $8.90 \text{ mg}$  in  $500 \text{ cm}^3$ .

Moles of  $\text{Na}[\text{PF}_6]$  in  $500 \text{ cm}^3$

$$\begin{aligned} &= \frac{500 \times 4.45 \times 10^{-6}}{1000} = 2.225 \times 10^{-6} \\ &= 2.23 \times 10^{-6} \text{ (to 3 sig. fig.)} \end{aligned}$$

Molecular mass of  $\text{Na}[\text{PF}_6] = 168 \text{ g mol}^{-1}$

Mass of  $\text{Na}[\text{PF}_6]$  in the sample

$$\begin{aligned} &= (2.23 \times 10^{-6}) \times 168 \\ &= 3.75 \times 10^{-4} \text{ g} \\ &= 0.375 \text{ mg} \end{aligned}$$

Therefore,  $8.90 \text{ mg}$  of  $[\text{X}][\text{PF}_6]_2 \cdot x\text{Na}[\text{PF}_6]$  contains  $0.375 \text{ mg Na}[\text{PF}_6]$ .

$x$  can be determined by finding the ratio of the number of moles of  $[\text{X}][\text{PF}_6]_2 : \text{Na}[\text{PF}_6]$ .

$8.90 \text{ mg}$  of  $[\text{X}][\text{PF}_6]_2 \cdot x\text{Na}[\text{PF}_6]$  is composed of  $0.375 \text{ mg Na}[\text{PF}_6]$  and  $8.53 \text{ mg } [\text{X}][\text{PF}_6]_2$ .

Amount of  $\text{Na}[\text{PF}_6]$  in  $0.375 \text{ mg} = 2.23 \mu\text{mol}$  (see above).

The molecular mass of  $[\text{X}][\text{PF}_6]_2 = 1362 \text{ g mol}^{-1}$

$$\begin{aligned} \text{Amount of } [\text{X}][\text{PF}_6]_2 \text{ in } 8.53 \text{ mg} &= \frac{8.53}{1362} = 6.26 \mu\text{mol} \\ &\text{(to 3 sig. fig.)} \end{aligned}$$

$$\begin{aligned} \text{Ratio of moles of } [\text{X}][\text{PF}_6]_2 : \text{Na}[\text{PF}_6] &= 6.26 : 2.23 \\ &= 1 : 0.36 \end{aligned}$$

Therefore,  $x = 0.36$ .

### Self-study exercises

- By referring to Section 7.12, comment on the structural features of  $[\text{X}]^{2+}$  (drawn on p. 91) that lead to  $\text{Na}^+$  ions being trapped in the complex.
- What is the physical significance of a value of  $x = 0.36$  on the solid state structure of the complex?

## 4.4 Compositional analysis: thermogravimetry (TG)

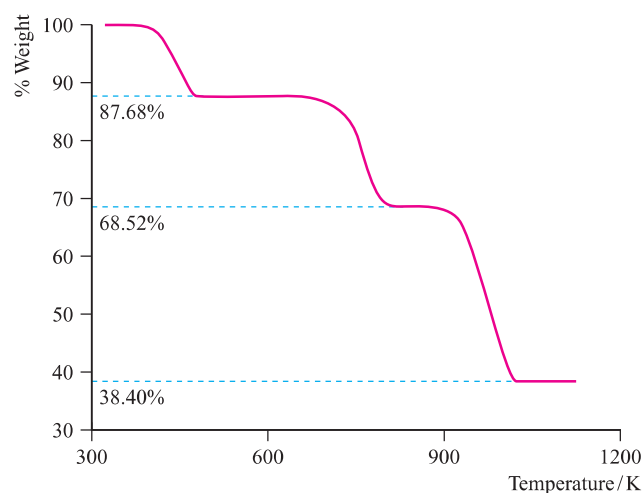
In *thermogravimetric analysis (TGA)*, the change in mass of a sample is monitored as the sample is heated.

When a compound crystallizes from solution, the crystals may contain solvent of crystallization. The compound is then called a *solvate*, and if the solvent is water, the compound is a *hydrate*. The presence of the solvent is revealed by elemental analysis, and thermogravimetric analysis (TGA) shows whether the solvent molecules are loosely or strongly bound in the crystal lattice. More generally, TGA is used to investigate the thermal degradation of inorganic compounds or polymers or the gas uptake of a solid (e.g.  $\text{H}_2$  uptake by  $\text{WO}_3$ ). A TGA instrument is able to simultaneously heat (at a constant rate) and record the mass of a sample. Samples are usually heated in air or  $\text{N}_2$ , or in an

atmosphere of a reactive gas (e.g.  $\text{H}_2$ ) for studying the uptake of a particular gas. The output data are presented as described in the example below.

### Worked example 4.2 Three-stage decomposition of $\text{CaC}_2\text{O}_4 \cdot \text{H}_2\text{O}$

TGA data for hydrated calcium oxalate,  $\text{CaC}_2\text{O}_4 \cdot \text{H}_2\text{O}$ , are shown below:



Explain the shape of the curve, and give a series of equations to summarize the thermal decomposition.

The curve shows three steps in the decomposition of  $\text{CaC}_2\text{O}_4 \cdot \text{H}_2\text{O}$ .

In the graph, the % weight losses are with respect to the original mass of  $\text{CaC}_2\text{O}_4 \cdot \text{H}_2\text{O}$ . Determine the % weight loss corresponding to each step.

$$\text{Weight loss in step 1} = 100 - 87.7 = 12.3\%$$

$$\text{Weight loss in step 2} = 87.7 - 68.5 = 19.2\%$$

$$\text{Weight loss in step 3} = 68.5 - 38.4 = 30.1\%$$

$$M_r(\text{CaC}_2\text{O}_4 \cdot \text{H}_2\text{O}) = 40.08 + 2(12.01) + 5(16.00) + 2(1.01) = 146.12 \text{ g mol}^{-1}$$

The weight loss of 12.3% corresponds to a mass of

$$\left(\frac{12.3}{100}\right) \times 146.12 = 18.0 \text{ g}$$

$$M_r(\text{H}_2\text{O}) = 18.02 \text{ g mol}^{-1}$$

Therefore, the lowest temperature thermal event is loss of  $\text{H}_2\text{O}$ .

The next weight loss of 19.2% corresponds to a mass of

$$\left(\frac{19.2}{100}\right) \times 146.12 = 28.1 \text{ g}$$

$$M_r(\text{CO}) = 28.01 \text{ g mol}^{-1}$$

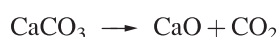
Therefore, CO is lost in step 2.

The next weight loss of 30.1% corresponds to a mass of

$$\left(\frac{30.1}{100}\right) \times 146.12 = 44.0 \text{ g}$$

This corresponds to loss of  $\text{CO}_2$  ( $M_r = 44.01 \text{ g mol}^{-1}$ ).

The three steps are therefore:



### Self-study exercises

- 100.09 mg of  $\text{CaCO}_3$  loses 43.97% of its weight when heated from 298 to 1100 K. Confirm that this corresponds to the formation of CaO.
- When 2.50 g of  $\text{CuSO}_4 \cdot 5\text{H}_2\text{O}$  are heated from 298 to 573 K, three decomposition steps are observed. The % weight losses for the consecutive steps with respect to the original mass are 14.42, 14.42 and 7.21%. Rationalize these data.

## 4.5 Mass spectrometry

**Mass spectrometry** is the separation of ions (atomic or molecular) according to their mass-to-charge ( $m/z$ ) ratio.

A variety of mass spectrometric techniques is available and we focus on electron ionization (or electron impact), fast atom bombardment, matrix-assisted laser desorption ionization time-of-flight and electrospray ionization methods, all of which are routinely available.

### Electron ionization (EI)

In **electron ionization (EI) mass spectrometry**, ions are produced by bombarding gaseous molecules with high-energy electrons. It is a 'hard' technique and causes fragmentation of the parent molecule.

A schematic representation of an electron ionization (EI) mass spectrometer is shown in Fig. 4.7. The compound (solid, liquid or gas) to be analysed is introduced into the instrument and is vaporized by heating (unless the sample is gaseous at 298 K). The vapour is subjected to a stream of high-energy ( $\approx 70 \text{ eV}$ ) electrons which ionizes the sample (eq. 4.1). The  $[\text{M}]^+$  ion is a radical cation and is strictly written as  $[\text{M}]^{\bullet+}$ . The energy of the electrons used for the bombardment is much greater than covalent bond energies and causes fragmentation of the parent molecule, M. Thus, in addition to the molecular (or parent) ion,

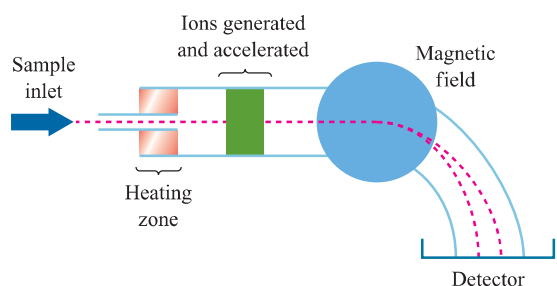
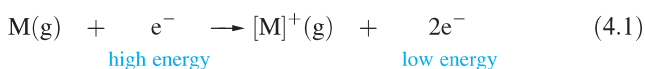


**Fig. 4.7** Schematic diagram of an electron ionization (or electron impact, EI) mass spectrometer. During operation, the interior of the instrument is evacuated.

$[M]^+$ , fragment ions are also formed. Electron ionization mass spectrometry is therefore classed as a ‘hard’ technique.

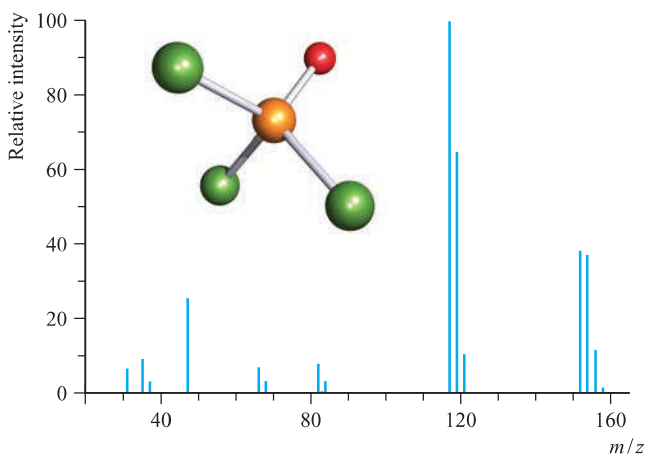


The positive ions pass through a magnetic field where their paths are deflected. The amount of deflection depends on the mass of the ion: the larger the  $m/z$  value, the larger the radius of the path that the ion follows (Fig. 4.7). The output from the mass spectrometer (a *mass spectrum*) is a plot of signal intensity against mass-to-charge ( $m/z$ ) ratio. For an ion with  $z = 1$ , the  $m/z$  value is the same as the molecular mass of the ion. If  $z = 2$ , the recorded mass is half the actual mass of the ion, and so on. In EI mass spectrometry, most ions have  $z = 1$ . In a mass spectrum, the signal intensity is plotted in terms of relative values, with the most intense signal (the *base peak*) being arbitrarily assigned a value of 100%.

In addition to fragmentation patterns, the appearance of a mass spectrum depends upon the naturally occurring isotopes of the elements (see Appendix 5). The presence of several isotopes of an element leads to the observation of *peak envelopes*.

### Worked example 4.3 EI mass spectrum of $POCl_3$

Assign the peaks in the EI mass spectrum of  $POCl_3$  shown below.



Look in Appendix 5 for the isotopes of P, O and Cl:

Cl	75.77% $^{35}\text{Cl}$ , 24.23% $^{37}\text{Cl}$
P	100% $^{31}\text{P}$
O	99.76% $^{16}\text{O}$ , 0.04% $^{17}\text{O}$ , 0.20% $^{18}\text{O}$ (i.e. close to 100% $^{16}\text{O}$ )

Note that, because Cl has two isotopes both of which are present in significant abundance, the mass spectrum exhibits groups of peaks (*peak envelopes*).

Determine the  $m/z$  value for the peak that you expect for the parent molecular ion,  $[M]^+$ , using the most abundant isotopes:

$$[M]^+ = [(^{31}\text{P})(^{16}\text{O})(^{35}\text{Cl})_3]^+ \quad m/z \ 152 \quad \text{for } z = 1$$

This matches the left-hand peak in the group of highest mass peaks in the mass spectrum. The peaks at  $m/z$  154, 156 and 158 arise from  $[(^{31}\text{P})(^{16}\text{O})(^{35}\text{Cl})_2(^{37}\text{Cl})]^+$ ,  $[(^{31}\text{P})(^{16}\text{O})(^{35}\text{Cl})(^{37}\text{Cl})_2]^+$  and  $[(^{31}\text{P})(^{16}\text{O})(^{37}\text{Cl})_3]^+$  and the relative intensities of these peaks correspond to the probabilities of finding the particular combinations of isotopes.

Now consider the possible fragmentations: cleavage of P–Cl or P–O bonds. The peaks at  $m/z$  117, 119 and 121 are assigned to  $[POCl_2]^+$  with two  $^{35}\text{Cl}$ , one  $^{35}\text{Cl}$  and one  $^{37}\text{Cl}$ , and two  $^{37}\text{Cl}$ , respectively. This ion can also be written as  $[M-Cl]^+$ .

The pairs of peaks at  $m/z$  82 and 84, and  $m/z$  66 and 68 have the same isotope pattern and this is diagnostic of one chlorine atom. The assignments are  $[M-2Cl]^+$  and  $[M-2Cl-O]^+$ .

The single peak at  $m/z$  must arise from an ion which does not contain Cl, i.e. to  $[M-3Cl]^+$ . The remaining peaks at  $m/z$  35 and 37, and at  $m/z$  31 are due to the atomic ions  $[Cl]^+$  and  $[P]^+$ .

Although EI mass spectrometry is widely used (especially for organic compounds), it has limitations. It is suitable for the mass determination of relatively low mass compounds ( $M_r < 1500$ ). If not a gas at 298 K, the compound must be volatile when heated and must be stable at the temperature required for vaporization. EI mass spectrometry cannot be used for ionic compounds.

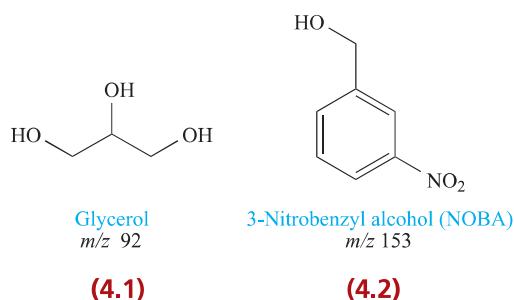
### Fast atom bombardment (FAB)

In *fast atom bombardment (FAB) mass spectrometry*, ions are produced by bombarding the sample (neutral molecules or ionic salts) with high energy xenon or argon atoms. It is a ‘soft’ technique and usually causes little fragmentation.

Fast atom bombardment (FAB) mass spectrometry was developed in the 1980s and has a number of advantages over EI: molecular masses up to  $\approx 10\,000$  can be determined, the instrument can be run in both positive and negative modes permitting both positive and negative ions to be



detected, and both ionic salts and neutral compounds can be investigated. Unlike EI, FAB mass spectrometry is a 'soft' technique and fragmentation of the parent ion is usually minimal.



The sample to be analysed is mixed with a high boiling point liquid matrix such as glycerol (4.1) or 3-nitrobenzyl alcohol (4.2). The mixture is applied to the probe of the instrument and is bombarded with fast Xe or Ar atoms (Fig. 4.8). These are generated in an atom gun by ionizing Xe to  $\text{Xe}^+$  (or Ar to  $\text{Ar}^+$ ), and then accelerating the ions in an environment where electron capture occurs to give a stream of atoms with energies  $\leq 10$  keV. The beam of atoms bombards the matrix/sample obliquely (Fig. 4.8) and sample ions are produced with energies close to 1 eV or  $96.5 \text{ kJ mol}^{-1}$ . When the instrument is run in positive mode, atom bombardment of the sample leads to:

- direct release of parent  $[\text{M}]^+$  ions from an ionic salt  $\text{M}^+\text{X}^-$ , or  $[\text{MX}]^+$  from an ionic salt  $\text{M}^{2+}(\text{X}^-)_2$ ;
- combination of a neutral molecule with a cation (usually  $\text{H}^+$  or  $\text{Na}^+$ ) to give  $[\text{M} + \text{H}]^+$  or  $[\text{M} + \text{Na}]^+$ ;
- ions such as  $[\text{M} - \text{H}]^+$ ;
- aggregation to form ions such as  $[2\text{M} + \text{H}]^+$ ,  $[2\text{M} + \text{Na}]^+$  or  $[\text{M} + \text{matrix} + \text{H}]^+$ .

With the instrument in negative mode, atom bombardment results in:

- direct release of  $[\text{X}]^-$  from an ionic salt containing  $\text{X}^-$  anions;

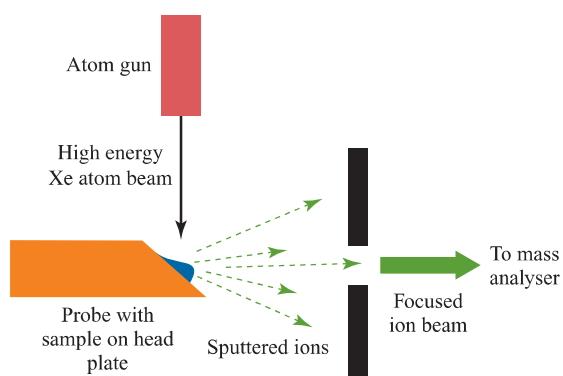


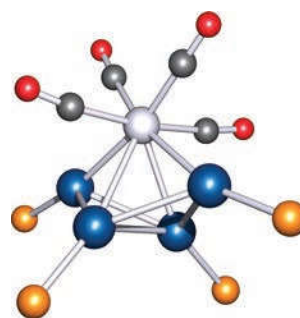
Fig. 4.8 Schematic representation of the components in a FAB mass spectrometer.

- combination of a neutral molecule with an anion (usually  $\text{H}^-$  or  $\text{Cl}^-$ ) to give  $[\text{M} + \text{H}]^-$  or  $[\text{M} + \text{Cl}]^-$ ;
- proton loss to give  $[\text{M} - \text{H}]^-$ ;
- aggregation to form ions such as  $[2\text{M} - \text{H}]^-$ .

The origin of  $\text{Na}^+$  and  $\text{Cl}^-$  ions may be impurities in the sample, but  $\text{NaCl}$  may be added to the analyte. The ions leaving the probe are said to be *sputtered*, and the beam of ions is focused for entry into the mass analyser (Fig. 4.8).

#### Worked example 4.4 Analysing a multinuclear metal cluster compound by FAB mass spectrometry

When  $\text{Ph}_3\text{PAuCl}$  reacts with  $[\text{HRe}_3(\text{CO})_{12}]^{2-}$ , and the product is treated with  $\text{K}[\text{PF}_6]$ , a yellow crystalline solid is isolated. The FAB (positive mode) mass spectrum exhibits peak envelopes at  $m/z$  2135.1, 1845.1 and 1582.8. Show that these data are consistent with the product being  $[(\text{Ph}_3\text{PAu})_4\text{Re}(\text{CO})_4][\text{PF}_6]$ , and assign all the peaks. The structure of the  $\{(\text{PAu})_4\text{Re}(\text{CO})_4\}$  core of the  $[(\text{Ph}_3\text{PAu})_4\text{Re}(\text{CO})_4]^+$  cation is shown below:



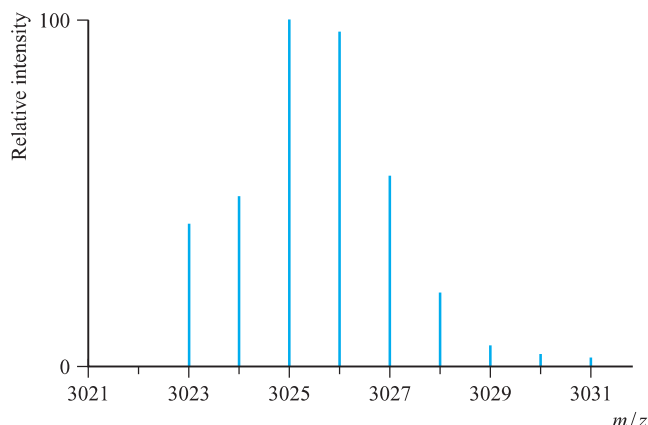
Colour code: Au, blue; P, orange; Re, silver; C, grey; O, red.  
[Data: G. Pivoriunas *et al.* (2005) *Inorg. Chim. Acta*, vol. 358, p. 4301]

The compound is ionic. In positive mode FAB MS, direct release of  $[(\text{Ph}_3\text{PAu})_4\text{Re}(\text{CO})_4]^+$  leads to an ion with calculated  $m/z$  2135.2. This is consistent with the observed value for the highest mass peak.

Fragmentation is expected to involve loss of CO or  $\text{PPh}_3$  ligands. The peaks at  $m/z$  1845.1 and 1582.8 are assigned to  $[\text{M} - \text{PPh}_3 - \text{CO}]^+$  and  $[\text{M} - 2\text{PPh}_3 - \text{CO}]^+$ , respectively.

#### Self-study exercises

1. In the FAB mass spectra of gold(I) triphenylphosphane complexes, a peak envelope at  $m/z$  721.2 is often observed. Assign this peak.
2. The highest mass peak envelope in the FAB (positive mode) mass spectrum of the compound  $[(\text{Ph}_3\text{PAu})_6\text{Re}(\text{CO})_3][\text{PF}_6]$  appears as follows:



(a) Explain how this series of peaks arises. (b) Additional peak envelopes are observed at  $m/z$  2763.4, 2501.3, 2239.5, 1977.6 and 459.0. Suggest identities for these singly charged ions.

### Matrix-assisted laser desorption ionization time-of-flight (MALDI-TOF)

In *matrix-assisted laser desorption ionization time-of-flight (MALDI-TOF) mass spectrometry*, a UV laser is used to generate atoms,  $M$ , of the sample;  $[M + H]^+$  or  $[M + Na]^+$  ions are typically detected. It is a ‘soft’ method and there is little fragmentation.

Matrix-assisted laser desorption ionization (MALDI) mass spectrometry uses a pulsed UV laser beam to produce ions for mass analysis. The coupling of MALDI with time-of-flight (TOF) mass analysis (Fig. 4.9) provides a sensitive technique which is especially useful for very high molecular mass species ( $M_r \leq 300\,000$ ) including biomolecules and polymers. The sample is mixed with a large excess of matrix (e.g. **4.3** or **4.4**) which is capable of absorbing photons from the UV laser. Both **4.3** and **4.4** absorb at  $\lambda = 337$  and  $355$  nm. The matrix/analyte is loaded onto a sample plate where it crystallizes. Energy provided by the pulsed laser is absorbed by the matrix causing desorption of the molecules of sample. Combination with  $H^+$  or  $Na^+$  produces  $[M + H]^+$  or  $[M + Na]^+$  ions and, since MALDI is a ‘soft’ method, there is usually little fragmentation of the parent ions. Multiply charged ions are rarely formed.

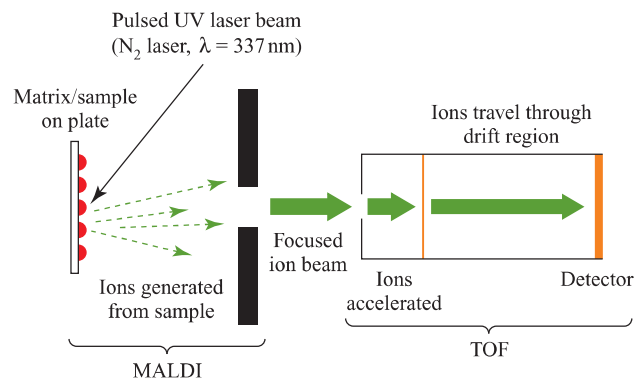
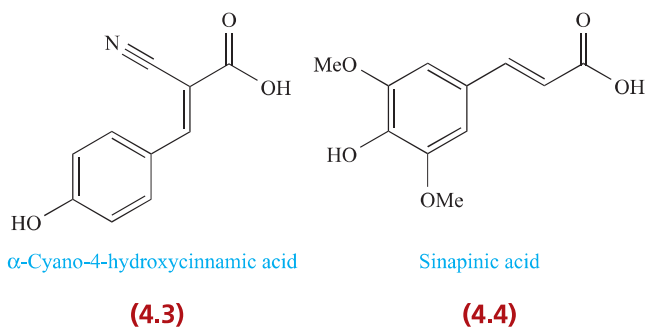
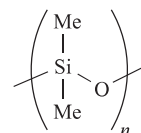


**Fig. 4.9** Schematic representation of the components in a MALDI-TOF mass spectrometer.

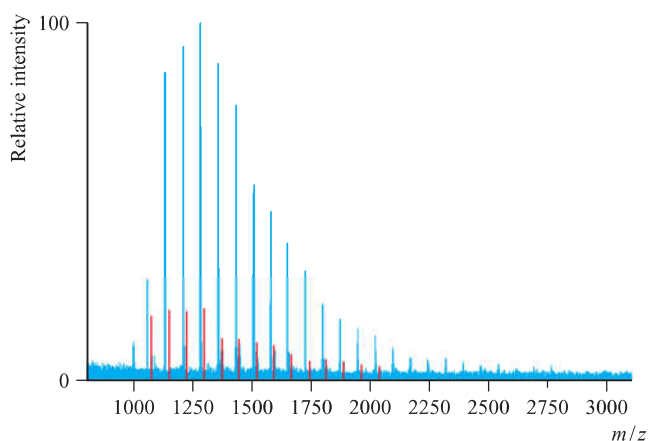
Ions leaving the sample plate are focused into a beam and accelerated in an electric field in such a way that all singly charged ions possess the same amount of kinetic energy. Since kinetic energy is  $\frac{1}{2}mv^2$ , ions with the highest masses have the lowest velocities and longer flight times along the drift region in the flight tube (Fig. 4.9), and vice versa. Ions with the same  $m/z$  ratio possess the same travel time and the data are converted into a conventional mass spectrum. However, the nature of the TOF method of analysis means that broader peaks are observed than in EI, FAB or ESI mass spectrometries with the result that isotope patterns are not usually well resolved.

### Worked example 4.5 MALDI-TOF mass spectrum of a polydimethylsiloxane

The figure below shows the MALDI-TOF mass spectrum (positive mode) of a sample of a polydimethylsiloxane elastomer, the repeat unit of which is:



Linear polymer chains may be terminated in Me or OH units; cyclic oligomers are also possible.



The main spectrum (in blue) is accompanied by a sub-spectrum (in red), and in each spectrum, the spacings between consecutive lines is  $m/z$  74. Rationalize the appearance of the mass spectrum.

[Data: S.M. Hunt *et al.* (2000) *Polym. Int.*, vol. 49, p. 633]

The value of  $m/z$  74 corresponds to an  $\text{Me}_2\text{SiO}$  monomer unit. Therefore the series of blue peaks arises from polymer chains of different lengths. Similarly for the set of red peaks. The observation of two series indicates that both cyclic and linear polymer chains are present. A cyclic oligomer has the formula  $(\text{Me}_2\text{SiO})_n$ . For a particular chain length, a linear oligomer has a higher molecular mass than the corresponding cyclic oligomer because of the presence of the end groups (Me or OH).

The relative intensities of the two spectra reveal that cyclic oligomers dominate over linear chains.

### Self-study exercises

These questions refer to the data in the worked example.

1. Polydimethylsiloxanes are neutral species. How do the positive ions observed in the MALDI-TOF experiment arise?
2. Give a formula for the positive ion observed at  $m/z$  985.
3. Use Appendix 5 to explain why each of the peaks shown in the figure above consists of an envelope of peaks.

### Electrospray ionization (ESI)

In *electrospray ionization (ESI) mass spectrometry*, ions are formed from a fine spray of solution under an applied electrical potential; it is a 'soft' technique used for both neutral molecules or ionic salts. Singly and multiply charged ions are observed.

The 'soft' technique of electrospray ionization (ESI) mass spectrometry has widespread applications in chemical and biochemical analysis of high-molecular mass compounds ( $M_r \leq 200\,000$ ). In contrast to the methods described above, both singly and multiply charged ions are observed, making the ESI technique valuable for analysis of ionic compounds.

The sample is dissolved in a volatile solvent (e.g. MeCN or MeOH) and the solution is converted into a fine spray (nebulized) at atmospheric pressure by the application of a high electrical potential (Fig. 4.10). The ESI mass spectrometer can be operated in positive-ion mode which gives positively charged droplets of sample, or in negative-ion mode which produces negatively charged droplets. An electrical potential is applied between the needle through which the sample is injected and a counter electrode. The charged droplets travel towards the counter electrode, during which time the solvent evaporates. The gas-phase ions so-formed pass into a mass analyser. Zoom scans of peaks in the mass spectrum reveal the isotope patterns and allow the peak separations to be determined. If the peaks in an envelope are one mass unit apart, the ion is singly charged. If they

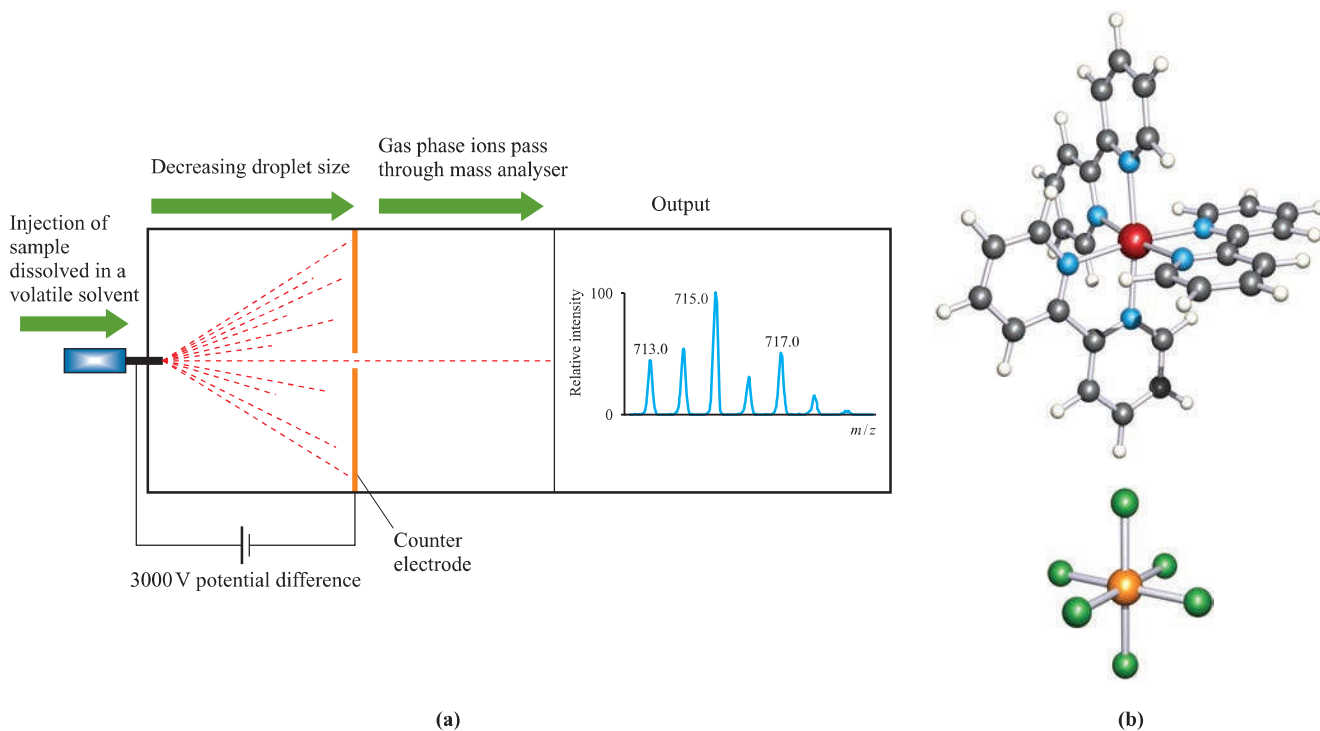
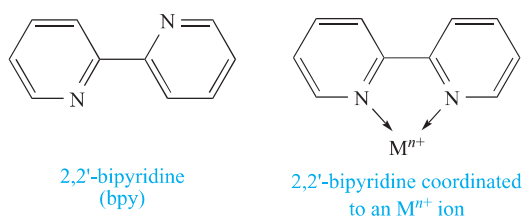


**Fig. 4.10** (a) Schematic representation of the components in an ESI mass spectrometer. The zoom scan shown on the right corresponds to the highest mass peak envelope in the ESI mass spectrum of the complex  $[\text{Ru}(\text{bpy})_3][\text{PF}_6]_2$  ( $\text{bpy} = 2,2'$ -bipyridine) and is assigned to the  $[\text{M}-\text{PF}_6]^+$  ion. (b) The structures of the  $[\text{Ru}(\text{bpy})_3]^{2+}$  and  $[\text{PF}_6]^-$  ions. Colour code: Ru, red; N, blue; C, grey; H, white; P, orange; F, green.

are half a mass unit apart, the ion is doubly charged, and so on. The zoom scan shown in Fig. 4.10 shows the highest mass peak envelope in the ESI mass spectrum of the coordination compound  $[\text{Ru}(\text{bpy})_3][\text{PF}_6]_2$  ( $\text{bpy} = 2,2'$ -bipyridine, 4.5). The pattern of peaks is largely controlled by the fact that Ru possesses seven naturally occurring isotopes (see Appendix 5), and the peak envelope is assigned to the  $[\text{M} - \text{PF}_6]^+$  ion.

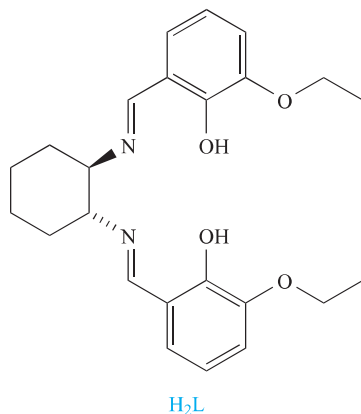


(4.5)

As in FAB and MALDI-TOF mass spectrometries, neutral molecules are converted to positive ions by combination with  $\text{H}^+$  or  $\text{Na}^+$  ions. Aggregation may also occur to produce ions of the type  $[2\text{M} + \text{Na}]^+$ , and combination with the solvent molecules gives ions such as  $[\text{M} + \text{MeCN} + \text{H}]^+$ .

### Self-study exercises

1.



The ligand,  $\text{H}_2\text{L}$ , reacts with copper(II) acetate to give a neutral complex. In the ESI mass spectrum of a  $\text{CH}_2\text{Cl}_2/\text{MeOH}$  solution of the product, the base peak is at  $m/z$  494.1 and exhibits an isotope pattern characteristic of one Cu atom. Assign the peak and, assuming no fragmentation occurs, suggest a formula for the complex.

2. Elemental analysis for an ionic cobalt(II) compound is consistent with a formula of  $\text{C}_{30}\text{H}_{22}\text{N}_6\text{CoP}_2\text{F}_{12}$ . (a) In the ESI mass spectrum of an MeCN solution of the compound, the highest group of peaks appears at  $m/z$  670.1 (100%), 671.1 (35%) and 672.1 (6%). By referring to Appendix 5, explain how this group of peaks arises.

(b) In a second group of peaks, the most intense peak has  $m/z$  262.6 and the peaks in the envelope are at half-mass separations. Rationalize these data.

## 4.6 Infrared and Raman spectroscopies

**Infrared (IR) and Raman spectroscopies** are concerned with transitions between vibrational energy levels. For a vibrational mode to be **IR active**, it must give rise to a **change in dipole moment**. For a vibrational mode to be **Raman active**, it must give rise to a **change in polarizability**.

Infrared (IR) and Raman spectroscopies are types of *vibrational spectroscopy*. In Chapter 3, we showed how to determine the number of degrees of vibrational freedom of a molecule, and stated the selection rules for an IR or Raman active mode of vibration (summarized above). We detailed the use of character tables to determine the types of vibrational modes and their symmetry labels.

### Energies and wavenumbers of molecular vibrations

The **zero point energy** of a molecule corresponds to the energy of its lowest vibrational level (vibrational ground state).

When a molecule absorbs infrared radiation, it undergoes vibrational motions (Section 3.7). Stretching a covalent bond is like stretching a spring, and molecules undergo *anharmonic oscillations*. The vibrational energies are quantized and are given by eq. 4.2. The energy level with  $v = 0$  is the *zero point energy* of the molecule. If, as is usually the case, we are concerned only with a transition from the vibrational ground state to the first excited state, then the motion is approximately that of a *simple harmonic oscillator* (eq. 4.3).<sup>†</sup>

$$E_v = (v + \frac{1}{2})h\nu - (v + \frac{1}{2})^2 h\nu x_e \quad (E_v \text{ in J}) \quad (4.2)$$

where:  $v$  is the vibrational quantum number

$h$  = Planck constant

$\nu$  = frequency of vibration

$x_e$  = anharmonicity constant

$$E_v = (v + \frac{1}{2})h\nu \quad (4.3)$$

Consider a diatomic molecule, XY. The vibrational frequency of the bond depends on the masses of atoms X and Y, and on the *force constant*,  $k$ , of the bond. The force constant is a property of the bond and is related to its strength. If we return to stretching a spring, then the force constant is a measure of the stiffness of the spring. If atoms X and Y are of similar mass, they contribute almost equally to the molecular vibration. However, if the masses

<sup>†</sup>For more basic detail, see Chapter 12 in: C.E. Housecroft and E.C. Constable (2010) *Chemistry*, 4th edn, Prentice Hall, Harlow.

are very different, the lighter atom moves more than the heavier one. It is therefore necessary to define a quantity that describes the mass of the oscillator in a way that reflects the relative masses of X and Y. This is the *reduced mass*,  $\mu$ , and for X and Y with masses of  $m_X$  and  $m_Y$ ,  $\mu$  is given by eq. 4.4.

$$\frac{1}{\mu} = \frac{1}{m_X} + \frac{1}{m_Y} \quad \text{or} \quad \mu = \frac{m_X m_Y}{m_X + m_Y} \quad (4.4)$$

For a diatomic molecule, the transition from the vibrational ground state to the first excited state gives rise to a *fundamental absorption* in the vibrational spectrum. Equation 4.5 gives the frequency of this absorption.

$$\nu = \frac{1}{2\pi} \sqrt{\frac{k}{\mu}} \quad (4.5)$$

where:  $\nu$  = fundamental vibrational frequency (Hz)

$k$  = force constant ( $\text{N m}^{-1}$ )

$\mu$  = reduced mass (kg)

Absorptions in IR spectra are usually quoted in wavenumbers (wavenumber =  $1/\text{wavelength}$ ,  $\bar{\nu} = 1/\lambda$ ) rather than frequencies, and eq. 4.5 then becomes eq. 4.6.

$$\bar{\nu} = \frac{1}{2\pi c} \sqrt{\frac{k}{\mu}} \quad (4.6)$$

where:  $\bar{\nu}$  = wavenumber ( $\text{cm}^{-1}$ )

$c$  = speed of light =  $3.00 \times 10^{10} \text{ cm s}^{-1}$

### The Fourier transform infrared (FT-IR) spectrometer and sample preparation

The IR region is from  $20 \text{ cm}^{-1}$  (far IR) to  $14\,000 \text{ cm}^{-1}$  (near IR), but most laboratory IR spectrometers probe only the mid-IR ( $400$  to  $4000 \text{ cm}^{-1}$ ). In addition to being invaluable as a routine analytical tool in the laboratory, IR spectroscopy has applications in fields as far apart as forensic sciences (Fig. 4.11) and astronomy. The output data may be in the



**Fig. 4.11** Fourier transform (FT) IR spectrometer in a forensic crime laboratory.

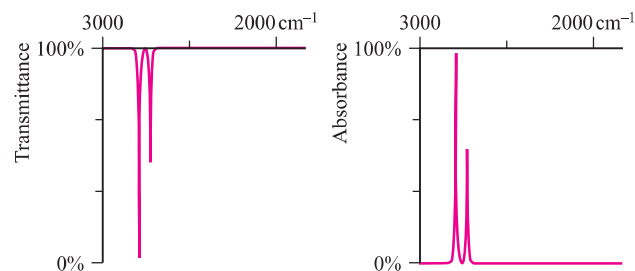


**Fig. 4.12** An IR spectrum can be recorded in terms of transmittance or absorbance, and provides information about the energy and intensity of an absorption.

form of an absorption or a transmission spectrum (Fig. 4.12): 100% transmission corresponds to 0% absorption.

Infrared spectra can be recorded using gaseous, liquid or solid samples. Spectra of gases usually exhibit rotational structure in addition to bands arising from vibrational modes. Solid samples have traditionally been prepared in the form of a mull in an organic oil (e.g. nujol) or as a pressed disc in which the sample is ground with an alkali metal halide (e.g. KBr). The disadvantage of a mull is the appearance of absorptions arising from the matrix, while the use of an alkali metal halide restricts the window of observation: KBr is optically transparent from  $4000$  to  $450 \text{ cm}^{-1}$ , whereas the window for NaCl is  $4000$  to  $650 \text{ cm}^{-1}$ . The use of a modern diamond attenuated total reflectance (ATR) accessory allows the IR spectrum of a solid to be measured directly, and avoids the need for mulls or pressed discs.

### Diagnostic absorptions

Infrared spectra of inorganic and organic compounds can generally be separated into two regions. Absorptions above  $1500 \text{ cm}^{-1}$  can typically be assigned to specific groups (Table 4.1), while bands below  $1500 \text{ cm}^{-1}$  tend to arise from single bond stretching modes, deformations, and vibrational modes of the molecular framework. This latter region is called the *fingerprint region* and the absorptions within it are usually taken together to provide a diagnostic signature of the compound. However, the distinction between the two regions is not definitive. For example, the  $T_{1u}$  vibrational mode (see Fig. 3.18) of the  $[\text{PF}_6]^-$  ion gives rise to a strong and easily recognizable absorption at  $865 \text{ cm}^{-1}$ . Table 4.2 lists IR active bands for some common inorganic anions with  $D_{3h}$ ,  $C_{3v}$ ,  $T_d$ ,  $D_{4h}$  or  $O_h$  symmetries; the vibrational modes are illustrated in Figs. 3.14–3.18. Table 4.2 shows that the vibrational wavenumbers for the  $D_{4h}$   $[\text{PdCl}_4]^{2-}$  and  $[\text{PtCl}_4]^{2-}$  ions are below  $400 \text{ cm}^{-1}$ , and the associated IR absorptions, like those of most other metal halides, are not observed using a typical laboratory mid-IR spectrometer.

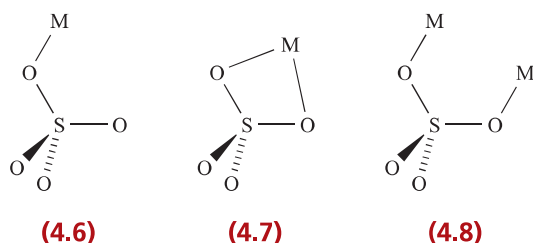
Ions such as  $[\text{NO}_3]^-$ ,  $[\text{CO}_3]^{2-}$ ,  $[\text{SO}_4]^{2-}$  and  $[\text{ClO}_4]^-$  can coordinate to metal centres and, as a result, the symmetry of the anion is lowered. Structures 4.6–4.8 illustrate common

**Table 4.1** Typical ranges of fundamental stretching wavenumbers of selected groups (M = metal atom).

Functional group	$\nu/\text{cm}^{-1}$	Functional group	$\nu/\text{cm}^{-1}$
O–H	3700–3500	CO ligand (terminal MCO) <sup>†</sup>	2200–1900
O–H (hydrogen bonded)	3500–3000	CO ligand (bridging M <sub>2</sub> CO) <sup>†</sup>	1900–1700
N–H	3500–3200	NO (terminal, linear MNO)	1900–1650
C–H	3000–2850	NO (terminal, bent MNO)	1690–1525
B–H (terminal)	2650–2350	CN ligand (terminal MCN)	2200–2000
B–H (bridge)	2100–1600	B–Cl	1000–600
S–H	2700–2550	C–Cl	1000–600
P–H	2450–2275	Si–Cl	750–600
Si–H	2250–2100	N–Cl	800–600
Al–H	1800–1700	P–Cl	600–450
C=O (organic)	1750–1650	O–Cl	1200–700
C=N (organic)	1690–1630	S–Cl	750–400

<sup>†</sup>See Fig. 24.2 and accompanying discussion.

coordination modes for the sulfato ligand; charges are ignored in the diagrams. The effects of coordination can be seen in Fig. 4.13 which shows part of the IR spectra of  $[\text{Co}(\text{NH}_3)_6][\text{SO}_4]_3 \cdot 5\text{H}_2\text{O}$  (which contains non-coordinated  $[\text{SO}_4]^{2-}$  ions) and  $[\text{Co}(\text{NH}_3)_5(\text{OSO}_3)]\text{Br}$  (which contains a metal-bound sulfato ligand in coordination mode 4.6).



Section 3.7 gives examples of the fundamental stretching wavenumbers of simple inorganic molecules and anions, as well as exercises to help you to relate an observed spectrum to the symmetry of a species.

### Deuterium/hydrogen exchange

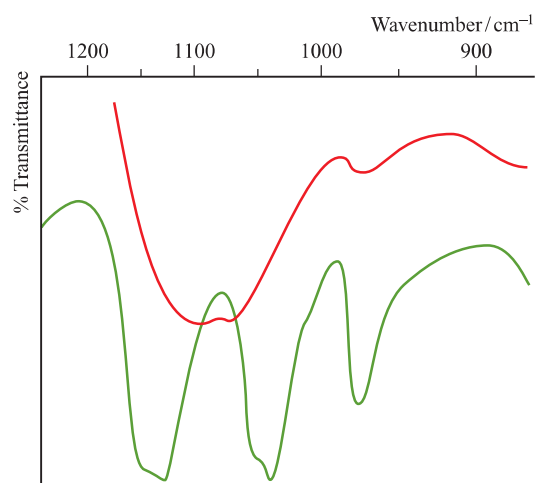
When the hydrogen atom in an X–H bond is exchanged by deuterium D,<sup>†</sup> the reduced mass of the pair of bonded atoms changes and shifts the position of the absorption in the IR spectrum due to the X–H stretching mode. Shifts of this kind can be used to confirm assignments in IR spectra.

<sup>†</sup>Rather than use the full notation for the  $^2_1\text{H}$  isotope, we use the less rigorous, but still unambiguous, notation with only the mass number, e.g.  $^2\text{H}$ . In addition, the label D for deuterium is introduced.

For example, N–H, O–H and C–H bonds all absorb around  $3000\text{--}3600\text{ cm}^{-1}$  (Table 4.1). However, if a compound containing C–H and N–H or O–H bonds is shaken with  $\text{D}_2\text{O}$ , usually, only the OH and NH groups undergo rapid *deuterium exchange reactions* (eq. 4.7). An H atom attached directly to C exchanges extremely slowly except in cases where it is acidic (e.g. a terminal alkyne).





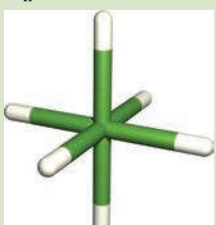


By observing which IR spectroscopic bands shift (and by how much), it is possible to confirm the assignment of an N–H, O–H or C–H absorption.



**Fig. 4.13** IR spectra of  $[\text{Co}(\text{NH}_3)_6]_2[\text{SO}_4]_3 \cdot 5\text{H}_2\text{O}$  (in red) and  $[\text{Co}(\text{NH}_3)_5(\text{OSO}_3)]\text{Br}$  (in green). [Redrawn with permission from: K. Nakamoto *et al.* (1957) *J. Am. Chem. Soc.*, vol. 79, p. 4904.]

**Table 4.2** Vibrational modes and wavenumbers of selected anions.<sup>†</sup> See Figs. 3.14–3.18 for schematic representations of the vibrational modes.

<b><math>D_{3h}</math></b>		$\nu_2 (A_2'')$	$\nu_3 (E')$	$\nu_4 (E')$			
							
$[\text{CO}_3]^{2-}$ (solid $\text{CaCO}_3$ )	879	1429–1492 broad	706				
$[\text{NO}_3]^-$ (solid $\text{NaNO}_3$ )	831	1405	692				
$[\text{NO}_3]^-$ (solid $\text{KNO}_3$ )	828	1370	695				
<b><math>C_{3v}</math></b>		$\nu_1 (A_1)$	$\nu_2 (A_1)$	$\nu_3 (E)$	$\nu_4 (E)$		
							
$[\text{SO}_3]^{2-}$	967	620	933	469			
$[\text{ClO}_3]^-$	933	608	977	477			
<b><math>D_{4h}</math></b>		$\nu_3 (A_{2u})$	$\nu_6 (E_u)$	$\nu_7 (E_u)$			
							
$[\text{PdCl}_4]^{2-}$	150	321	161				
$[\text{PtCl}_4]^{2-}$	147	313	165				
<b><math>T_d</math></b>		$\nu_3 (T_2)$	$\nu_4 (T_2)$	<b><math>O_h</math></b>		$\nu_3 (T_{1u})$	$\nu_4 (T_{1u})$
							
$[\text{BF}_4]^-$	1070	533		$[\text{SiF}_6]^{2-}$	741	483	
$[\text{BCl}_4]^-$	722	278		$[\text{PF}_6]^-$	865	559	
$[\text{AlCl}_4]^-$	498	182		$[\text{PCl}_6]^-$	444	285	
$[\text{SiO}_4]^{4-}$	956	527		$[\text{AsF}_6]^-$	700	385	
$[\text{PO}_4]^{3-}$	1017	567		$[\text{AsCl}_6]^-$	333	220	
$[\text{SO}_4]^{2-}$	1105	611		$[\text{SbF}_6]^-$	669	350	
$[\text{ClO}_4]^-$	1119	625		$[\text{SbCl}_6]^-$	353	180	

<sup>†</sup>Data: K. Nakamoto (1997) *Infrared and Raman Spectra of Inorganic and Coordination Compounds*, Part A, 5th edn, Wiley, New York.

**Worked example 4.6** The effects of deuteration on  $\bar{\nu}_{\text{O-H}}$  in an IR spectrum

An absorption at  $3650\text{ cm}^{-1}$  in the IR spectrum of a compound X has been assigned to an O–H stretching mode. To what wavenumber is this band expected to shift upon deuteration? What assumption have you made in the calculation?

The vibrational wavenumber,  $\bar{\nu}$ , is given by:

$$\bar{\nu} = \frac{1}{2\pi c} \sqrt{\frac{k}{\mu}}$$

If we assume that the force constants of O–H and O–D bonds are the same, then the only variables in the equation are  $\bar{\nu}$  and  $\mu$ . Thus, the O–H vibrational wavenumber,  $\bar{\nu}$ , is related to the reduced mass,  $\mu$ , by the equation:

$$\bar{\nu}_{\text{O-H}} \propto \frac{1}{\sqrt{\mu_{\text{O-H}}}}$$

For comparison of the O–H and O–D stretching frequencies, we can write:

$$\frac{\bar{\nu}_{\text{O-D}}}{\bar{\nu}_{\text{O-H}}} = \frac{\sqrt{\mu_{\text{O-H}}}}{\sqrt{\mu_{\text{O-D}}}}$$

and since we are now dealing with a *ratio*, it is not necessary to convert the atomic masses to kg (see eq. 4.5). The relative atomic masses of O, H and D are 16.00, 1.01 and 2.01, respectively. The reduced masses of O–H and O–D bonds are found as follows:

$$\frac{1}{\mu_{\text{O-H}}} = \frac{1}{m_1} + \frac{1}{m_2} = \frac{1}{16.00} + \frac{1}{1.01} = 1.0526 \quad \mu_{\text{O-H}} = 0.9500$$

$$\frac{1}{\mu_{\text{O-D}}} = \frac{1}{m_1} + \frac{1}{m_2} = \frac{1}{16.00} + \frac{1}{2.01} = 0.5600 \quad \mu_{\text{O-D}} = 1.7857$$

The vibrational wavenumber of the O–D bond is therefore:

$$\begin{aligned} \bar{\nu}_{\text{O-D}} &= \bar{\nu}_{\text{O-H}} \times \sqrt{\frac{\mu_{\text{O-H}}}{\mu_{\text{O-D}}}} = 3650 \times \sqrt{\frac{0.9500}{1.7857}} = 2662\text{ cm}^{-1} \\ &= 2660\text{ cm}^{-1} \text{ (to 3 sig. fig.)} \end{aligned}$$

The calculation makes the assumption that the force constants of O–H and O–D bonds are the same.

**Self-study exercises**

Data: atomic masses H = 1.01; D = 2.01; N = 14.01; C = 12.01; O = 16.00

- Show that upon converting  $\text{NH}_3$  to  $\text{ND}_3$ , an absorption in the vibrational spectrum at  $3337\text{ cm}^{-1}$  shifts to  $2440\text{ cm}^{-1}$ .
- An absorption at  $3161\text{ cm}^{-1}$  in an IR spectrum is assigned to a C–H stretching mode. Show that upon deuteration, the band appears at  $2330\text{ cm}^{-1}$ .

- An absorption in the IR spectrum of a compound containing an X–H bond shifts from  $3657$  to  $2661\text{ cm}^{-1}$  upon deuteration. Show that X is likely to be O rather than C. What assumption have you made in the calculation?

Spectroscopic studies of isotopically substituted molecules often involve special syntheses which must be designed so as to make the best possible use of the isotope to be incorporated. For example, deuterated ammonia,  $\text{ND}_3$ , would not be prepared by exchange between  $\text{NH}_3$  and  $\text{D}_2\text{O}$  since a large proportion of the deuterium is wasted in conversion to  $\text{HOD}$ . A better method is to react  $\text{D}_2\text{O}$  with  $\text{Mg}_3\text{N}_2$  (eq. 4.8).

**Raman spectroscopy**

The nature of the selection rules for IR and Raman spectroscopies results in these techniques being complementary. Chandrasekhara V. Raman was awarded the 1930 Nobel Prize in Physics ‘for his work on the scattering of light and for the discovery of the effect named after him’. When radiation (usually from a laser, Fig. 4.14) of a frequency,  $\nu_0$ , falls on a vibrating molecule, most of the radiation is scattered without a change in frequency. This is called *Rayleigh scattering*. A small amount of the scattered radiation has frequencies of  $\nu_0 \pm \nu$ , where  $\nu$  is the fundamental frequency of a vibrating mode of the molecule. This is *Raman scattering*. For recording the Raman spectra of inorganic compounds, the radiation source is usually a visible noble gas laser (e.g. a red krypton laser,  $\lambda = 647\text{ nm}$ ). One of the advantages of Raman spectroscopy is that it extends to lower wavenumbers than routine laboratory IR spectroscopy, thereby permitting the observation of,

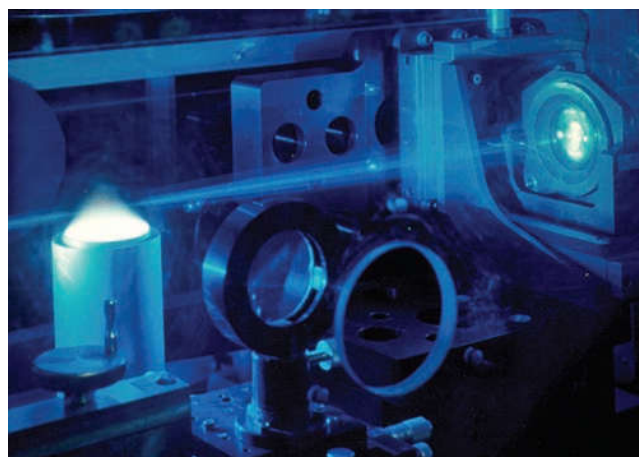


**Fig. 4.14** Laser Raman spectroscopy being used to measure ambient flame pressure at the Combustion Research Facility and Sandia National Laboratory, California. The research is aimed at creating heat engines and systems that burn fuel more efficiently while creating less pollution.



## APPLICATIONS

## Box 4.1 Analysing paints and pigments

Analysis of paints is a routine part of forensic investigations of hit-and-run accidents or collisions involving vehicles. Paints have complex formulations. Automotive paints are applied in layers and the sequence and colours of the layers provide information on the origins of the vehicle. By matching IR and Raman spectroscopic data from a vehicle paint sample to those in databases (e.g. the European Collection of Automotive Paints and Paint Data Query), it is possible to determine the vehicle's manufacturer and year of production. The main components of a paint fall into four categories:

- binders (resins)
- pigments
- solvents
- additives.

Binders are typically organic resins, while pigments include inorganic compounds. The table below gives IR spectroscopic absorptions that can be used to identify some of the most common inorganic pigments. For the identification of a wider range of pigments, Raman spectroscopy must be used.

Pigment	Dominant IR absorptions/cm <sup>-1</sup>
TiO <sub>2</sub> (rutile)	600
BaCrO <sub>4</sub>	860
Al <sub>2</sub> Si <sub>2</sub> O <sub>5</sub> (OH) <sub>4</sub> (kaolinite)	3700, 3620, 1030, 1010
Fe <sub>2</sub> O <sub>3</sub>	560
BaSO <sub>4</sub>	1180, 1080, 630

Raman spectroscopy plays an important role in the identification of pigments in artwork. In *Raman microscopy*, a sample is irradiated with a laser beam and the scattered light is detected by a combination of an optical microscope and a Raman spectrometer. This relatively new technique is ideally suited to the analysis of pigments in manuscripts and artwork, because analysis takes place *in situ* without the need for scraping samples from the source material. In addition to identifying pigments, art historians gain insight into methods of conservation (e.g. do pigments degrade with time?) and are aided in authenticating an artwork. Over the centuries, a wide variety of artistic inorganic pigments has been used. Of those listed below, all occur naturally except for Prussian blue which was first manufactured in 1704, and viridian (Guignet's green) which has been manufactured since the mid-1800s.

Pigment	Chemical formula	Colour
Azurite	2CuCO <sub>3</sub> · Cu(OH) <sub>2</sub>	Blue
Lazurite (lapis lazuli)	Na <sub>8</sub> [Al <sub>6</sub> Si <sub>6</sub> O <sub>24</sub> ][S <sub>n</sub> ]	Blue
Prussian blue	Fe <sub>4</sub> [Fe(CN) <sub>6</sub> ] <sub>3</sub> · nH <sub>2</sub> O	Blue
Ochre	Fe <sub>2</sub> O <sub>3</sub> · H <sub>2</sub> O	Brown/orange
Malachite	CuCO <sub>3</sub> · Cu(OH) <sub>2</sub>	Green
Realgar	As <sub>4</sub> S <sub>4</sub>	Red
Orpiment	As <sub>2</sub> S <sub>3</sub>	Yellow
Barytes	BaSO <sub>4</sub>	White
Cadmium yellow	CdS	Yellow
Viridian	Cr <sub>2</sub> O <sub>3</sub> · 2H <sub>2</sub> O	Green
Litharge	PbO	Red
Vermilion (Cinnabar)	HgS	Red

## Further reading

- P. Buzzini and W. Stoecklein (2005) in *Encyclopedia of Analytical Science*, 2nd edn, eds. P. Worsfold, A. Townshend and C. Poole, Elsevier, Oxford, p. 453 – 'Paints, varnishes and lacquers'.
- R.J.H. Clark (1995) *Chem. Soc. Rev.*, vol. 24, p. 187 – 'Raman microscopy: application to the identification of pigments in medieval manuscripts'.
- R.J.H. Clark (2002) *C. R. Chimie*, vol. 5, p. 7 – 'Pigment identification by spectroscopic means: an arts/science interface'.
- R.J.H. Clark (2007) *Appl. Phys. A*, vol. 89, p. 833 – 'The scientific investigation of artwork and archaeological artefacts: Raman microscopy as a structural, analytical and forensic tool'.



Illustrations in medieval manuscripts used natural pigments from plants, animals and minerals.

for example, metal–ligand vibrational modes. A disadvantage of the Raman effect is its insensitivity because only a tiny percentage of the scattered radiation undergoes Raman scattering. This can be overcome by using the Fourier transform (FT) technique. For coloured compounds, sensitivity can be enhanced by using *resonance Raman spectroscopy*. This relies on using laser excitation wavelengths that coincide with wavelengths of absorptions in the electronic spectrum of a compound. This leads to resonance enhancement and an increase in the intensities of lines in the Raman spectrum.

An early success of Raman spectroscopy was in 1934 when Woodward reported the spectrum of mercury(I) nitrate. After the assignment of lines to the  $[\text{NO}_3]^-$  ion, a line at  $169\text{ cm}^{-1}$  remained which he assigned to the stretching mode of the Hg–Hg bond in  $[\text{Hg}_2]^{2+}$ . This was one of the first pieces of evidence for the dimeric nature of the ‘mercury(I) ion’. Resonance Raman spectroscopy is now used extensively for the investigation of coloured *d*-block metal complexes and for probing the active metal sites in metalloproteins. Application of Raman spectroscopy in pigment analysis is described in Box 4.1.

### Self-study exercises

1. The fundamental stretching vibration for  $\text{O}_2$  is at  $1580\text{ cm}^{-1}$ . Why would you use Raman, and not IR, spectroscopy to observe this absorption?
2. Each of the Raman and IR spectra of  $\text{O}_3$  exhibits three bands at  $1135$ ,  $1089$  and  $716\text{ cm}^{-1}$ . Explain why this provides evidence that  $\text{O}_3$  is a non-linear molecule.
3. Why is the fundamental stretching vibration of NO both Raman and IR active?

## 4.7 Electronic spectroscopy

*Electronic spectroscopy* is concerned with transitions of electrons between energy levels and covers both *absorption and emission spectroscopies*.

Electronic spectra arise from transitions of electrons between energy levels. Transitions from lower to higher energy levels produce absorption spectra, while those from higher to lower energy levels give rise to emission spectra. *Atomic* absorption and emission spectra were discussed in Sections 1.4 and 4.3. In this section, we describe the electronic spectra of *molecular species*.

### UV-VIS absorption spectroscopy

Molecular orbitals may be bonding ( $\sigma$  or  $\pi$ ), non-bonding ( $n$ ) or antibonding ( $\sigma^*$  or  $\pi^*$ ) in character. If a molecule

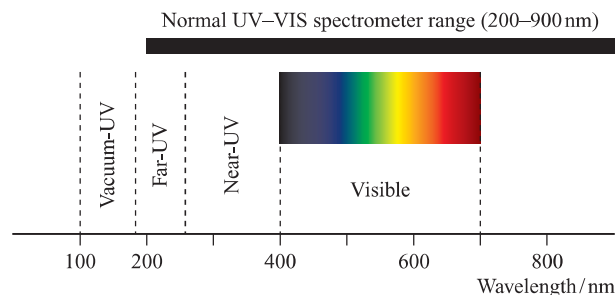


**Fig. 4.15** The ultraviolet (UV) and visible regions of the electromagnetic spectrum. Normal laboratory UV-VIS spectrophotometers operate between 200 and 900 nm.

absorbs an appropriate amount of energy, an electron in an occupied orbital is excited to an unoccupied or partially occupied orbital. The HOMO-LUMO separation (HOMO = highest occupied MO, LUMO = lowest occupied MO) is such that absorption spectra are usually observed in the ultraviolet (UV) or visible region of the electromagnetic spectrum (Fig. 4.15). The energies of MOs are quantized, and so an electronic transition is associated with a specific amount of energy,  $\Delta E$ . You might expect, therefore, that transitions from one electronic level to another in a molecular species would give rise to sharp spectral lines just as they do in atomic absorption spectra. However, molecular electronic absorption spectra usually consist of broad bands. Unlike atoms, molecules undergo vibrational and rotational motions and these are much slower than the absorption of a photon ( $\approx 10^{-18}\text{ s}$ ): the *Franck–Condon approximation* states that electronic transitions are very much faster than nuclear motion (because nuclear mass is far greater than electronic mass). Thus, an electronic transition is a ‘snapshot’ of the molecule in a particular vibrational and rotational state. Molecular orbital energies depend on the molecular geometry, and so a range of  $\Delta E$  values (corresponding to different vibrational and rotational states as the molecular geometry changes) is observed. The result is that broad bands are observed in electronic absorption spectra. Sharper spectra may be seen at low temperatures because less energy is available for molecular motion. A spectrum is also sharp if electronic transitions are localized on a single atomic centre, e.g. for compounds of the *f*-block metals (see Chapter 27).

### Types of absorption

The *notation for electronic transitions* shows the higher energy level first.

Emission: (high energy level)  $\rightarrow$  (low energy level),  
e.g.  $\pi^* \rightarrow \pi$ .

Absorption: (high energy level)  $\leftarrow$  (low energy level),  
e.g.  $\pi \leftarrow \pi^*$ .

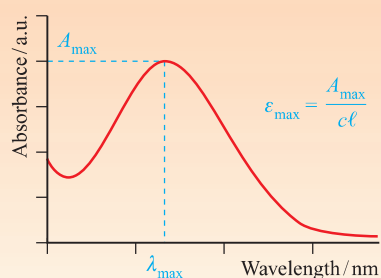
Electronic transitions giving rise to absorption spectra usually fall into the following categories:

- $\sigma^* \leftarrow \sigma$
- $\sigma^* \leftarrow n$
- $\pi^* \leftarrow \pi$
- $\pi^* \leftarrow n$
- charge transfer
- 'd-d'

The energies of most  $\sigma^* \leftarrow \sigma$  electronic transitions are too high (i.e. the wavelength is too short and occurs in the vacuum UV) to be observed using a normal UV-VIS spectrophotometer. The most intense absorptions in the 200–800 nm region (Fig. 4.15) typically arise from  $\pi^* \leftarrow \pi$ ,  $\sigma^* \leftarrow n$ ,  $\pi^* \leftarrow n$  or charge transfer transitions. Examples of the latter include metal-to-ligand and ligand-to-metal charge transfer in which electronic charge is transferred between metal and ligand orbitals (see Section 20.7).

### Absorbance and the Beer–Lambert law

Absorption bands in *molecular electronic spectra* are often broad, and may be described in terms of wavelength,  $\lambda_{\max}$  (nm), and the molar extinction (or absorption) coefficient,  $\epsilon_{\max}$  ( $\text{dm}^3 \text{mol}^{-1} \text{cm}^{-1}$ ):



A UV-VIS spectrophotometer typically records absorption spectra in the 200–800 nm range, and Fig. 4.16 shows a simplified diagram of the instrument. The light source consists of a deuterium lamp and a tungsten or halogen lamp which cover the UV and visible regions, respectively. The solution sample and a solvent reference are held in quartz cuvettes, usually with a 1 cm path length; the path length is the distance that

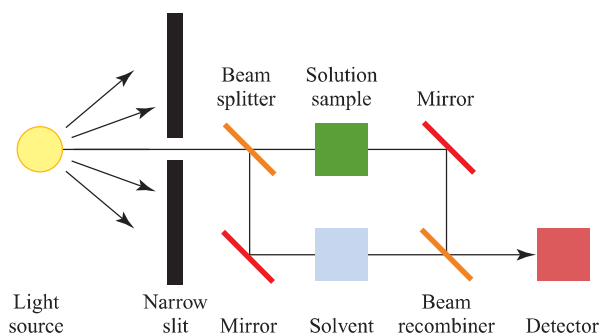


**Fig. 4.16** Schematic representation of a double beam UV-VIS spectrophotometer.

the radiation travels through the cuvette. The two cuvettes are placed between the source of radiation and a detector and are simultaneously irradiated. The detector monitors the radiation transmitted through the sample. The *transmittance*,  $T$ , of the sample is equal to the ratio of the intensity of the transmitted radiation ( $I$ ) to that of the incident radiation ( $I_0$ ), and eq. 4.9 shows how the absorbance,  $A$ , of the sample is determined. This is done automatically by the spectrophotometer and the data are output as an absorption spectrum. The whole range of wavelengths is detected simultaneously using a diode array detector (DAD), and the double beam set up allows the absorption spectrum of the solvent to be subtracted from that of the sample solution.

$$\text{Absorbance, } A = -\log T = -\log \frac{I}{I_0} \quad (4.9)$$

It can be seen from eq. 4.9 that absorbance is dimensionless. The absorbance is related to the concentration of the solution by the Beer–Lambert law (eq. 4.10) where  $\epsilon$  is the *molar extinction* (or *absorption*) *coefficient* of the dissolved sample. The extinction coefficient is a property of the compound and is independent of concentration for dilute solutions. Solution concentrations of the order of  $10^{-5} \text{mol dm}^{-3}$  are typical, giving absorbance values  $\leq 3$ .

$$\text{Absorbance, } A = \epsilon \times c \times \ell \quad (4.10)$$

Since the concentration,  $c$ , is measured in  $\text{mol dm}^{-3}$  and the cell path length,  $\ell$ , in cm, the units of  $\epsilon$  are  $\text{dm}^3 \text{mol}^{-1} \text{cm}^{-1}$ . Values of  $\epsilon_{\max}$  range from close to zero (a very weak absorption) to  $>10\,000 \text{dm}^3 \text{mol}^{-1} \text{cm}^{-1}$  (an intense absorption).

Electronic absorption spectra may be presented as plots of absorbance against wavenumber or wavelength, or as plots of  $\epsilon_{\max}$  against wavenumber or wavelength (Fig. 4.17).

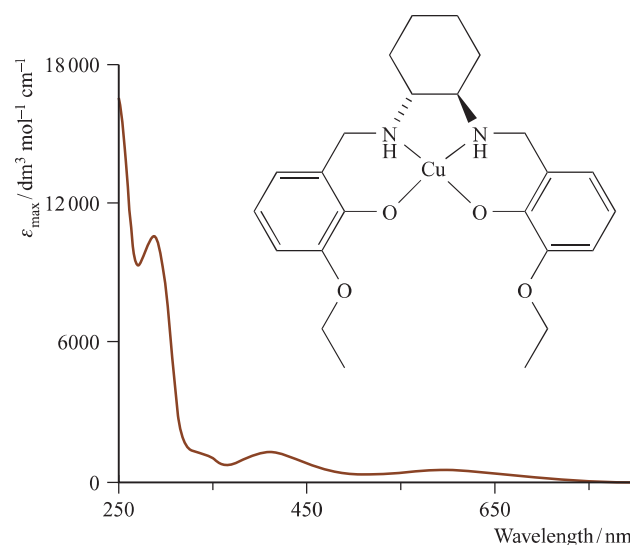


**Fig. 4.17** The UV-VIS spectrum of a  $\text{CH}_2\text{Cl}_2$  solution ( $8.8 \times 10^{-5} \text{mol dm}^{-3}$ ) of the copper(II) complex shown in the figure. Absorption maxima are at 252, 292, 347 (shoulder), 415 and 612 nm. [G. Zhang is thanked for recording the spectrum.]

The advantage of plotting  $\epsilon_{\max}$  rather than absorbance on the vertical axis is that spectra of different compounds can be readily compared with one another. Remember that  $\epsilon_{\max}$  is the characteristic of a given compound, whereas absorbance depends on both  $\epsilon_{\max}$  and concentration. The effect of plotting wavenumber,  $\bar{\nu}$  (in  $\text{cm}^{-1}$ ), rather than wavelength,  $\lambda$  (in nm), is to invert the spectrum; from eq. 4.11, it follows that  $400 \text{ nm} = 25\,000 \text{ cm}^{-1}$  and  $200 \text{ nm} = 50\,000 \text{ cm}^{-1}$ .

$$\bar{\nu} = \frac{1}{\lambda} \quad (4.11)$$

When comparing spectra, we are often interested in whether bands shift to lower or higher energy. A *bathochromic effect* or *red shift* is a shift in an absorption towards the red end of the spectrum (longer wavelengths, lower energy). A *hypsochromic effect* or *blue shift* is a shift in a band towards shorter wavelength (i.e. towards the blue end of the spectrum, higher energy).

#### Worked example 4.7 The UV-VIS spectrum of a copper(II) complex

Figure 4.17 shows the UV-VIS spectrum of a  $\text{CH}_2\text{Cl}_2$  solution of a copper(II) complex. A 1 cm cuvette was used for the measurement. Solutions of the complex are brown. The intense bands in the spectrum arise from ligand-based  $\pi^* \leftarrow \pi$  transitions. (a) Suggest how the  $\pi^* \leftarrow \pi$  transitions arise. (b) Which absorption or absorptions give rise to the observed colour of the complex in solution? (c) Calculate the absorbance that corresponds to the absorption at 292 nm.

(a) A  $\pi^* \leftarrow \pi$  transition can occur when an electron in a high-lying  $\pi$ -orbital is promoted to a low-lying, vacant  $\pi^*$ -orbital. The question states that the transitions are ‘ligand-based’. Therefore, the  $\pi$ - and  $\pi^*$ -orbitals must be associated with the arene rings.

(b) The visible region is 400–700 nm. The absorption at 612 nm is in the visible region, and that at 415 nm is partly in the visible region.

(c) Use the Beer–Lambert law:

$$\text{Absorbance, } A = \epsilon \times c \times \ell$$

$\ell$  is the path length = 1 cm

From Fig. 4.17, for the 292 nm absorption,  $\ell \approx 10\,000 \text{ dm}^3 \text{ mol}^{-1} \text{ cm}^{-1}$  and  $c = 8.8 \times 10^{-5} \text{ mol dm}^{-3}$  (see the figure caption). Therefore:

$$\begin{aligned} A &= (10\,000 \text{ dm}^3 \text{ mol}^{-1} \text{ cm}^{-1}) \times (8.8 \times 10^{-5} \text{ mol dm}^{-3}) \times (1 \text{ cm}) \\ &= 0.88 \text{ (dimensionless)} \end{aligned}$$

#### Self-study exercises

1. Show that  $625 \text{ nm} = 16\,000 \text{ cm}^{-1}$ .
2. The data in Fig. 4.17 are redrawn as a plot of  $\epsilon_{\max}$  against wavenumber. Sketch the appearance of this absorption spectrum, and include the scales.
3. Show that for the absorption at 415 nm in Fig. 4.17,  $A \approx 0.1$ .

Further details and applications of electronic absorption spectra and the assignment of absorptions are given in Sections 17.4 (charge transfer complexes of the halogens), 19.5 (colours of *d*-block metal complexes), 20.7 (electronic spectra of *d*-block metal complexes) and 27.4 (electronic spectra of *f*-block metal complexes).

#### Emission spectroscopy

The energy of the absorbed radiation corresponds to the energy of a transition from ground to an excited state. Decay of an excited state back to the ground state may take place by a radiative or non-radiative process. The spontaneous emission of radiation from an electronically excited species is called *luminescence* and this term covers both *fluorescence* and *phosphorescence*. A discussion of these phenomena requires an understanding of the electronic states of multi-electron systems, and we return to emission spectra in Section 20.8.

### 4.8 Nuclear magnetic resonance (NMR) spectroscopy

*Nuclear magnetic resonance (NMR) spectroscopy* is a resonance technique involving absorption of radiofrequency energy. The magnetic environment of a nucleus affects its resonance frequency and allows structural information to be deduced.

In this section we introduce one of the most important routine analytical tools of the synthetic chemist: nuclear magnetic resonance (NMR) spectroscopy. It is used to determine the relative numbers and environments of NMR active nuclei, and to investigate (usually in solution) the dynamic behaviour of molecular species. Although  $^1\text{H}$  and  $^{13}\text{C}$  NMR spectra are most commonly recorded, many more nuclei can be studied by this technique.

#### NMR active nuclei and isotope abundance

Many nuclei possess a property described as spin. The nuclear spin (nuclear angular momentum) is quantized and is described by the spin quantum number  $I$  which can have

values of  $0, \frac{1}{2}, 1, \frac{3}{2}, 2, \frac{5}{2}$  etc. If the value of  $I$  for a nucleus is zero, the nucleus is *NMR inactive*, e.g.  $^{12}\text{C}$ . For both  $^1\text{H}$  and  $^{13}\text{C}$ ,  $I = \frac{1}{2}$  and these nuclei are *NMR active*. Later, we introduce other NMR active nuclei with different (non-zero) values of  $I$ . In the absence of an applied magnetic field, the different nuclear spin states of a nucleus are degenerate. However, when a magnetic field is applied, they are split (become non-degenerate) and this allows nuclear spin transitions to occur when radiofrequency (RF) radiation is absorbed.

When a  $^1\text{H}$  NMR spectrum of a hydrogen-containing compound is recorded, virtually all the H atoms in the sample contribute to the observed spectrum; in a naturally occurring hydrogen sample, the abundance of  $^1\text{H}$  is 99.985%. The fact that only 1% of naturally occurring carbon is  $^{13}\text{C}$  means that if a  $^{13}\text{C}$  NMR spectrum of a carbon-containing compound is recorded, only 1% of the carbon atoms present are observed. This has important consequences with respect to  $^1\text{H}$ - $^{13}\text{C}$  coupling as we see below.

### Which nuclei are suitable for NMR spectroscopic studies?

A wide range of nuclei may be observed by NMR spectroscopy, but the inherent properties of some nuclei (e.g. a large quadrupole moment) may make their observation difficult. The main criterion is that the nucleus possesses a value of the nuclear spin quantum number  $I \geq \frac{1}{2}$  (Table 4.3). Secondly, it is advantageous (but not essential) for the nucleus to occur in significant abundance. Carbon-13 is an example of a low-abundance isotope which is, nevertheless, extensively used for NMR spectroscopy. Isotopic enrichment may be used to improve signal:noise ratios. A third requirement is that the nucleus possesses a relatively short *spin-relaxation time* ( $\tau_1$ ). This property depends not only on the nucleus itself but also on its molecular environment. Some elements exhibit more than one NMR active nucleus and the choice for experimental observation may depend upon the relative inherent values of  $\tau_1$ . For example,  $^6\text{Li}$  and  $^7\text{Li}$  are NMR active, but whereas  $\tau_1$  values for  $^7\text{Li}$

**Table 4.3** Properties of selected NMR active nuclei.

Nucleus	Natural abundance / %	$I$	Frequency of observation / MHz (referred to $^1\text{H}$ at 100 MHz) <sup>†</sup>	Chemical shift reference ( $\delta$ 0 ppm) <sup>‡</sup>
$^1\text{H}$	>99.9	$\frac{1}{2}$	100	$\text{SiMe}_4$
$^2\text{H}$	0.015	1	15.35	$\text{SiMe}_4$
$^7\text{Li}$	92.5	$\frac{3}{2}$	38.9	$\text{LiCl}$ (1 M in $\text{H}_2\text{O}$ )
$^{11}\text{B}$	80.1	$\frac{3}{2}$	32.1	$\text{F}_3\text{B}\cdot\text{OEt}_2$
$^{13}\text{C}$	1.1	$\frac{1}{2}$	25.1	$\text{SiMe}_4$
$^{17}\text{O}$	0.04	$\frac{5}{2}$	13.5	$\text{H}_2\text{O}$
$^{19}\text{F}$	100	$\frac{1}{2}$	94.0	$\text{CFCl}_3$
$^{23}\text{Na}$	100	$\frac{3}{2}$	26.45	$\text{NaCl}$ (1 M in $\text{H}_2\text{O}$ )
$^{27}\text{Al}$	100	$\frac{5}{2}$	26.1	$[\text{Al}(\text{OH}_2)_6]^{3+}$
$^{29}\text{Si}$	4.67	$\frac{1}{2}$	19.9	$\text{SiMe}_4$
$^{31}\text{P}$	100	$\frac{1}{2}$	40.5	$\text{H}_3\text{PO}_4$ (85%, aq)
$^{77}\text{Se}$	7.6	$\frac{1}{2}$	19.1	$\text{SeMe}_2$
$^{103}\text{Rh}$	100	$\frac{1}{2}$	3.2	Rh (metal)
$^{117}\text{Sn}$	7.68	$\frac{1}{2}$	35.6	$\text{SnMe}_4$
$^{119}\text{Sn}$	8.58	$\frac{1}{2}$	37.3	$\text{SnMe}_4$
$^{129}\text{Xe}$	26.4	$\frac{1}{2}$	27.7	$\text{XeOF}_4$
$^{183}\text{W}$	14.3	$\frac{1}{2}$	4.2	$\text{Na}_2\text{WO}_4$ (in $\text{D}_2\text{O}$ )
$^{195}\text{Pt}$	33.8	$\frac{1}{2}$	21.5	$\text{Na}_2[\text{PtCl}_6]$
$^{199}\text{Hg}$	16.84	$\frac{1}{2}$	17.9	$\text{HgMe}_2$

<sup>†</sup> The operating frequency of an instrument is defined by the field of the magnet and is designated by the frequency at which the  $^1\text{H}$  nuclei of  $\text{SiMe}_4$  resonate.

<sup>‡</sup> It is important to quote the reference when reporting NMR spectra since alternative references may be used.

are typically <3 s, those for  ${}^6\text{Li}$  lie in the range  $\approx 10\text{--}80$  s.  ${}^7\text{Li}$  is thus more appropriate for NMR spectroscopic observation and this choice is also favoured by the fact that  ${}^7\text{Li}$  is more abundant (92.5%) than  ${}^6\text{Li}$ . Another nuclear property that may militate against easy observation is the *quadrupole moment* arising from a non-spherical charge distribution of the nucleus and which is associated with values of  $I > \frac{1}{2}$ . Although the possession of a quadrupole moment leads to short values of  $\tau_1$ , it generally causes the signals in the NMR spectrum to be broad (e.g.  ${}^{11}\text{B}$ ). Signal broadening is also seen in the spectra of nuclei *attached* to nuclei with quadrupole moments, e.g. the  ${}^1\text{H}$  NMR spectrum of protons attached to  ${}^{11}\text{B}$ .

### Resonance frequencies and chemical shifts

A particular nucleus (e.g.  ${}^1\text{H}$ ,  ${}^{13}\text{C}$ ,  ${}^{31}\text{P}$ ) absorbs characteristic radiofrequencies, i.e. it *resonates* at a characteristic frequency. If an NMR spectrometer is tuned to a particular resonance frequency, *only* a selected NMR active nucleus is observed. For example, only  ${}^1\text{H}$  nuclei are observed if a 400 MHz spectrometer is tuned to 400 MHz, but if the same spectrometer is retuned to 162 MHz, only  ${}^{31}\text{P}$  nuclei are observed. This is analogous to tuning a radio and receiving only one station at a time.

In a  ${}^1\text{H}$  NMR experiment, protons in different chemical environments resonate at different frequencies. The same is true of, for example, non-equivalent  ${}^{13}\text{C}$  nuclei in a  ${}^{13}\text{C}$  NMR experiment, or non-equivalent  ${}^{19}\text{F}$  nuclei in a  ${}^{19}\text{F}$  NMR spectroscopic experiment, and so on. Each signal in an NMR spectrum is denoted by a *chemical shift value*,  $\delta$ , a value that is given relative to the signal observed for a specified reference compound (see below).

The parameter  $\delta$  is independent of the applied magnetic field strength and is defined as follows. The frequency difference ( $\Delta\nu$ ), in Hz, between the signal of interest and some defined reference frequency ( $\nu_0$ ) is divided by the absolute frequency of the reference signal (eq. 4.12):

$$\delta = \frac{(\nu - \nu_0)}{\nu_0} = \frac{\Delta\nu}{\nu_0} \quad (4.12)$$

Typically, this leads to a very small number. In order to obtain a more convenient number for  $\delta$ , it is usual to multiply the ratio in eq. 4.12 by  $10^6$ . This gives  $\delta$  in units of parts per million, ppm. The IUPAC<sup>†</sup> defines  $\delta$  according to eq. 4.12, but eq. 4.13 gives a method of calculating  $\delta$  in ppm.

$$\delta \text{ in ppm} = \frac{(\nu - \nu_0) \text{ in Hz}}{\nu_0 \text{ in MHz}} \quad (4.13)$$

It follows that you use eq. 4.14 to work out the frequency difference between two spectroscopic peaks in Hz when

the chemical shifts have been measured in ppm.

$$\Delta\nu \text{ (in Hz)} = (\text{spectrometer frequency in MHz}) \times \Delta\delta \text{ (in ppm)} \quad (4.14)$$

The standard reference (for which  $\delta$  is defined as 0 ppm) for both  ${}^1\text{H}$  and  ${}^{13}\text{C}$  NMR spectroscopies is tetramethylsilane,  $\text{SiMe}_4$  (TMS). When the NMR spectrum of a compound is recorded, signals due to particular nuclei are said to be *shifted* with respect to the standard reference signal. A shift to more positive  $\delta$  is ‘shifted to higher frequency’ and a shift to negative (or to less positive)  $\delta$  is ‘shifted to lower frequency’. Older terminology which may still be encountered relates a positive  $\delta$  value to a ‘downfield shift’ and a negative  $\delta$  value to an ‘upfield shift’.

### Chemical shift ranges

The range of chemical shifts over which NMR spectroscopic signals appear is dependent on the nucleus. The most commonly observed nucleus is  ${}^1\text{H}$  and, in organic compounds, a *spectral window* from  $\delta +15$  to 0 ppm usually encompasses most signals. In inorganic compounds, the window may have to be widened if, for example,  ${}^1\text{H}$  nuclei attached to metal centres are to be observed, or if signals are *paramagnetically shifted* (see Box 4.2). The chemical shift range for  ${}^{13}\text{C}$  NMR spectra is typically  $\delta +250$  to  $-50$  ppm, for  ${}^{31}\text{P}$  NMR spectra,  $\approx \delta +300$  to  $-300$  ppm, and for  ${}^{77}\text{Se}$  NMR spectra  $\approx \delta +2000$  to  $-1000$  ppm. Figure 4.18 illustrates the change in chemical shift for the  ${}^{31}\text{P}$  nucleus on going from triphenylphosphane to the corresponding oxide. Such a shift to higher frequency is typical when a tertiary phosphane ( $\text{R}_3\text{P}$ ) is oxidized, and also tends to occur when a phosphane ligand coordinates to a *d*-block metal centre.

### Solvents for solution studies

Samples for solution NMR spectroscopy are generally prepared using *deuterated solvents*. One reason for this is that, were non-deuterated solvents to be used (e.g.  $\text{CH}_3\text{Cl}$  in place of  $\text{CD}_3\text{Cl}$ ) for a  ${}^1\text{H}$  NMR spectroscopic experiment, the signals due to the solvent would ‘swamp’ those due to the sample. Deuterated solvents are commercially available, typically with >99.5%  ${}^2\text{H}$  label incorporated. The remaining unlabelled compound provides a useful *internal reference* signal in the  ${}^1\text{H}$  NMR spectrum of the sample under study.

### Integration of signals and signal broadening

Under normal conditions of measuring  ${}^1\text{H}$  NMR spectra, the ratio of the peak areas (*integrals*) of the signals in the spectrum is proportional to the number of nuclei giving rise to the signals. For example, in a  ${}^1\text{H}$  NMR spectrum of  $\text{HC}\equiv\text{CCH}_3$ , two signals with relative integrals 1:3 are observed. However, the integration of signals must be treated

<sup>†</sup> R.K. Harris, E.D. Becker, S.M. Cabral de Menezes, R. Goodfellow and P. Granger (2001) *Pure and Applied Chemistry*, vol. 73, p. 1795 – ‘NMR nomenclature. Nuclear spin properties and conventions for chemical shifts (IUPAC recommendations 2001)’.



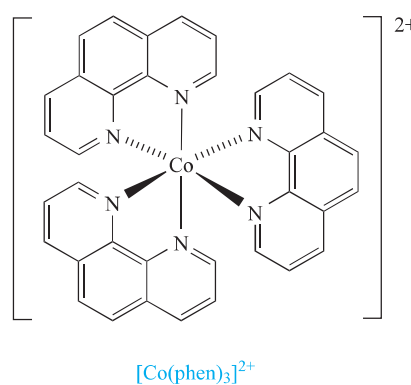
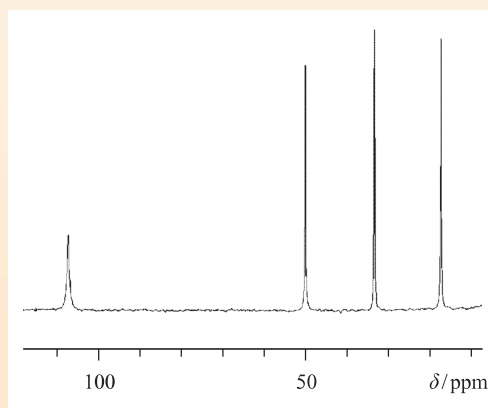
## THEORY

Box 4.2 Paramagnetically shifted  $^1\text{H}$  NMR spectra

The presence of a paramagnetic centre (i.e. a centre with one or more unpaired electrons) in a compound has significant consequences on the  $^1\text{H}$  NMR spectrum of the compound. Firstly, the *local magnetic field* at each  $^1\text{H}$  nucleus is affected. The energy difference between nuclear spin states – a consequence of applying an external magnetic field in an NMR experiment – arises from the interaction of the magnetic fields of the spinning nuclei with the applied field. However, the local field experienced by the nuclei is not the same as the applied field because electron pairs in the vicinity of the  $^1\text{H}$  nucleus generate small local magnetic fields. The local magnetic field is the sum of the applied and all the smaller fields. The latter depend on the chemical environment of the  $^1\text{H}$  nucleus. Typically, the differences in local magnetic fields for protons in different environments are small and, as a consequence, the chemical shift range over which the  $^1\text{H}$  NMR signals occur is not large. In a paramagnetic compound, there is an additional factor: a large, local magnetic field arising from the unpaired

electron or electrons on the paramagnetic centre. This contributes to the energy difference between nuclear spin states, and as a consequence, the chemical shift range for the  $^1\text{H}$  NMR signals is much larger than in a diamagnetic compound. The second effect that is observed in  $^1\text{H}$  NMR spectra of paramagnetic compounds is a broadening of the signals. This effect has its origins in a significant shortening of the excited state lifetime, i.e. the relaxation time is very short. In some cases, the broadening is so great that no well-resolved signals are observed.

An example of a paramagnetic centre is a  $\text{Co}^{2+}$  ion which, in an octahedral complex, has one or three unpaired electrons (see Chapter 20). The figure below shows the  $^1\text{H}$  NMR spectrum of the  $\text{Co}^{2+}$  complex  $[\text{Co}(\text{phen})_3]^{2+}$  (phen = 1,10-phenanthroline), the structure of which is shown below. There are four different aromatic proton environments in the complex, and the chemical shifts of the signals assigned to these  $^1\text{H}$  nuclei fall in the range  $\delta +110$  to  $+15$  ppm.



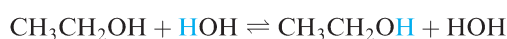
[Barbara Brisig is acknowledged for recording the spectrum shown above.]

## Further reading

I. Bertini and C. Luchinat (1996) *Coord. Chem. Rev.*, vol. 150 – ‘NMR of paramagnetic substances’.

with caution since the peak integral is dependent upon the *relaxation time* of the nucleus in question, i.e. the time taken for the nucleus to relax from an excited to ground state during the NMR spectroscopic experiment. (Further details of this phenomenon may be found in references cited at the end of this chapter.) One particular problem is the relative integrals of signals in a  $^{13}\text{C}$  NMR spectrum.

In some cases, signals may be broadened and this can affect the measurement of the relative integrals of signals. For example, signals arising from protons attached to N are broadened due to *quadrupolar relaxation* by  $^{14}\text{N}$  ( $I = 1$ ). Exchange with solvent protons also causes broadening, e.g.:

Homonuclear spin–spin coupling:  $^1\text{H}$ – $^1\text{H}$ 

A  $^1\text{H}$  nucleus ( $I = \frac{1}{2}$ ) may be in one of two spin states ( $m_I = +\frac{1}{2}$ ,  $m_I = -\frac{1}{2}$ ) and the energy difference between the spin states depends on the applied magnetic field of the NMR spectrometer. Consider a system in which there are two magnetically non-equivalent  $^1\text{H}$  nuclei,  $\text{H}_\text{A}$  and  $\text{H}_\text{B}$ . There are two possible situations:

- The local magnetic field generated by the spin of  $\text{H}_\text{A}$  is *not* detected by  $\text{H}_\text{B}$ ; the  $^1\text{H}$  NMR spectrum consists of two resonances, each a *singlet* because there is *no coupling* between the two  $^1\text{H}$  nuclei.
- $\text{H}_\text{A}$  is affected by the magnetic fields associated with  $\text{H}_\text{B}$ ; the  $^1\text{H}$  NMR signal for  $\text{H}_\text{A}$  is *split into two equal lines*

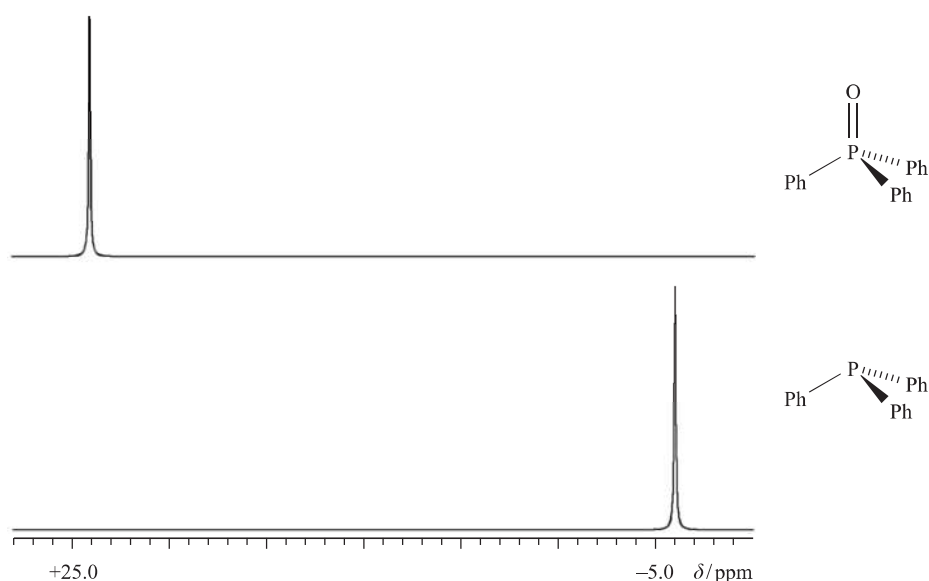


**Fig. 4.18** The 162 MHz  $^{31}\text{P}$  NMR spectra of  $\text{PPh}_3$  and  $\text{O}=\text{PPh}_3$ . A shift to more positive  $\delta$  (higher frequency) generally accompanies the oxidation of a tertiary phosphane and recording the  $^{31}\text{P}$  NMR spectrum of a phosphane before use in the laboratory is an easy way of checking the purity of phosphanes which are readily oxidized in air.

depending on which of the two spin states of  $\text{H}_\text{B}$  (equal probabilities) it ‘sees’. Similarly, the signal for  $\text{H}_\text{B}$  is composed of two equal lines. Protons  $\text{H}_\text{A}$  and  $\text{H}_\text{B}$  *couple* with each other and the spectrum consists of two *doublets*.

The separation between the two lines in each of the doublets described above must be equal, and this splitting is called the *coupling constant*,  $J$ , and is measured in hertz (Hz). In general, coupling to one proton gives a doublet, to two equivalent protons gives a triplet, to three equivalent protons gives a quartet, and so on. The relative intensities of the lines in the *multiplet* are given by a binomial distribution, readily determined using a Pascal’s triangle:

1				← singlet		
	1	1		← doublet		
	1	2	1	← triplet		
	1	3	3	1	← quartet	
	1	4	6	4	1	← quintet

The number and spins of the *attached nuclei* determine the **multiplicity** (number of lines) and pattern of the NMR spectroscopic signal of the observed nucleus. The coupling constant between nuclei X and Y is denoted as  $J_{\text{XY}}$  and is measured in Hz.

In general the multiplicity of an NMR spectroscopic signal can be determined using eq. 4.15 where the nucleus being observed is coupling to  $n$  equivalent nuclei with quantum number  $I$ .

$$\text{Multiplicity (number of lines)} = 2nI + 1 \quad (4.15)$$

### Self-study exercise

The 100 MHz  $^1\text{H}$  NMR spectrum of butanone is shown in Fig. 4.19 and consists of a quartet, a singlet and a triplet. The coupling constants  $J$  for the triplet and quartet are equal. Account for the observed spectrum.

### Heteronuclear spin–spin coupling: $^{13}\text{C}$ – $^1\text{H}$

Each of the nuclei  $^1\text{H}$  and  $^{13}\text{C}$  has a magnetic spin quantum number  $I = \frac{1}{2}$ , and when  $^{13}\text{C}$  and  $^1\text{H}$  nuclei are in close proximity, they can couple. However, in molecules containing a natural isotopic distribution of carbon atoms, only 1% are  $^{13}\text{C}$  nuclei. From a statistical consideration, it follows that in a  $^1\text{H}$  NMR spectrum of, for example, acetone,  $^{13}\text{C}$ – $^1\text{H}$  coupling is *not* observed, although it is observed in the  $^{13}\text{C}$  NMR spectrum of the *same* sample. The  $^{13}\text{C}$  NMR spectrum of acetone exhibits a singlet due to the  $\text{C}=\text{O}$  carbon atom, and a quartet due to the two equivalent methyl  $^{13}\text{C}$  nuclei.

### Self-study exercise

Why do you not observe  $^{13}\text{C}$ – $^{13}\text{C}$  coupling in the  $^{13}\text{C}$  NMR spectrum of acetone?

The following case studies illustrate the use of NMR spectroscopy to study compounds containing spin-active nuclei other than  $^1\text{H}$  and  $^{13}\text{C}$ .



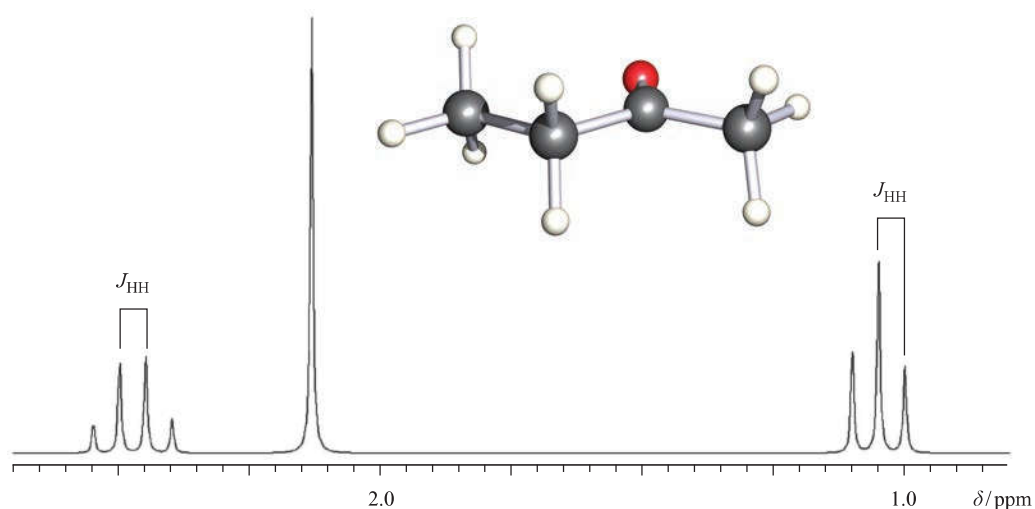


**Fig. 4.19** The 100 MHz NMR spectrum of butanone. In the structure, the colour code is: C, grey; H, white; O, red.

## Case studies

### Case study 1: $^{31}\text{P}$ NMR spectrum of $[\text{PF}_6]^-$

The  $^{31}\text{P}$  NMR spectrum of a salt containing the octahedral  $[\text{PF}_6]^-$  ion exhibits a binomial septet (Fig. 4.20) consistent with six equivalent  $^{19}\text{F}$  nuclei ( $I = \frac{1}{2}$ ) attached to the central  $^{31}\text{P}$  centre. The large value of  $J_{\text{PF}}$  708 Hz is typical of  $^{31}\text{P}$ – $^{19}\text{F}$  coupling constants for *directly attached* nuclei; the magnitudes of coupling constants usually diminish with nuclear separation, but a consequence of large values for directly attached nuclei is that *long-range couplings* may be observed (see Case study 2).

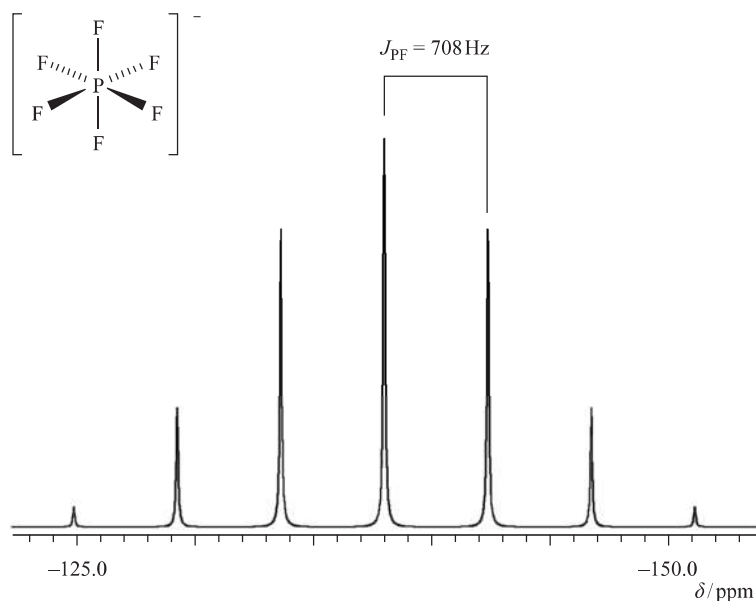
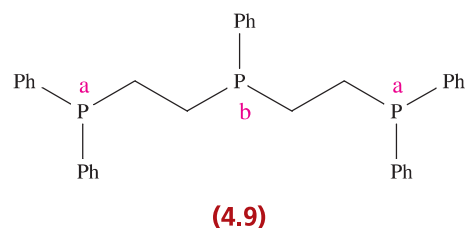


**Fig. 4.20** The 162 MHz  $^{31}\text{P}$  NMR spectrum of a salt of  $[\text{PF}_6]^-$  consists of a binomial septet. The value of  $J_{\text{PF}}$  can be measured between any pair of adjacent lines in the signal.

### Case study 2: $^{31}\text{P}$ NMR spectrum of $\text{Ph}_2\text{PCH}_2\text{CH}_2\text{P}(\text{Ph})\text{CH}_2\text{CH}_2\text{PPh}_2$



Structure **4.9** shows that  $\text{Ph}_2\text{PCH}_2\text{CH}_2\text{P}(\text{Ph})\text{CH}_2\text{CH}_2\text{PPh}_2$  contains two phosphorus environments, labelled a and b.

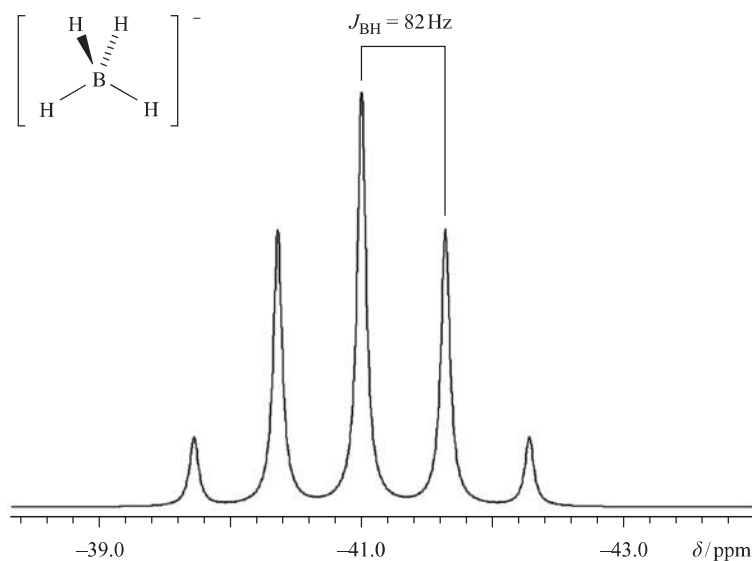


**Fig. 4.21** The 128 MHz  $^{11}\text{B}$  NMR spectrum of a solution of  $\text{NaBH}_4$  in  $\text{CD}_3\text{C}(\text{O})\text{CD}_3$ . The value of  $J_{\text{BH}}$  can be measured between any pair of adjacent lines in the signal.

The  $^{31}\text{P}$  NMR spectrum exhibits two signals with an integral ratio of 1:2. For directly attached inequivalent phosphorus atoms, values of  $J_{\text{PP}}$  are typically 450–600 Hz; in compound 4.9, *long-range coupling* between non-equivalent  $^{31}\text{P}$  nuclei is observed. The signals due to atoms  $\text{P}_b$  and  $\text{P}_a$  are a triplet and doublet respectively; values of  $J_{\text{PP}}$  (29 Hz) measured from the two signals are necessarily equal. Additionally, coupling between the  $^{31}\text{P}$  and closest  $^1\text{H}$  nuclei may be observed. Two types of heteronuclear NMR spectra are routinely recorded: one in which coupling to protons is observed and one in which protons are instrumentally *decoupled* from the observed nucleus.

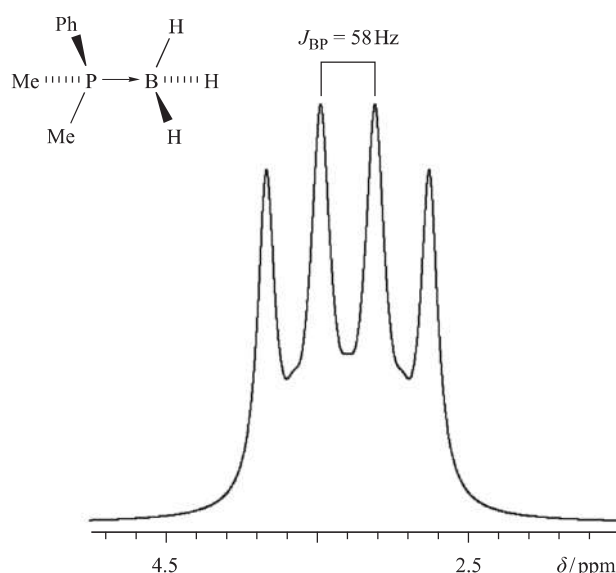
The notation  $^{31}\text{P}\{^1\text{H}\}$  means *proton-decoupled*  $^{31}\text{P}$ ; corresponding notations are used for other proton-decoupling.

### Case study 3: $^{11}\text{B}$ NMR spectrum of $[\text{BH}_4]^-$

The  $^{11}\text{B}$  NMR spectrum of  $\text{Na}[\text{BH}_4]$  is shown in Fig. 4.21. The 1:4:6:4:1 pattern of signal integrals corresponds to the binomial quintet expected for four equivalent  $^1\text{H}$  nuclei coupling to  $^{11}\text{B}$ . Although  $I = \frac{3}{2}$  for  $^{11}\text{B}$ , it is the  $I = \frac{1}{2}$  of the attached protons that determines the nature of the signal in the  $^{11}\text{B}$  NMR spectrum of  $[\text{BH}_4]^-$ .

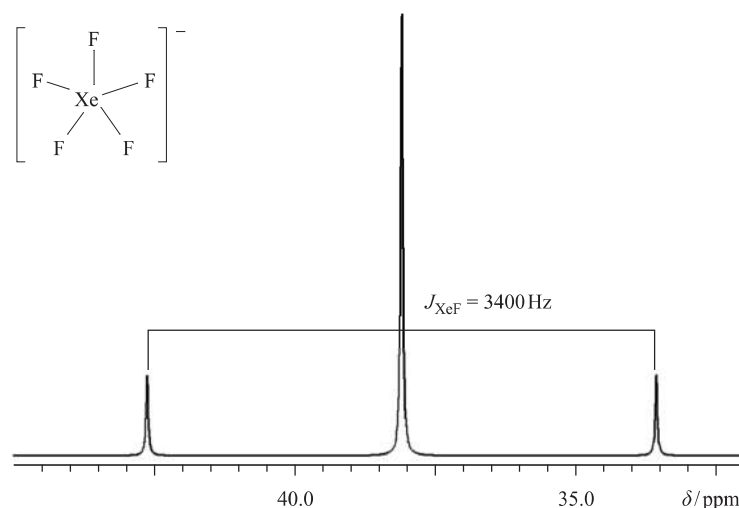
### Case study 4: $^{31}\text{P}\{^1\text{H}\}$ NMR spectrum of $\text{PhMe}_2\text{P}\cdot\text{BH}_3$

Figure 4.22 shows the structure of the adduct  $\text{PhMe}_2\text{P}\cdot\text{BH}_3$  and its  $^{31}\text{P}\{^1\text{H}\}$  NMR spectrum. The signal is a four-line multiplet (but *not* a binomial quartet) and arises primarily from coupling between  $^{31}\text{P}$  and  $^{11}\text{B}$  nuclei. For  $^{11}\text{B}$ ,  $I = \frac{3}{2}$ ;



**Fig. 4.22** The 162 MHz  $^{31}\text{P}\{^1\text{H}\}$  NMR spectrum of the adduct  $\text{PhMe}_2\text{P}\cdot\text{BH}_3$ . The four-line pattern is *not* a binomial quartet but an approximate 1:1:1:1 multiplet.

this means there are four spin states with values  $+\frac{3}{2}$ ,  $+\frac{1}{2}$ ,  $-\frac{1}{2}$  and  $-\frac{3}{2}$ . There is an *equal probability* that the  $^{31}\text{P}$  nucleus will ‘see’ the  $^{11}\text{B}$  nucleus in each of the four spin states, and this gives rise to the  $^{31}\text{P}$  signal being split into four equal intensity lines: a 1:1:1:1 multiplet. The observed signal is complicated by the fact that  $^{11}\text{B}$  has an 80% abundance and the second isotope,  $^{10}\text{B}$ , is also NMR active ( $I = 3$ ). It too couples to the  $^{31}\text{P}$  nucleus, giving a seven-line multiplet (1:1:1:1:1:1:1), but the value of  $J_{^{31}\text{P}^{10}\text{B}}$  is smaller than  $J_{^{31}\text{P}^{11}\text{B}}$ . The result is two overlapping signals, but the dominant feature is the 1:1:1:1 multiplet,



**Fig. 4.23** The 376 MHz  $^{19}\text{F}$  NMR spectrum of  $[\text{XeF}_5]^-$ , simulated using literature parameters. The isotopic abundance of  $^{129}\text{Xe}$  is 26.4%; the centre of the doublet coincides with the position of the singlet. (K.O. Christie *et al.* (1991) *J. Am. Chem. Soc.*, vol. 113, p. 3351.)

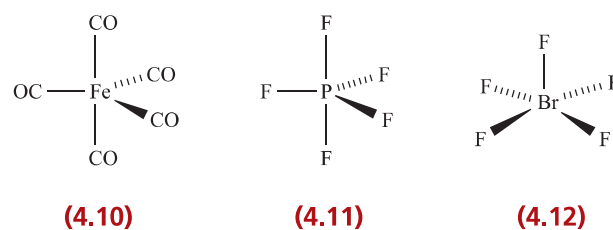
the signal shape of which is affected by both the underlying seven-line multiplet and relaxation effects.

#### Case study 5: $^{19}\text{F}$ NMR spectrum of $[\text{XeF}_5]^-$

The planar  $[\text{XeF}_5]^-$  ion contains five equivalent F atoms (see worked example 2.7). Both the  $^{19}\text{F}$  and  $^{129}\text{Xe}$  nuclei are NMR active:  $^{19}\text{F}$ ,  $I = \frac{1}{2}$ , 100% abundance;  $^{129}\text{Xe}$ ,  $I = \frac{1}{2}$ , 26.4%. The  $^{19}\text{F}$  NMR spectrum of  $[\text{XeF}_5]^-$  is shown in Fig. 4.23. The chemical equivalence of the  $^{19}\text{F}$  nuclei gives rise to one signal. However, 26.4% of the F centres are attached to  $^{129}\text{Xe}$ , while the remainder are bonded to other Xe nuclei. The spectrum can be interpreted in terms of a singlet (the central line) due to 73.6% of the  $^{19}\text{F}$  nuclei, plus an overlapping doublet due to the 26.4% of the  $^{19}\text{F}$  nuclei that couple to  $^{129}\text{Xe}$ . The centre of the doublet coincides with the position of the singlet because *all* the  $^{19}\text{F}$  nuclei resonate at the same frequency. The two side peaks in Fig. 4.23 are called *satellite peaks*.

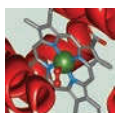
#### Stereochemically non-rigid species

The NMR spectroscopic examples discussed so far have assumed that, with the exception of free rotation about single bonds, the molecule or ion is static in solution. For the majority of organic and inorganic species, this assumption is valid, but the possibility of *stereochemical non-rigidity (fluxionality) on the NMR spectroscopic timescale* must be considered. Five-coordinate species such as  $\text{Fe}(\text{CO})_5$ , **4.10**,  $\text{PF}_5$ , **4.11**, and  $\text{BrF}_5$ , **4.12**, constitute one group of compounds for which the activation barrier for dynamic behaviour in solution is relatively low, and exchange of substituent positions is facile.



The inclusion of the qualifier ‘on the NMR spectroscopic timescale’ is important. The timescale<sup>†</sup> of the NMR spectroscopic technique ( $10^{-1}$  to  $10^{-5}$  s, depending on the observed nucleus) is relatively long, and is significantly longer than that of IR spectroscopy;  $\text{Fe}(\text{CO})_5$  appears static on the IR spectroscopic timescale, but dynamic within the timescale of a  $^{13}\text{C}$  NMR spectroscopic experiment. Lowering the temperature slows down the dynamic behaviour, and *may* make it slower than the spectroscopic timescale. However, some fluxional processes have very low energy barriers. Even at 103 K, the axial and equatorial CO groups in  $\text{Fe}(\text{CO})_5$  exchange positions and the  $^{13}\text{C}$  NMR spectrum consists of one signal corresponding to the average  $^{13}\text{C}$  environment. On the other hand, the room temperature solution  $^{19}\text{F}$  NMR spectrum of  $\text{BrF}_5$  exhibits a doublet and a binomial quintet (due to  $^{19}\text{F}$ – $^{19}\text{F}$  coupling) with relative integrals of 4:1, and this is consistent with structure **4.12**. Above 450 K, one signal is observed, indicating that the five F atoms are equivalent on the NMR timescale, i.e. the  $\text{BrF}_5$  molecule is fluxional. On going from the low to high temperature limit, the two signals *coalesce* to give a single resonance.

<sup>†</sup> See: A.B.P. Lever (2003) in *Comprehensive Coordination Chemistry II*, eds J.A. McCleverty and T.J. Meyer, Elsevier, Oxford, vol. 2, p. 435 – ‘Notes on time frames’.



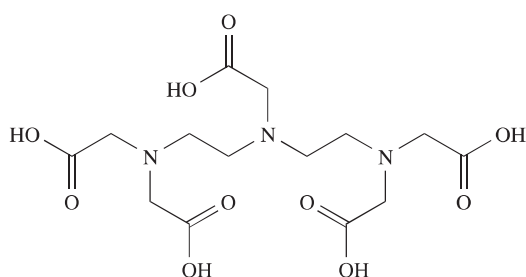
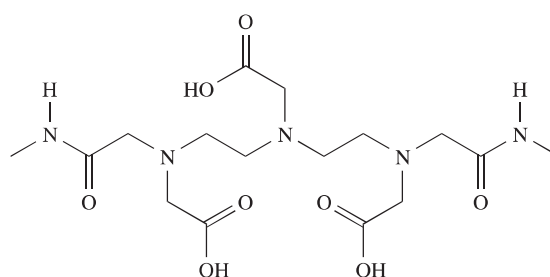
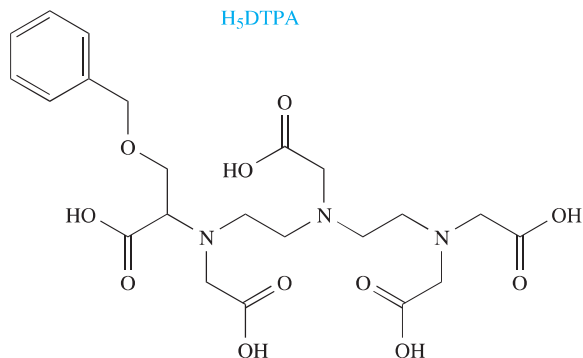
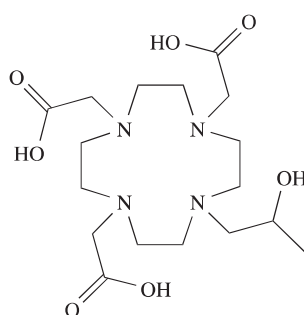
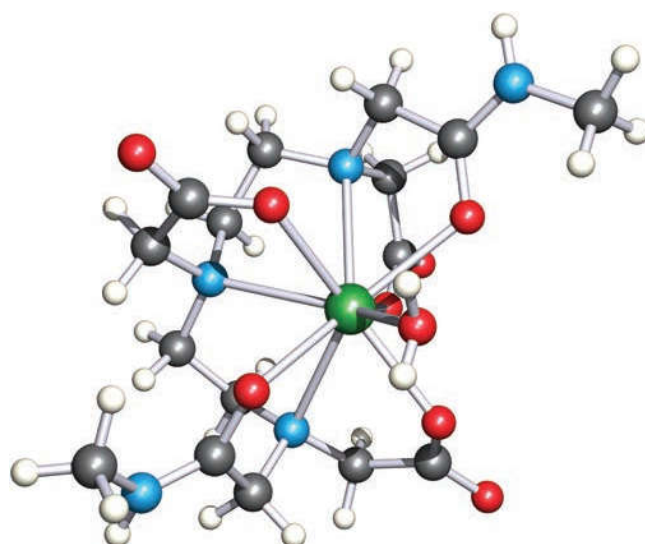
## BIOLOGY AND MEDICINE



## Box 4.3 Magnetic resonance imaging (MRI)

Magnetic resonance imaging (MRI) is a rapidly expanding clinical technique to obtain an image of, for example, a human organ or tumour. In 2003, approximately 10 000 MRI units performed  $\approx 75$  million scans worldwide and since then these numbers have risen dramatically. The impact of this non-invasive technique on clinical medicine was recognized by the award of the 2003 Nobel Prize in Medicine to Paul Lauterbur and Peter Mansfield. The MRI image is generated from information obtained from the  $^1\text{H}$  NMR spectroscopic signals of water. The signal intensity depends upon the proton relaxation times and the concentration of water. The relaxation times can be altered, and the image enhanced, by using *MRI contrast agents*. Coordination complexes containing paramagnetic  $\text{Gd}^{3+}$ ,  $\text{Fe}^{3+}$  or  $\text{Mn}^{2+}$  are potentially suitable as contrast agents and, of these, complexes containing the  $\text{Gd}^{3+}$  ion have so far proved to be especially useful. As a free ion,  $\text{Gd}^{3+}$  is extremely toxic and, therefore, to minimize side-effects in patients,  $\text{Gd}^{3+}$  must be

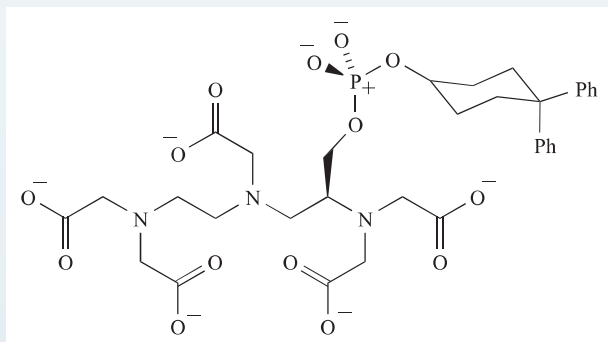
introduced in the form of a complex that will not dissociate in the body. Chelating ligands are particularly suitable (see Chapter 7 for a discussion of stability constants). Ligands such as  $[\text{DTPA}]^{5-}$  (the conjugate base of  $\text{H}_5\text{DTPA}$ , drawn below) possess both *O*- and *N*-donor atoms, and form gadolinium(III) complexes in which the  $\text{Gd}^{3+}$  ion exhibits a high coordination number (see Chapter 19). For example, in  $[\text{Gd}(\text{DTPA})(\text{OH}_2)]^{2-}$ , the  $\text{Gd}^{3+}$  centre is 9-coordinate. The complex  $[\text{Gd}(\text{DTPA})(\text{OH}_2)]^{2-}$  was approved in 1988 for medical use as an MRI contrast agent and is used under the brand name of Magnevist. Two other approved contrast agents are  $[\text{Gd}(\text{DTPA-BMA})(\text{OH}_2)]$  (trade name Omniscan) and  $[\text{Gd}(\text{HP-DO3A})(\text{OH}_2)]$  (ProHance). The solid state structure of  $[\text{Gd}(\text{DTPA-BMA})(\text{OH}_2)]$  is shown below, and confirms a 9-coordinate metal centre. Magnevist, Omniscan and ProHance are classed as *extra-cellular* contrast agents, meaning that, once injected into a patient, they are distributed non-specifically

 $\text{H}_5\text{DTPA}$  $\text{H}_3\text{DTPA-BMA}$  $\text{H}_3\text{BOPTA}$  $\text{H}_3\text{HP-DO3A}$ 

The molecular structure of  $[\text{Gd}(\text{DTPA-BMA})(\text{OH}_2)]$  (Omniscan) determined by X-ray diffraction [A. Aukrust *et al.* (2001) *Org. Proc. Res. Develop.*, vol. 5, p. 361]. Colour code: Gd, green; N, blue; O, red; C, grey; H, white.

throughout the plasma and extra-cellular fluids in the body. Clearance through the kidneys occurs rapidly, the elimination half-life being  $\approx 90$  minutes.

Two other types of MRI contrast agents are *hepatobiliary* and *blood pool* agents. Hepatocytes are the main cell types present in the liver, and a hepatobiliary contrast agent is designed to target the liver, and then be excreted through the bile ducts, gall bladder and intestines. The gadolinium(III) complex  $[\text{Gd}(\text{BOP-TA})(\text{OH}_2)]^{2-}$  (brand name Multihance) is an approved hepatobiliary contrast agent.  $[\text{BOPTA}]^{5-}$  is the conjugate base of  $\text{H}_5\text{BOPTA}$ , the structure of which is shown opposite.  $[\text{BOPTA}]^{5-}$  is structurally similar to  $[\text{DTPA}]^{5-}$ , differing only in the presence of the pendant hydrophobic group which is responsible for making Multihance cell-specific. Blood pool contrast agents remain intravascular for a significant period of time. In 2005, MS-325 (trade name Vasovist) received approval by the European Commission and US Food and Drug Administration for medical use. The chelating ligand in Vasovist is structurally related to  $[\text{DTPA}]^{5-}$ , but carries a phosphate-containing group. The structure of the ligand,  $\text{L}^{6-}$ , in Vasovist is shown below. Vasovist itself is the sodium salt  $\text{Na}_3[\text{GdL}(\text{OH}_2)]$ , and the ligand binds  $\text{Gd}^{3+}$  in the same environment as in Omniscan (structure opposite).



The introduction of the diphenylcyclohexylphosphate group increases the hydrophilic character of the contrast agent and this allows Vasovist to bind reversibly to human serum albumin. This results in enhanced images of vascular structures. This particular type of MR imaging is known as *magnetic resonance angiography* (MRA) and is a significant development in imaging techniques. Prior to the availability of non-invasive MRA, vascular structures could only be imaged by conventional angiography, an invasive procedure that involves injection into the blood of a substance that absorbs X-rays. An angiogram is then obtained by exposing the patient to X-rays.

A second class of MRI contrast agents consists of iron oxide nanoparticles (magnetite,  $\text{Fe}_3\text{O}_4$ , and maghemite,  $\gamma\text{-Fe}_2\text{O}_3$ ). These paramagnetic materials are able to shorten proton relaxation times. They are categorized according to particle size: superparamagnetic iron oxide (SPIO) nanoparticles have diameters of 50 nm to hundreds of nanometres, whereas ultrasmall superparamagnetic iron oxide (USPIO) nanoparticles are  $< 50$  nm in diameter. The nanoparticles can be prepared by a number of routes, the simplest of which involves precipitation from aqueous solution under carefully controlled pH conditions starting with a mixture of iron(II) and iron(III) salts (e.g. chlorides):



The iron oxide nanoparticles are coated in polysaccharides (dextran or carboxydextran) to make them biocompatible and are administered to patients as aqueous colloids. Clinical MRI contrast agents of this type include Feridex, Resovist and Combidex which are selectively taken up by the liver, spleen and bone marrow. The synthesis and potential applications in MRI of related iron oxide nanoparticles is currently an active area of research.



Doctors with a patient entering an MRI scanner.

Dependence upon the observation of proton signals in some organs (e.g. lungs) presents problems with respect to MRI. The use of  $^{129}\text{Xe}$  magnetic imaging has been tested as a means of overcoming some of the difficulties associated with proton observation. Under the right conditions, gaseous  $^{129}\text{Xe}$  taken into mouse lungs allows excellent images to be observed.

### Further reading

- A. Accardo, D. Tesauro, L. Aloj, C. Pedone and G. Morelli (2009) *Chem. Rev.*, vol. 253, p. 2193 – ‘Supramolecular aggregates containing lipophilic Gd(III) complexes as contrast agents in MRI’.
- P. Hermann, J. Kotek, V. Kubiček and I. Lukeš (2008) *Dalton Trans.*, p. 3027 – ‘Gadolinium(III) complexes as MRI contrast agents: ligand design and properties of the complexes’.
- S. Laurent, D. Forge, M. Port, A. Roch, C. Robic, L. Vander Elst and R.N. Muller (2008) *Chem. Rev.*, vol. 108, p. 2064 – ‘Magnetic iron oxide nanoparticles: synthesis, stabilization, vectorization, physicochemical characterizations and biological applications’.
- H.B. Na and T. Hyeon (2009) *J. Mater. Chem.*, vol. 19, p. 6267 – ‘Nanostructured T1 MRI contrast agents’.
- H.B. Na, I.C. Song and T. Hyeon (2009) *Adv. Mater.*, vol. 21, p. 2133 – ‘Inorganic nanoparticles for MRI contrast agents’.
- E.L. Que and C.J. Chang (2010) *Chem. Soc. Rev.*, vol. 39, p. 51 – ‘Responsive magnetic resonance imaging contrast agents as chemical sensors for metals in biology and medicine’.
- O. Taratula and I.J. Dmochowski (2010) *Curr. Opin. Chem. Biol.*, vol. 14, p. 97 – ‘Functionalized  $^{129}\text{Xe}$  contrast agents for magnetic resonance imaging’.

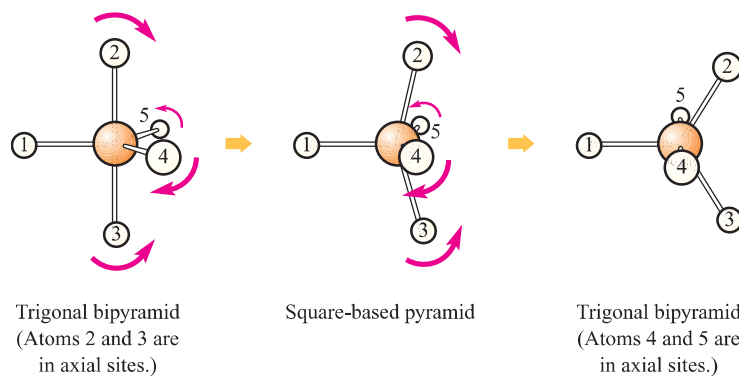


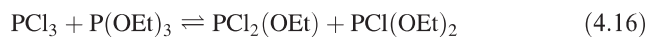
**Fig. 4.24** Berry pseudo-rotation interconverts one trigonal bipyramidal structure into another via a square-based pyramidal transition state. The numbering scheme illustrates that axial and equatorial sites in the trigonal bipyramid are interchanged.

The usual dynamic process in which 5-coordinate species are involved in solution is *Berry pseudo-rotation*.<sup>†</sup> Although ligand–ligand repulsions are minimized in a trigonal bipyramidal arrangement, only a small amount of energy is needed to convert it into a square-based pyramid. The interconversion involves small perturbations of the bond angles subtended at the central atom, and continued repetition of the process results in each substituent ‘visiting’ both equatorial and axial sites in the trigonal bipyramidal structure (Fig. 4.24).

### Exchange processes in solution

A number of hydrated cations in aqueous solution undergo exchange with the solvent at rates slow enough to be observed on the NMR spectroscopic timescale by using <sup>17</sup>O isotopic labelling; <sup>17</sup>O has  $I = \frac{5}{2}$ , while both <sup>16</sup>O and <sup>18</sup>O are NMR inactive. Different chemical shifts are observed for the <sup>17</sup>O nuclei in bulk and coordinated water, and from the signal intensity ratios, hydration numbers can be obtained. For example, Al<sup>3+</sup> has been shown to be present as [Al(OH<sub>2</sub>)<sub>6</sub>]<sup>3+</sup>.

Reactions such as that in eq. 4.16 are known as *redistribution reactions*.



A **redistribution reaction** is one in which substituents exchange between species but the types and numbers of each type of bond remain the same.

The position of equilibrium can be followed by using <sup>31</sup>P NMR spectroscopy, since each of the four species has a characteristic chemical shift. Rate data are obtained by following the variation in relative signal integrals with

<sup>†</sup> A discussion that goes beyond Berry pseudo-rotation and considers the ‘lever mechanism’ in SF<sub>4</sub> (based on a trigonal bipyramidal structure with an equatorial site occupied by a lone pair of electrons) and related species is: M. Mauksch and P. von R. Schleyer (2001) *Inorg. Chem.*, vol. 40, p. 1756.

time, and equilibrium constants (and hence values of  $\Delta G^\circ$  since  $\Delta G^\circ = -RT \ln K$ ) can be found from the relative signal integrals when no further change takes place (i.e. equilibrium has been established). By determining  $\Delta G^\circ$  at different temperatures, values of  $\Delta H^\circ$  and  $\Delta S^\circ$  can be found using eqs. 4.17 and 4.18.

$$\Delta G^\circ = \Delta H^\circ - T\Delta S^\circ \quad (4.17)$$

$$\frac{d \ln K}{dT} = \frac{\Delta H^\circ}{RT^2} \quad (4.18)$$

Values of  $\Delta H^\circ$  for these types of reactions are almost zero, the redistribution of the groups being driven by an increase in the entropy of the system.

## 4.9 Electron paramagnetic resonance (EPR) spectroscopy

### What is EPR spectroscopy?

*Electron paramagnetic resonance (EPR) spectroscopy* is a resonance technique involving microwave-induced transitions between magnetic energy levels of electrons which possess a net spin and orbital angular momentum. An EPR spectrum provides information about **paramagnetic species**.

Electron paramagnetic resonance (EPR) spectroscopy (also called electron spin resonance (ESR) spectroscopy), is used to study paramagnetic species with one or more unpaired electrons, e.g. free radicals, diradicals, metal complexes containing paramagnetic metal centres, defects in semiconductors and irradiation effects in solids. While diamagnetic materials are EPR silent, paramagnetic species always exhibit an EPR spectrum. This consists of one or more lines, depending on the interactions between the unpaired electron (which acts as a ‘probe’) and the molecular framework in which it is located. Analysis of the shape of the EPR spectrum (the number and positions of EPR lines, their intensities and line widths) provides information

about the paramagnetic species, e.g. the structure of a free radical, characterization of the coordination sphere around the metal centre in a coordination complex, or the presence of multiple paramagnetic species.

EPR spectroscopic measurements can be performed at high, room or low ( $\geq 4$  K) temperature. Samples may be solid (single crystal or powder) or liquid (fluid or frozen solution, a 'glass'). In this introduction to EPR spectroscopy, we shall be concerned only with *magnetically dilute systems* in which the unpaired electrons are involved in intramolecular (not intermolecular) interactions. We shall focus attention on the application of the technique to mono-nuclear, metal-containing systems.

### The Zeeman electronic effect

For a paramagnetic metal ion such as  $\text{Ti}^{3+}$  ( $d^1$ ),  $\text{V}^{4+}$  ( $d^1$ ) or  $\text{Cu}^{2+}$  ( $d^9$ ) with a single unpaired electron, the total spin quantum number  $S = \frac{1}{2}$ . There are two possible spin states:  $M_S = +\frac{1}{2}$  and  $M_S = -\frac{1}{2}$  (see Box 1.4 for one-electron systems and Section 20.6 for quantum numbers for multi-electron systems). In the absence of a magnetic field, these states are degenerate. Consider a one-electron case. By applying a magnetic field,  $B_0$ , the interaction between the unpaired electron and the magnetic field leads to a splitting of the energy levels (Fig. 4.25). This is called the Zeeman electronic effect and the energy difference,  $\Delta E$ , is given by eq. 4.19.

$$\Delta E = g\mu_B B_0 \quad (4.19)$$

where:  $g$  = Landé  $g$ -factor (' $g$ -value')

$B_0$  = applied magnetic field (in tesla, T)

$\mu_B$  = Bohr magneton

$$(1\mu_B = eh/4\pi m_e = 9.2740 \times 10^{-24} \text{ J T}^{-1})$$

The  $g$ -value is given by the ratio  $2\mu_e/\mu_B$  where  $\mu_e$  is the electron magnetic moment ( $9.2848 \times 10^{-24} \text{ J T}^{-1}$ );  $g$  is dimensionless. For a free electron,  $g = 2.0023$ . For a metal ion, spin-orbit coupling (see Chapter 20) leads to  $g$ -values that are significantly different from that of a free electron. The energy separation between the  $\alpha$  and  $\beta$  states (Fig. 4.25) corresponds to the microwave region of the elec-

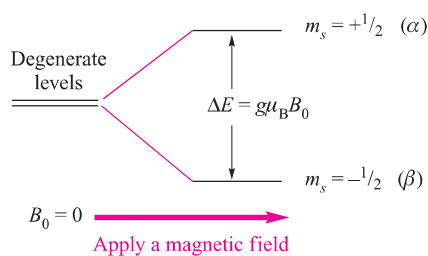


**Fig. 4.25** Under an applied magnetic field,  $B_0$ , the interaction between an unpaired electron and the magnetic field results in a splitting of the energy levels (the Zeeman electronic effect).

tromagnetic spectrum. Thus, by supplying appropriate microwave radiation to the sample, electron spin transitions between the two energy states occur. The system is then *in resonance*, and the recording of these transitions represents the EPR spectrum. (Compare this with the nuclear spin transitions resulting from radiofrequency radiation in NMR spectroscopy described in Section 4.8.) Usually, an EPR spectrometer operates at a constant microwave frequency (measured in gigahertz, GHz) and the magnetic field (measured in gauss or tesla,  $1 \text{ G} = 10^{-4} \text{ T}$ ) is varied until the energy separation of the two spin states coincides with the microwave radiation energy. Standard EPR spectrometers operate at 9–10 GHz (so-called 'X-band'), but there are also domains of lower and higher microwave frequencies: 1–2 GHz (L-band), 2–4 GHz (S-band), 35 GHz (Q-band) and 95 GHz (W-band). Recently developed FT-EPR spectrometers (as opposed to continuous wave instruments) produce increased spectral resolution and their use has widened the scope of systems that can be investigated (e.g. the second coordination sphere around a paramagnetic metal centre in a metalloprotein).

### EPR spectra

The form in which an EPR spectrum is recorded is the first derivative of an absorption peak (Fig. 4.26), because in this form the detection is more sensitive and the signal:noise ratio is improved due to intrinsic electronic properties resulting from modulation of the magnetic field. The point at which the derivative curve is zero (i.e. crosses the baseline) corresponds to the absorption maximum (the hashed line in Fig. 4.26), and the magnetic field,  $B_{\text{sample}}$ , at this

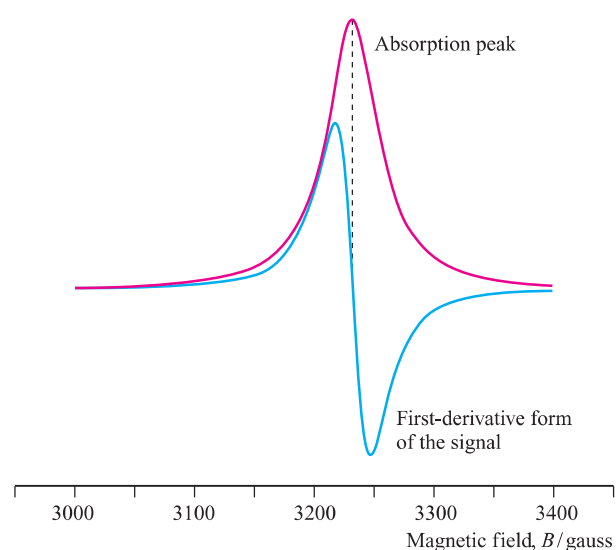


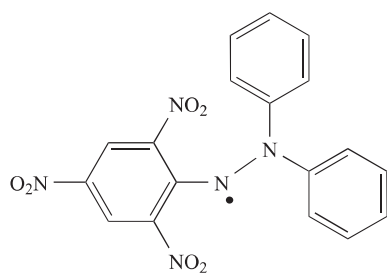
**Fig. 4.26** The typical appearance of a simple EPR spectrum is shown by the blue line. This is the first derivative of the absorption peak (shown in red).

point is recorded. The  $g$ -value for the sample is found by substituting the value of  $B_{\text{sample}}$  into eq. 4.19 (eq. 4.20).

$$\Delta E = h\nu = g_{\text{sample}} \times \mu_{\text{B}} \times B_{\text{sample}} \quad (4.20)$$

The experimental  $g$ -value can be found directly since the frequency,  $\nu$ , of a modern spectrometer is known accurately,  $h$  = Planck constant, and  $\mu_{\text{B}}$  = Bohr magneton (a constant). For old spectrometers, or where a calibration is required,  $g_{\text{sample}}$  can be found by comparing the value of  $B_{\text{sample}}$  with that of an internal reference material for which  $g$  is known (e.g. for the reference DPPH, 4.13,  $g = 2.0036$ ). Equation 4.21 follows from  $\Delta E = g\mu_{\text{B}}B_0$  because  $\mu_{\text{B}}$  is a constant.

$$g_{\text{sample}} \times B_{\text{sample}} = g_{\text{reference}} \times B_{\text{reference}} \quad (4.21)$$



2,2-Diphenyl-1-picrylhydrazyl radical (DPPH)

(4.13)

The  $g$ -value obtained from an EPR experiment provides diagnostic information about the system being investigated. For a paramagnetic metal centre, the  $g$ -value is characteristic of the oxidation state (i.e. the number of unpaired electrons), the coordination environment and the molecular symmetry. However, unless a system has cubic symmetry (i.e. it belongs to the  $T_d$ ,  $O_h$  or  $I_h$  point groups and is *isotropic*), the  $g$ -value depends on the orientation of the molecular principal axis with respect to the magnetic field. Such systems are said to be *anisotropic*. By rotation of the sample placed in the magnetic field in three orthogonal planes, three  $g$ -values are therefore obtained. Each  $g$ -value is associated with one of the three orthogonal axes. Three cases must now be considered:

- For an *isotropic* system (e.g. an  $\text{MX}_6$  species with  $O_h$  symmetry), the three  $g$ -values are equal to one another ( $g_{xx} = g_{yy} = g_{zz} = g_{\text{iso}}$ ).
- A system that is *anisotropic*, but has *axial symmetry*, has two axes ( $x$  and  $y$ ) that are equivalent but are different from the principal axis,  $z$ . This gives rise to two  $g$ -values labelled  $g_{\parallel}$  and  $g_{\perp}$  ( $g_{xx} = g_{yy} = g_{\parallel}$  and  $g_{zz} = g_{\perp}$ ) depending on whether the molecular principal axis is aligned parallel to or perpendicular to the magnetic field.
- An *anisotropic* system in which each of the  $x$ ,  $y$  and  $z$  axes is unique gives rise to three  $g$ -values ( $g_{xx}$ ,  $g_{yy}$  and  $g_{zz}$ ).

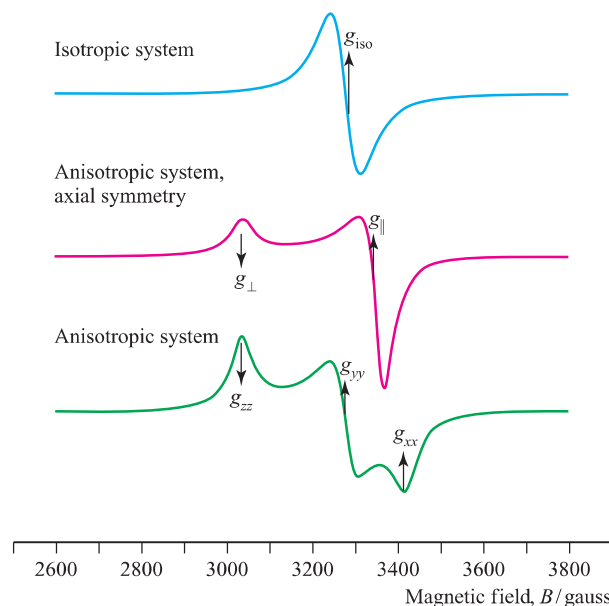


**Fig. 4.27** Typical line shapes for EPR spectra of an isotropic system (blue line), an anisotropic system with axial symmetry (red line), and an anisotropic system (green line). [Spectra simulated by Dr C. Palivan, University of Basel.]

These three cases are illustrated in Fig. 4.27. In addition to the information available from  $g$ -values, we can obtain information about nuclei with nuclear spin quantum number  $I \neq 0$  which are close to the paramagnetic centre. The spins of such nuclei interact magnetically with the unpaired electron and give rise to a *hyperfine interaction*. There is a direct analogy here with coupling of nuclear spins in NMR spectroscopy. The hyperfine interaction is added to the Zeeman electronic interaction, leading to a further splitting of the energy levels (eq. 4.22).

$$\Delta E = g\mu_{\text{B}}B_0 + SAI \quad (4.22)$$

where:  $S$  = total electron spin quantum number

$A$  = hyperfine coupling constant (in MHz)

$I$  = nuclear spin quantum number

The additional term  $SAI$  results in an EPR spectrum that is more complicated than those illustrated in Fig. 4.27. The EPR spectrum of one line (as for a scalar gyromagnetic factor) is split and the number of lines in the hyperfine pattern is given by  $2nI + 1$ , where  $n$  is the number of equivalent nuclei with spin quantum number  $I$  (compare this with eq. 4.15). For example, cobalt possesses one isotope,  $^{59}\text{Co}$ , with  $I = \frac{7}{2}$ . An unpaired electron on a  $\text{Co}^{2+}$  centre couples to the  $^{59}\text{Co}$  nucleus giving rise to an 8-line splitting pattern (Fig. 4.28a). Many elements possess more than one isotope (see Appendix 5). For example, naturally occurring Cu consists of  $^{63}\text{Cu}$  (69.2%,  $I = \frac{3}{2}$ ) and  $^{65}\text{Cu}$  (30.8%,  $I = \frac{3}{2}$ ). An unpaired electron on a  $\text{Cu}^{2+}$  ion couples to  $^{63}\text{Cu}$  and to  $^{65}\text{Cu}$ , giving rise to two, superimposed 4-line hyperfine patterns (in the case of a scalar gyromagnetic factor). As



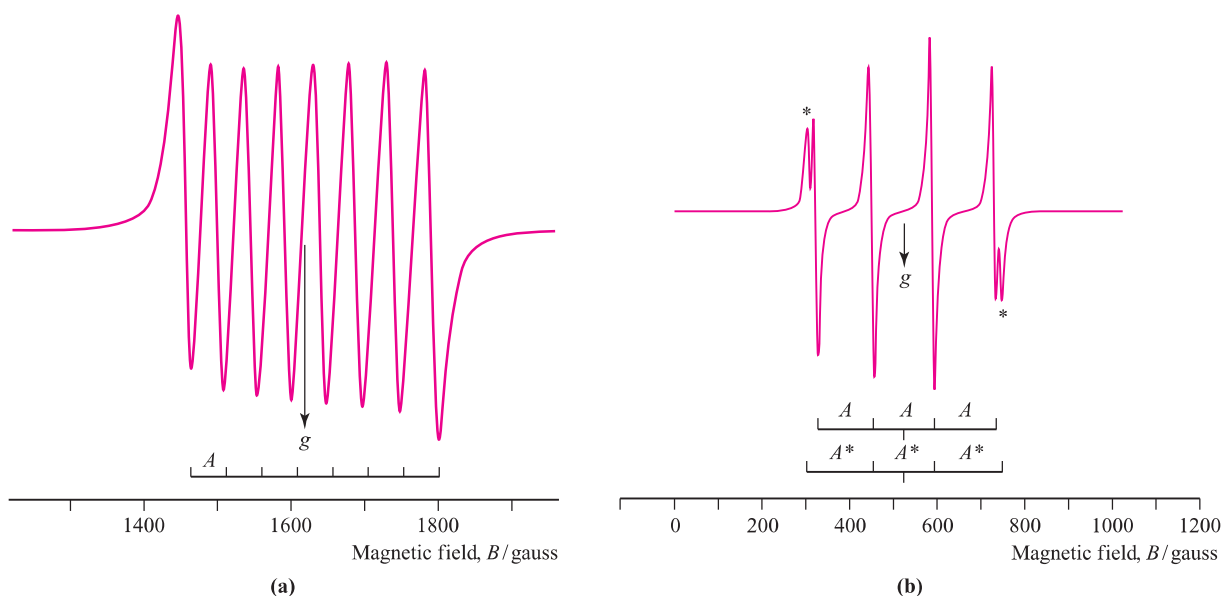


**Fig. 4.28** (a) Coupling between an unpaired electron on a  $\text{Co}^{2+}$  ion with the  $^{59}\text{Co}$  nucleus (100%,  $I = \frac{7}{2}$ ) gives rise to an 8-line hyperfine splitting pattern for the EPR signal (microwave frequency = 9.785 GHz). (b) Coupling between an unpaired electron on a  $\text{Cu}^{2+}$  ion with the  $^{63}\text{Cu}$  and  $^{65}\text{Cu}$  nuclei (69.2% and 30.8%, respectively, both  $I = \frac{3}{2}$ ) produces two superimposed 4-line splitting patterns.  $A$  and  $A^*$  are the hyperfine coupling constants. [Spectra simulated by Dr C. Palivan, University of Basel.]

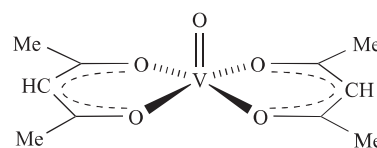
$A(^{65}\text{Cu}) = 1.07 \times A(^{63}\text{Cu})$ , a well-resolved spectrum is still observed (Fig. 4.28b,  $A$  and  $A^*$  are the hyperfine coupling constants for  $^{63}\text{Cu}$  and  $^{65}\text{Cu}$ , respectively). Hyperfine interactions will also arise if there is delocalization of the unpaired electron from the paramagnetic metal centre onto ligands in the first coordination sphere, atoms in which possess  $I > 0$  (e.g.  $^{19}\text{F}$ , 100%,  $I = \frac{1}{2}$ ). In this case, the spectrum is more complex because of the presence of the transitions arising from this so called, ‘superhyperfine’ interaction.

As in the case of  $g$ -values, hyperfine coupling constants,  $A$ , can be either isotropic or anisotropic depending on the symmetry of the system, and the shape of the EPR spectra reflects this. As a result,  $g$  and  $A$ -values can be used to give detailed information about the coordination sphere of a paramagnetic metal centre (e.g. geometry, symmetry, nature of adjacent nuclei having  $I > 0$ ). Depending on the paramagnetic metal centre, further insight into their structure can be gained by considering other interactions (e.g. zero field interactions, quadrupolar interaction, Zeeman nuclear interactions).

EPR spectroscopy has a wide range of applications, including its use in bioinorganic systems, for example, blue copper proteins (see Section 29.4).

#### Worked example 4.8 EPR spectrum of $[\text{VO}(\text{acac})_2]$

The complex  $[\text{VO}(\text{acac})_2]$  has the structure shown below (Hacac = pentane-2,4-dione or acetylacetonone). Vanadium has two isotopes ( $^{50}\text{V}$ , 0.25%,  $I = 6$ ;  $^{51}\text{V}$ , 99.75%,  $I = \frac{7}{2}$ ).



The solution EPR spectrum of  $[\text{VO}(\text{acac})_2]$  at 298 K shows an 8-line signal ( $A = 120 \text{ G}$ ,  $g = 1.971$ ). When the sample is frozen in liquid  $\text{N}_2$  (77 K), the EPR spectrum consists of two overlapping 8-line patterns for which the  $g$ -values are 1.985 and 1.942, respectively. Rationalize these data.

[Data: A. Serianz *et al.* (1976) *J. Chem. Educ.*, vol. 53, p. 394.]

Vanadium is in group 5 and in  $[\text{VO}(\text{acac})_2]$ , it is in oxidation state +4. Therefore the V centre has one unpaired electron.

Vanadium is almost monotypic. The pattern in the EPR spectrum is dominated by hyperfine coupling between the unpaired electron and the  $^{51}\text{V}$  nucleus (99.75% abundant). The  $I = \frac{7}{2}$  spin gives rise to the 8-line pattern:

$$2nI + 1 = 2(1)(\frac{7}{2}) + 1 = 8$$

Look at the structure of the  $[\text{VO}(\text{acac})_2]$  molecule. It is not spherically symmetrical, but instead has axial symmetry. The principal axis contains the  $\text{V}=\text{O}$  unit. At 298 K, the EPR spectrum corresponds to an isotropic system and this is because the molecules are tumbling rapidly in solution and an average orientation is observed. On cooling to

77 K, the spectrum splits into two superimposed 8-line patterns. This corresponds to the principal axis of the molecule aligning parallel or perpendicular to the applied magnetic field. The two  $g$  values of 1.985 and 1.942 correspond to  $g_{\parallel}$  and  $g_{\perp}$ . The value at 298 K ( $g = 1.971$ ) is in between the values of  $g_{\parallel}$  and  $g_{\perp}$ .

### Self-study exercises

1. Why is copper(I) EPR silent?
2. Manganese is monatomic ( $^{55}\text{Mn}$ ). The EPR spectrum of an aqueous solution of  $[\text{Mn}(\text{OH}_2)_6]^{2+}$  shows a 6-line pattern. Why is  $[\text{Mn}(\text{OH}_2)_6]^{2+}$  isotropic? What is the value of  $I$  for  $^{55}\text{Mn}$ ?
3. Show that the spectrum in Fig. 4.28a is consistent with a  $g$ -value of 4.32.

## 4.10 Mössbauer spectroscopy

### The technique of Mössbauer spectroscopy

The *Mössbauer effect* is the emission and resonant absorption of nuclear  $\gamma$ -rays studied under conditions such that the nuclei have negligible recoil velocities when  $\gamma$ -rays are emitted or absorbed. This is only achieved by working with *solid samples* in which the nuclei are held rigidly in a crystal lattice. The energy, and thus the frequency of the  $\gamma$ -radiation involved, corresponds to the transition between the ground state and the short-lived excited state of the nuclide concerned. Table 4.4 lists properties of several nuclei which can be observed using Mössbauer spectroscopy.

We illustrate the study of the Mössbauer effect by reference to  $^{57}\text{Fe}$  spectroscopy. The basic apparatus includes a radioactive source, a solid absorber with the  $^{57}\text{Fe}$ -containing sample and a  $\gamma$ -ray detector. For  $^{57}\text{Fe}$  samples, the radioactive source is  $^{57}\text{Co}$  and is incorporated into stainless steel; the  $^{57}\text{Co}$  source decays by capture of an extra-nuclear electron to give the excited state of  $^{57}\text{Fe}$  which emits  $\gamma$ -radiation as it decays to its ground state. If  $^{57}\text{Fe}$  is present in the

same form in both source and absorber, resonant absorption occurs and no radiation is transmitted. However, if the  $^{57}\text{Fe}$  in the source and absorber is present in two different forms, absorption does *not* occur and  $\gamma$ -radiation reaches the detector. Moving the source at different velocities towards or away from the  $^{57}\text{Fe}$  absorber has the effect of varying the energy of the  $\gamma$ -radiation (i.e. by the Doppler effect). The velocity of movement required to bring about maximum absorption relative to stainless steel (defined as an arbitrary zero for iron) is called the *isomer shift* of  $^{57}\text{Fe}$  in the sample, with units of  $\text{mm s}^{-1}$  (see Fig. 20.31).

### What can isomer shift data tell us?

The isomer shift gives a measure of the electron density on the  $^{57}\text{Fe}$  centre, and isomer shift values can be used to determine the oxidation state of the Fe atom. Similarly, in  $^{197}\text{Au}$  Mössbauer spectroscopy, isomer shifts can be used to distinguish between Au(I) and Au(III). Three specific examples are chosen here from iron chemistry.

The cation  $[\text{Fe}(\text{NH}_3)_5(\text{NO})]^{2+}$  has presented chemists with an ambiguity in terms of the description of the bonding which has, in some instances, been described in terms of an  $[\text{NO}]^+$  unit bound to an Fe(I) centre. Results of  $^{57}\text{Fe}$  Mössbauer spectroscopy have revealed that the correct description is that of an  $[\text{NO}]^-$  ligand bound to an Fe(III) centre.

The formal oxidation states of the iron centres in  $[\text{Fe}(\text{CN})_6]^{4-}$  and  $[\text{Fe}(\text{CN})_6]^{3-}$  are +2 and +3. However, the closeness of the isomer shifts for these species suggests that the actual oxidation states are similar and this may be interpreted in terms of the extra electron in  $[\text{Fe}(\text{CN})_6]^{4-}$  being delocalized on the cyanido ligands rather than the iron centre.


Differences in isomer shifts can be used to distinguish different iron environments in the same molecule: the existence of two signals in the Mössbauer spectrum of  $\text{Fe}_3(\text{CO})_{12}$  provided the first evidence for the presence of two types of iron atom in the solid state structure (Fig. 4.29), a fact that has been confirmed by X-ray diffraction methods.

**Table 4.4** Properties of selected nuclei observed by Mössbauer spectroscopy. The radioisotope source provides the  $\gamma$ -radiation required for the Mössbauer effect.

Nucleus observed	Natural abundance / %	Ground spin state	Excited spin state	Radioisotope source <sup>†</sup>
$^{57}\text{Fe}$	2.2	$\frac{1}{2}$	$\frac{3}{2}$	$^{57}\text{Co}$
$^{119}\text{Sn}$	8.6	$\frac{1}{2}$	$\frac{3}{2}$	$^{119\text{m}}\text{Sn}$
$^{99}\text{Ru}$	12.7	$\frac{3}{2}$	$\frac{5}{2}$	$^{99}\text{Rh}$
$^{197}\text{Au}$	100	$\frac{3}{2}$	$\frac{1}{2}$	$^{197\text{m}}\text{Pt}$

<sup>†</sup> m = metastable.

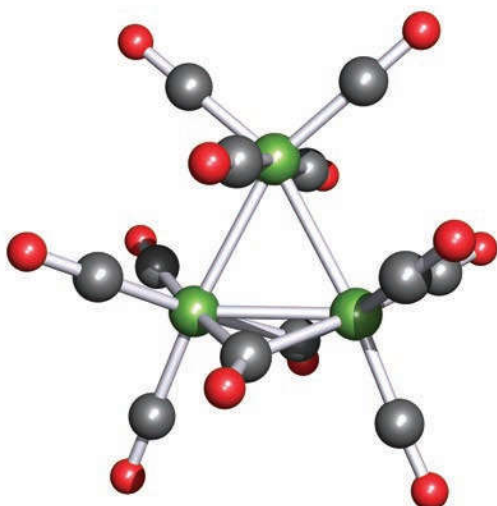


 **Fig. 4.29** The solid state structure of  $\text{Fe}_3(\text{CO})_{12}$  as determined by X-ray diffraction methods. The molecule contains two Fe environments by virtue of the arrangement of the CO groups. Colour code: Fe, green; C, grey; O, red.

The use of Mössbauer spectroscopy to investigate different electronic spin states of iron(II) is exemplified in Fig. 20.31 and the accompanying discussion.

#### 4.11 Structure determination: diffraction methods

Chemists rely on diffraction methods for the structural determination of molecular solids (i.e. solids composed of discrete molecules), non-molecular solids (e.g. ionic materials) and, to a lesser extent, gaseous molecules. As the technique has been developed, its range of applications has expanded to include polymers, proteins and other macromolecules. The most commonly applied techniques are single crystal and powder X-ray diffraction. Electron diffraction is important for the structural elucidation of molecules in the gas phase and for the study of solid surfaces. Neutron diffraction is used for the accurate location of light atoms (e.g. H, D or Li), or if one needs to distinguish between atoms of similar atomic numbers, e.g. C and N, or Ni and Cu.

##### X-ray diffraction (XRD)

In *X-ray diffraction (XRD)*, X-rays are diffracted by electrons surrounding the nuclei in atoms in a crystalline or polycrystalline solid.

The wavelength of X-rays ( $\approx 10^{-10}$  m, i.e.  $\approx 100$  pm) is of the same order of magnitude as the internuclear distances in molecules or non-molecular solids. As a consequence of this, diffraction is observed when X-rays interact with the electrons in an array of atoms in the crystalline solid.



**Fig. 4.30** A Kappa-CCD diffractometer equipped with a nitrogen gas, low-temperature cryostat (upper, centre in the photograph). The X-ray source and the detector are on the left- and right-hand sides of the photograph, respectively. The crystal is mounted on the goniometer head (centre). The black 'tube' shown at the upper left is a microscope.

This permits atomic resolution to be achieved when a structure is determined from the X-ray diffraction data which are collected. An X-ray diffractometer (Fig. 4.30) typically consists of an X-ray source, a mounting for the crystal, turntables which allow the operator to alter the orientation of the crystal with respect to the incident X-ray beam, and an X-ray detector. The source provides *monochromatic radiation*, i.e. X-rays of a single wavelength. The detector records X-rays that are scattered by the crystal. Modern diffractometers incorporate *imaging plate detectors* or *charge-coupled device (CCD) area detectors* which make the process of data collection much faster. For both these detectors, radiation must be converted to light before it can be recorded. Currently, *pixel detectors* are being developed which detect radiation directly, and their use will avoid the step of transforming radiation to light.

X-rays are scattered by the electrons surrounding the nuclei in atoms in the solid. Because the *scattering power*

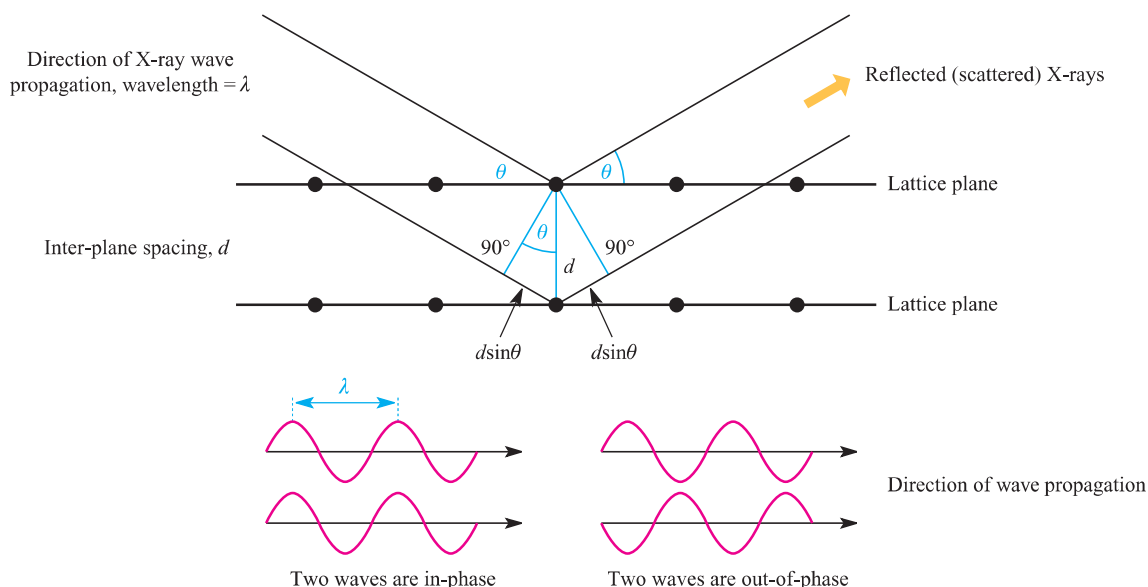


**Fig. 4.31** Schematic representation of the interaction of X-rays with layers of atoms in a crystal. This leads to the derivation of Bragg's equation (eq. 4.23).

of an atom depends on the number of electrons, it is possible to distinguish different types of atoms. However, it is difficult (often impossible) to locate H atoms in the presence of heavy atoms.

Figure 4.31 shows an ordered array of atoms with the latter represented as black dots. The atoms are arranged in layers or *lattice planes*. Consider the case in which the two waves of incident radiation are in-phase. Let one wave be reflected from an atom in the first lattice plane, and the second wave reflected from an atom in the second lattice plane (Fig. 4.31). The two scattered (reflected) waves will be in-phase only if the additional distance travelled by the second wave is equal to a multiple of the wavelength, i.e.  $n\lambda$ . If the *lattice spacing* (the distance between the planes of atoms in the crystal) is  $d$ , then by trigonometry it follows that the additional distance travelled by the second wave is  $2d \times \sin \theta$ . For the two waves (originally in-phase) to stay in-phase as they are scattered, eq. 4.23 must hold. This relationship between the wavelength,  $\lambda$ , of the incident X-ray radiation and the lattice spacings,  $d$ , of the crystal is Bragg's equation and is the basis of the techniques of X-ray and neutron diffraction.

$$2d \sin \theta = n\lambda \quad \text{Bragg's equation} \quad (4.23)$$

The angle  $\theta$  in eq. 4.23 is half of the diffraction angle (Fig. 4.31), and diffraction data are often referred to in terms of an angle  $2\theta$ . Scattering data are collected over a wide range of  $\theta$  (or  $2\theta$ ) values and for a range of crystal orientations. Each setting results in a different *diffraction pattern* as discussed below.

## Single crystal X-ray diffraction

Analysis by *single crystal X-ray diffraction* leads to the full determination of the structure of a compound.

Single crystals suitable for X-ray diffraction can be grown by a number of methods,<sup>†</sup> all of which lower the solubility of the compound in solution:

- evaporation of solvent from a solution of the compound;
- cooling a solution of the compound;
- diffusing a solvent in which the compound is insoluble or poorly soluble into a solution of the compound in a second solvent;
- allowing the vapour of a volatile solvent to diffuse into a solution of the compound in a second solvent;

In addition, it may be possible to grow crystals by sublimation or from a melt. Problems sometimes occur with the intergrowth of two crystals (*crystal twinning*). Large crystals are not necessary for use with modern diffractometers, and ideal crystal dimensions are 0.1 to 0.3 mm.

A single crystal gives rise to a diffraction pattern consisting of well-defined spots. Figure 4.32a shows the diffraction pattern in one *frame* recorded during a data collection of a single crystal of 4'-azido-2,2':6':2''-terpyridine (**4.14**). This is an example of an organic ligand used in metal coordination chemistry (see Sections 7.11 and 19.7).

<sup>†</sup>See: W. Clegg (2004) in *Comprehensive Coordination Chemistry II*, eds. J.A. McCleverty and T.J. Meyer, Elsevier, Oxford, vol. 1, p. 579.

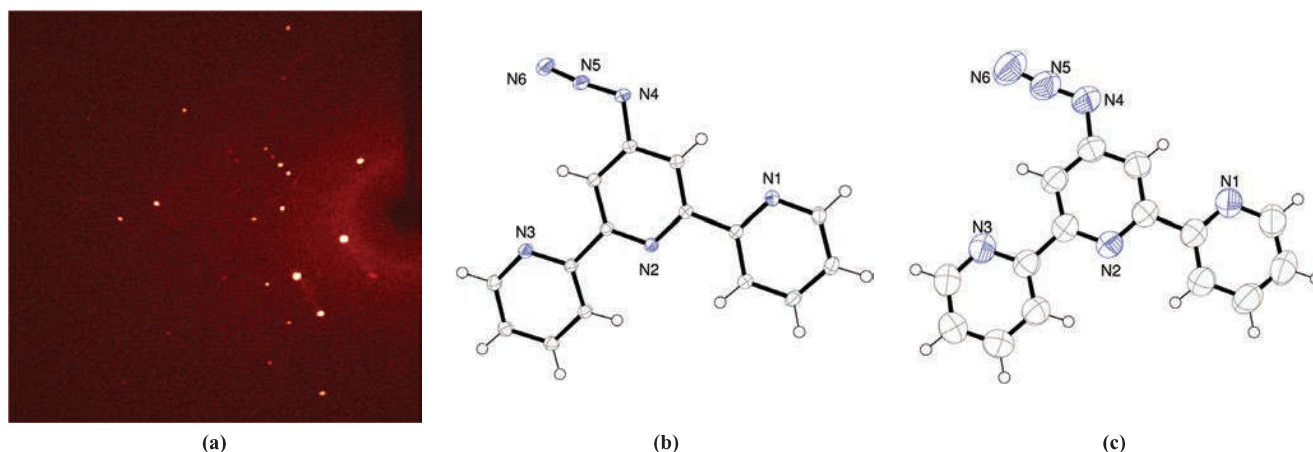
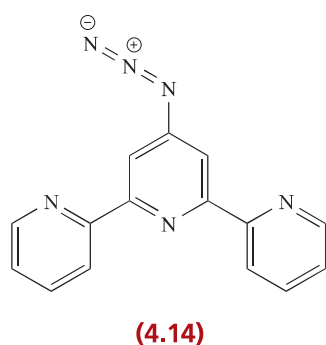


**Fig. 4.32** Solving the structure of the ligand 4'-azido-2,2':6',2''-terpyridine. (a) One photographic frame from the single crystal X-ray data collection showing diffraction spots. ORTEP drawings of the molecular structure of 4'-azido-2,2':6',2''-terpyridine from data collected at (b) 123 K and (c) 293 K with ellipsoids plotted at a 50% probability level. The H atoms were refined isotropically (see text). Colour code for atoms: C, grey; N, blue; H, white. [Data: M. Neuburger and N. Hostettler, University of Basel; R. Al-Fallahpour *et al.* (1999) *Synthesis*, p. 1051.]



In order to obtain a complete data set (i.e. enough reflection data to solve the structure of the compound under investigation), many hundreds or thousands of frames are recorded. Each frame contains diffraction data from different reflections, and at the end of the experiment, the data are extracted and assembled to produce a numerical datafile. The methods of solving a crystal structure from the reflection data are beyond the scope of this book, and further details can be found in the texts listed at the end of the chapter.

Compounds such as **4.14** consist of discrete molecules, and the results of a structural determination are usually discussed in terms of molecular structure (atomic coordinates, bond distances, bond angles and torsion angles) and in terms of the packing of the molecules in the lattice. Packing involves intermolecular interactions (e.g. hydrogen bonding, van der Waals forces,  $\pi$ -stacking of aromatic rings). Molecular structures are routinely represented as ORTEP diagrams (Figs. 4.32b and c),<sup>†</sup> in which the atoms are drawn as ellipsoids. Each ellipsoid delineates the volume

in space in which there is a probability of finding a particular atom and indicates the *thermal motion* of the atom. Since this motion depends upon the amount of energy that the molecule possesses, the temperature of the X-ray data collection is important. Accurate bond distances and angles can only be obtained if thermal motions are minimized. A comparison of Figs. 4.32b and c reveals the differences in thermal motion of the atoms in compound **4.14** at 123 and 293 K. Low-temperature data collection is now a routine part of single crystal X-ray structure determination. Note that the H atoms in Figs. 4.32b and c are drawn as circles (*isotropic*) rather than as ellipsoids (*anisotropic*). This is because the H atoms are not directly located. Instead, their positions are fixed in chemically sensible sites with respect to the C atoms which have been directly located using the X-ray diffraction data. It is not uncommon for solid state structures to suffer from *disorder* (see Box 15.5).

In Chapter 6, we discuss solid state structures of metals and ionic compounds, and detail the *unit cells* of a number of prototype structures. The unit cell is the smallest repeating unit in a crystal lattice, and its dimensions are characteristic of a particular *polymorph* of a compound. A unit cell is characterized by three cell edge lengths ( $a$ ,  $b$  and  $c$ ) and three angles ( $\alpha$ ,  $\beta$  and  $\gamma$ ). Distances are often given in the non-SI unit of the ångström ( $\text{Å}$ ), because  $1 \text{ Å} = 10^{-10} \text{ m}$  and bond distances typically lie in the range 1–3 Å; in this book we use SI units of the picometre ( $1 \text{ pm} = 10^{-12} \text{ m}$ ).

The smallest repeating unit in a solid state lattice is the *unit cell*.

*Polymorphs* are different phases of the same chemical compound with different crystal structures.

<sup>†</sup>ORTEP software: [www.chem.gla.ac.uk/~louis/software/](http://www.chem.gla.ac.uk/~louis/software/); L.J. Farrugia (1997) *J. Appl. Cryst.*, vol. 30, p. 565.

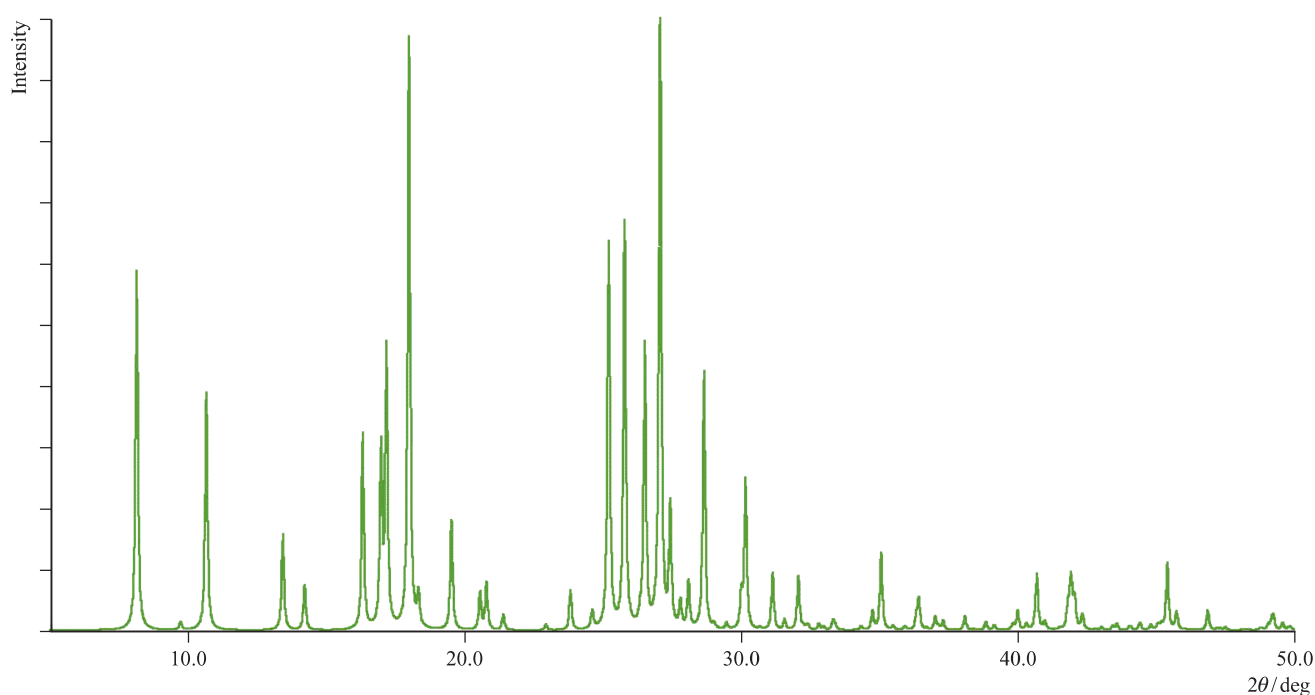


**Fig. 4.33** Calculated powder pattern for 4'-azido-2,2':6',2''-terpyridine (compound **4.14**) using single crystal X-ray diffraction data. The pattern is a fingerprint of the bulk powder material.

## Powder X-ray diffraction

A powder is a polycrystalline sample; **powder X-ray diffraction** data are routinely used for identifying a bulk sample of a material, and for screening different phases of a compound.

Powders (as distinct from amorphous materials) consist of huge numbers of microcrystals and are classed as polycrystalline materials. When X-rays interact with powders, they are scattered in all directions because the microcrystals lie in random orientations. This simultaneously provides all the reflection data that are produced in a single crystal experiment by making changes to the orientation of the crystal with respect to the incident X-ray beam. As a consequence, and in contrast to the single crystal diffraction experiment, all information about the relative orientations of the scattering vectors in space is lost, and the data consist of scattered intensities as a function of diffraction angle ( $2\theta$ ). The output from a powder diffractometer is in the form of a powder pattern (Fig. 4.33) and this is a diagnostic fingerprint of the polycrystalline compound. Different phases of the same compound exhibit different powder patterns and powder X-ray diffraction is a powerful tool for distinguishing between phases. Under certain conditions, it is possible to solve a molecular structure using powder data. This can be achieved for relatively

simple molecules,<sup>†</sup> but it is not the aim of most powder diffraction experiments. On the other hand, if a single crystal structure is known, a powder pattern can be calculated and Fig. 4.33 shows the calculated powder pattern of compound **4.14**. Having this pattern to hand allows you to match it to powder patterns obtained for new bulk samples of the compound that are synthesized, giving a means of rapidly screening bulk materials. This is particularly important in the pharmaceutical industry where different phases of a drug exhibit different pharmacological properties.

## Single crystal neutron diffraction

In **neutron diffraction**, Bragg scattering of neutrons occurs when neutrons interact with the nuclei of the atoms in a single crystal; both light and heavy atoms can be directly detected.

Neutron diffraction is less commonly used than X-ray diffraction because of the limitations and costs of sources of neutrons. However, because the technique relies upon the diffraction of neutrons by atomic nuclei, neutron diffraction

<sup>†</sup>See: K.D.M. Harris, R.L. Johnston, E.Y. Cheung, G.W. Turner, S. Habershon, D. Albesa-Jové, E. Tedesco and B.M. Kariuki (2002) *CrystEngComm*, vol. 4, p. 356; W.I.F. David, K. Shankland, J. van de Streek, E. Pidcock, W.D.S. Motherwell and J.C. Cole (2006) *J. Appl. Cryst.*, vol. 39, p. 910.]

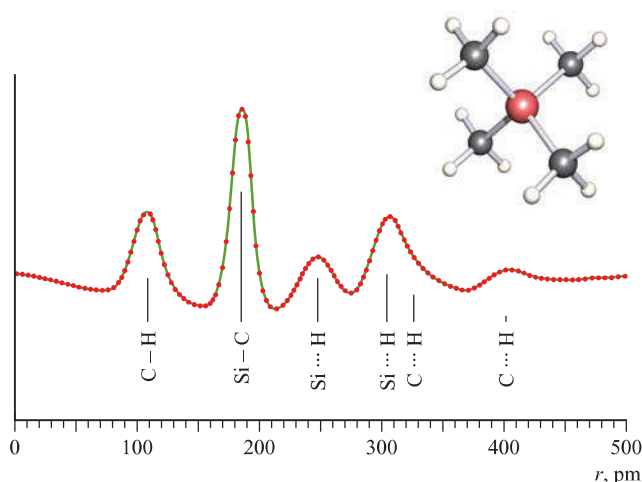


**Fig. 4.34** Experimental (dots) and calculated (solid line) radial distributions for  $\text{SiMe}_4$ . The vertical scale is arbitrary. The shortest distances (C–H and Si–C) correspond to bonded contacts, and the remaining ones to non-bonded contacts. [Redrawn with permission from I. Hargittai *et al.* (2009) *Encyclopedia of Spectroscopy and Spectrometry*, Elsevier, p. 461.]

has the advantage that it can accurately locate light atoms such as H. Before a beam of neutrons from a nuclear reactor can be used for a neutron diffraction experiment, its energy must be reduced. Neutrons released from the fission of  $^{235}_{92}\text{U}$  nuclei lose most of their kinetic energy by passage through a moderator such as heavy water ( $\text{D}_2\text{O}$ ). It follows from the deBroglie relationship (eq. 1.11) that the energy of the thermal neutrons so-produced corresponds to a wavelength of 100–500 pm (1–5 Å), i.e. appropriate for diffraction by a molecular or ionic solid. The scattering of neutrons follows Bragg's equation, and the diffraction experiment is similar to that for X-ray diffraction.

## Electron diffraction

In *gas phase electron diffraction*, electrons are scattered by the electric fields of atomic nuclei in gas phase molecules; intramolecular bond parameters are determined.

Electrons that have been accelerated through a potential difference of 50 kV possess a wavelength of 5.5 pm (from the de Broglie relationship, eq. 1.11). A monochromated beam of 50 kV electrons is therefore suitable for diffraction by molecules in the gas phase. An electron diffraction apparatus is maintained under high vacuum and the electron beam interacts with a gas stream emerging from a nozzle. Unlike X-rays and neutrons, electrons are charged, and electron scattering is mainly caused by the interactions of the electrons with the electric fields of the atomic nuclei in a sample. Because the sample molecules are in the gas phase, they are continually in motion and are, therefore, in random orientations and well separated from one another.

Thus, the diffraction data mainly provide information about *intramolecular* bond parameters.

The initial electron diffraction data relate scattering angle of the electron beam to intensity. Corrections must be made for atomic, inelastic and extraneous scatterings, and after this, *molecular scattering data* are obtained. Fourier transformation of these data produces radial distribution data which reveal the interatomic distances between all pairs of bonded and non-bonded atoms in the gaseous molecule. Converting these data into a 3-dimensional molecular structure is not trivial, particularly for large molecules. Experimental radial distribution curves are compared to those calculated for modelled structures. This is shown for  $\text{SiMe}_4$  in Fig. 4.34, where the best match between experimental and calculated radial distributions is found for a molecule with  $T_d$  symmetry, Si–C and C–H bond distances of 187.7 and 111.0 pm, and Si–C–H bond angles of  $111.0^\circ$ .

## Self-study exercise

Results of electron diffraction data for  $\text{BCl}_3$  give bonded B–Cl distances of 174 pm (all bonds of equal length) and non-bonded Cl...Cl distances of 301 pm (three equal distances). Show that these data are consistent with  $\text{BCl}_3$  being trigonal planar rather than trigonal pyramidal.

## Low-energy electron diffraction (LEED)

Electron diffraction is not confined to the study of gases. Low-energy electrons (10–200 eV) are diffracted from the surface of a solid and the diffraction pattern so obtained provides information about the arrangement of atoms on the surface of the solid.

## Structural databases

Structural data are stored in, and can be accessed from, three primary databases which are continually updated. Data for organic and metal–organic compounds and boranes are compiled by the Cambridge Structural Database ([www.ccdc.cam.ac.uk](http://www.ccdc.cam.ac.uk)), while crystallographic data for purely inorganic compounds (e.g. metal and non-metal halides and oxides) are deposited in the Inorganic Crystal Structure Database ([www.fiz-karlsruhe.de](http://www.fiz-karlsruhe.de)). Structural data for biological macromolecules are collected in the Protein Data Bank ([www.rcsb.org/pdb](http://www.rcsb.org/pdb)).

## 4.12 Photoelectron spectroscopy (PES, UPS, XPS, ESCA)

*Photoelectron spectroscopy (PES)* is a technique used to study the energies of occupied atomic or molecular orbitals.

The technique of *photoelectron spectroscopy* (PES, also called *photoemission spectroscopy*), was developed in the 1960s independently by Turner (in Oxford), Spicer (in Stanford), Vilesov (in Leningrad, now St. Petersburg) and Siegbahn (in Uppsala). In a PES experiment, atoms or molecules are excited with monochromated electromagnetic radiation of energy,  $E_{\text{ex}}$ , causing electrons to be ejected, i.e. photoionization occurs (eq. 4.24).



The atom or molecule X is in its ground state, and  $X^+$  is in either its ground or an excited state. The ejected electrons are called *photoelectrons*. Each electron in an atom or molecule possesses a characteristic *binding energy* and must absorb an amount of energy equal to, or in excess of, the binding energy to be ionized. The kinetic energy,  $KE$ , of the ejected photoelectron is the energy in excess of the ionization (or binding) energy,  $IE$  (eq. 4.25).

$$KE = E_{\text{ex}} - IE \quad (4.25)$$

Since the excess energy can be measured and  $E_{\text{ex}}$  is known, the binding energy of the electron can be determined. A photoelectron spectrum records the number of photoelectrons with a particular kinetic energy against binding energy. The quantization of energy states leads to a photoelectron spectrum having a discrete band structure. *Koopmans' theorem* relates ionization energy to the energy of the atomic or molecular orbital in which the electron resides before ejection. Thus, binding energies measured from PES give a measure of atomic or molecular orbital energies.

As an example, consider the photoelectron spectrum of gaseous  $\text{N}_2$ , one of the first PES results reported by Turner in

1963. A helium(I) lamp ( $E_{\text{ex}} = 21.2 \text{ eV}$ ) is a suitable source of photons for this experiment since 21.2 eV exceeds the binding energies of interest. The photoelectron spectrum of  $\text{N}_2$  consists of three peaks corresponding to binding energies of 15.57, 16.72 and 18.72 eV. These three ionizations arise from the ejection of an electron from the  $\sigma_g(2p)$ ,  $\pi_u(2p)$  or  $\sigma_u^*(2s)$  MOs of  $\text{N}_2$  (Fig. 2.10), respectively.

The applications of PES can be diversified by using different irradiation sources. In the example above, a helium(I) emission photon source with energy of 21.2 eV was used; the 'He(I) emission' corresponds to a transition from an excited state of configuration  $1s^1 2p^1$  to the ground state ( $1s^2$ ) of He. The ionization of more tightly bound electrons can be achieved by using higher energy sources. For example, a 'helium(II) source' corresponds to radiation from  $\text{He}^+$ , and a helium(II) lamp provides an excitation energy of 40.8 eV. Both helium(I) and helium(II) radiation are in the vacuum UV region of the electromagnetic spectrum and therefore PES using these excitation energies is known as UPS (*UV photoelectron spectroscopy*). The ionization of core electrons in molecules can be achieved using excitation sources in the X-ray region. The Mg and Al X-ray emissions (Mg  $K\alpha$  with  $E_{\text{ex}} = 1254 \text{ eV}$ , and Al  $K\alpha$  with  $E_{\text{ex}} = 1487 \text{ eV}$ ) are typical examples. With an X-ray source, the technique is referred to as XPS (*X-ray photoelectron spectroscopy*) and Fig. 4.35 shows a modern X-ray photoelectron spectrometer. XPS is also known as *electron spectroscopy for chemical analysis*, ESCA, and is a valuable analytical tool because core ionization energies have characteristic values for a given element. Thus, the technique can be applied for the detection of any element except for hydrogen, and can also be used to differentiate between oxidation states of an element. XPS is widely used for the analysis of surfaces, and applications include that in the semiconductor industry (e.g. to distinguish between Si and  $\text{SiO}_2$ ) and the study of surface corrosion.



**Fig. 4.35** An X-ray photoelectron spectrometer (XPS) being used to analyse the surface of a material.

### 4.13 Computational methods

Computational methods are now used extensively by experimental chemists. Information that can be calculated includes the equilibrium geometry of a molecule, transition state geometries, heats of formation, composition of molecular orbitals, vibrational frequencies, electronic spectra, reaction mechanisms and (from molecular mechanics calculations) strain energies. The last 20 years have witnessed a huge increase in the use of computational methods in chemistry. Two factors have revolutionized the ways in which computational chemistry may be applied. The first is that calculations can now be performed on small computers (including laptops) or small clusters of computers, instead of on a mainframe computer. The second is the development of the computational methods themselves. The importance of



the latter was recognized by the award of the 1998 Nobel Prize in Chemistry jointly to John Pople ‘for his development of computational methods in quantum chemistry’ and to Walter Kohn ‘for his development of the density-functional theory’. Many of the computational packages available to chemists fall into the following categories: *ab initio* methods, self-consistent field (SCF) MO methods, semi-empirical methods, density functional methods and molecular mechanics.

### Hartree–Fock theory

The Schrödinger equation (Section 1.5) can be solved exactly only for one-electron species, i.e. hydrogen-like systems. This is very restrictive and quantum chemists have invested a great deal of effort into finding ways to obtain approximate solutions to the Schrödinger equation for many-electron systems. Towards this end, the work of Hartree, Fock and Slater in the 1930s led to the development of Hartree–Fock theory. Equations in Hartree–Fock theory are solved by an iterative process and the calculation *converges to self-consistency*, hence the term ‘self-consistent’. Various levels of theory deal differently with the approximations made when solving the Schrödinger equation, in particular with regard to electron correlation (i.e. taking into account interactions between electrons). The higher the level of calculation, the closer the result should come to experimental observation. A number of semi-empirical methods, which are parameterized and consider only valence electrons, have been developed. These include CNDO (*complete neglect of differential overlap*), INDO (*intermediate neglect of differential overlap*), MNDO (*modified neglect of diatomic overlap*), AM1 (*Austin model 1*) and PM3 (*parametric method 3*). While these methods reduce the time required for computation, they may not always produce reliable results for complex systems. Hence, they should be used with a degree of caution.

### Density functional theory

In contrast to other methods, density functional theory (DFT) focuses on the electron density distribution in a system rather than on many-electron wavefunctions. Within DFT, there are several levels of calculation, two common ones being BLYP (after Becke, Lee, Yang and Parr) and B3LYP. The great advantage of DFT is that it can be applied to a wide variety of systems, ranging from transition metal complexes to solids, surfaces and metalloproteins. The computation time is not excessive, and the results are generally reliable. Conventional DFT cannot be used to investigate systems in which van der Waals (dispersion) forces are a dominant feature (e.g. biomolecules).

Development of the theory to allow these intermolecular interactions to be accurately computed is currently (as of 2011) ongoing.<sup>†</sup>

### Hückel MO theory

At a simple level, Hückel MO theory (proposed in the 1930s by Erich Hückel) works well for dealing with the  $\pi$ -systems of unsaturated organic molecules. By extending the basis set and including overlap and all interactions ( $\sigma$  and  $\pi$ ), Roald Hoffmann showed that *extended Hückel theory* could be applied to most hydrocarbons. This theory has since been developed further and continues to be a useful method to determine the relative energies of different conformers of an organic molecule.

### Molecular mechanics (MM)

Before attempting a new chemical synthesis, you might wish to compute the structure of the target molecule in order to investigate, for example, steric crowding of substituents. For this purpose, *molecular mechanics* (MM) has become a routine tool. Pure MM does not have a quantum mechanical basis. Instead, it calculates a *strain energy* which is the sum of energy terms involving bond deformation, angle deformation, torsion deformation and non-bonded interactions. The equation for the strain energy together with a number of input parameters that describe the atoms and bonds are known as a *force field*. When an MM calculation is running, the conformation of the molecule changes until it reaches an optimized structure for which the strain energy is minimized. As well as minimizing a ground state structure, it is also possible to investigate time-dependent processes by using *molecular dynamics* (MD). Force fields for such modelling take into account the cleavage and formation of bonds, so that MD simulations can explore potential energy surfaces associated with the dynamic systems. Examples of MD force fields are AMBER (*assisted model building and energy refinement*) and CHARMM (*chemistry at Harvard macromolecular mechanics*). Molecular mechanics and dynamics can be applied to both small (discrete molecules) and large (e.g. nucleic acids and proteins) systems. Force field parameters for metal ions bound in the active sites of metalloproteins have been, and continue to be, developed, permitting the application of molecular dynamics simulations to these systems.

<sup>†</sup>See: E.R. Johnson, I.D. Mackie and G.A. DiLabio (2009) *J. Phys. Org. Chem.*, vol. 22, p. 1127; F.O. Kannemann and A.D. Becke (2010) *J. Chem. Theory Comput.*, vol. 6, p. 1081; V.R. Cooper (2010) *Phys. Rev. B*, vol. 81, p. 161104.

## KEY TERMS

The following terms were introduced in this chapter. Do you know what they mean and what the techniques are used for?

- |  |   |   |
|--|---|---|
| <input type="checkbox"/> gas chromatography  | <input type="checkbox"/> zero point energy                        | <input type="checkbox"/> electron paramagnetic resonance spectroscopy |
| <input type="checkbox"/> column liquid chromatography                                  | <input type="checkbox"/> fingerprint region (in an IR spectrum)   | <input type="checkbox"/> <i>g</i> -value (in EPR spectroscopy)        |
| <input type="checkbox"/> plate liquid chromatography                                   | <input type="checkbox"/> Raman spectroscopy                       | <input type="checkbox"/> isotropic and anisotropic                    |
| <input type="checkbox"/> high-performance liquid chromatography                        | <input type="checkbox"/> resonance Raman spectroscopy             | <input type="checkbox"/> Mössbauer spectroscopy                       |
| <input type="checkbox"/> mobile and stationary phases                                  | <input type="checkbox"/> electronic spectroscopy                  | <input type="checkbox"/> isomer shift (in Mössbauer spectroscopy)     |
| <input type="checkbox"/> recrystallization   | <input type="checkbox"/> absorption spectroscopy                  | <input type="checkbox"/> X-ray diffraction                            |
| <input type="checkbox"/> atomic absorption spectroscopy                                | <input type="checkbox"/> Beer–Lambert law                         | <input type="checkbox"/> solvate                                      |
| <input type="checkbox"/> aspirate  | <input type="checkbox"/> Franck–Condon approximation              | <input type="checkbox"/> hydrate                                      |
| <input type="checkbox"/> nebulize  | <input type="checkbox"/> molar extinction coefficient             | <input type="checkbox"/> monochromatic radiation                      |
| <input type="checkbox"/> thermogravimetric analysis                                    | <input type="checkbox"/> bathochromic effect (red shift)          | <input type="checkbox"/> scattering power of an atom (in XRD)         |
| <input type="checkbox"/> electron ionization mass spectrometry                         | <input type="checkbox"/> hypsochromic effect (blue shift)         | <input type="checkbox"/> Bragg's equation                             |
| <input type="checkbox"/> fast atom bombardment mass spectrometry                       | <input type="checkbox"/> emission spectroscopy                    | <input type="checkbox"/> unit cell                                    |
| <input type="checkbox"/> matrix-assisted laser desorption ionization mass spectrometry | <input type="checkbox"/> nuclear magnetic resonance spectroscopy  | <input type="checkbox"/> polymorph                                    |
| <input type="checkbox"/> time-of-flight  | <input type="checkbox"/> spin-active nucleus                      | <input type="checkbox"/> neutron diffraction                          |
| <input type="checkbox"/> electrospray mass spectrometry                                | <input type="checkbox"/> chemical shift (in NMR spectroscopy)     | <input type="checkbox"/> electron diffraction                         |
| <input type="checkbox"/> infrared spectroscopy   | <input type="checkbox"/> spin–spin coupling (in NMR spectroscopy) | <input type="checkbox"/> low-energy electron diffraction              |
| <input type="checkbox"/> force constant  | <input type="checkbox"/> proton decoupled NMR spectrum            | <input type="checkbox"/> photoelectron spectroscopy                   |
| <input type="checkbox"/> reduced mass  | <input type="checkbox"/> stereochemical non-rigidity              | <input type="checkbox"/> Koopmans' theorem                            |
|  |   | <input type="checkbox"/> computational methods                        |

## IMPORTANT ACRONYMS: WHAT DO THEY STAND FOR?

- |                                    |                                 |                               |
|------------------------------------|---------------------------------|-------------------------------|
| <input type="checkbox"/> GC        | <input type="checkbox"/> ESI    | <input type="checkbox"/> UPS  |
| <input type="checkbox"/> LC        | <input type="checkbox"/> IR     | <input type="checkbox"/> XPS  |
| <input type="checkbox"/> TLC       | <input type="checkbox"/> UV-VIS | <input type="checkbox"/> ESCA |
| <input type="checkbox"/> HPLC      | <input type="checkbox"/> NMR    | <input type="checkbox"/> CNDO |
| <input type="checkbox"/> AAS       | <input type="checkbox"/> MRI    | <input type="checkbox"/> MNDO |
| <input type="checkbox"/> TGA       | <input type="checkbox"/> EPR    | <input type="checkbox"/> AM1  |
| <input type="checkbox"/> EI        | <input type="checkbox"/> XRD    | <input type="checkbox"/> PM3  |
| <input type="checkbox"/> FAB       | <input type="checkbox"/> LEED   | <input type="checkbox"/> DFT  |
| <input type="checkbox"/> MALDI-TOF | <input type="checkbox"/> PES    | <input type="checkbox"/> MM   |

## FURTHER READING

## General

- A.K. Brisdon (1998) *Inorganic Spectroscopic Methods*, Oxford University Press, Oxford – An OUP Primer covering basic vibrational and electronic spectroscopies and mass spectrometry.
- J.R. Dean, A.M. Jones, D. Holmes, R. Reed, J. Weyers and A. Jones (2002) *Practical Skills in Chemistry*, Pearson, Harlow – An excellent introduction to a

wide range of experimental techniques with many examples.

- S. Duckett and B. Gilbert (2000) *Foundations of Spectroscopy*, Oxford University Press, Oxford – An OUP Primer that introduces mass spectrometry, IR, UV-VIS and NMR spectroscopies and X-ray diffraction.
- R.P. Wayne (1994) *Chemical Instrumentation*, Oxford University Press, Oxford – An introductory text focusing on the operations of instruments.

**Mass spectrometry**

- W. Henderson and J.S. McIndoe (2005) *Mass Spectrometry of Inorganic and Organometallic Compounds*, Wiley, Chichester – A useful textbook that focuses on applications in inorganic chemistry.
- J.T. Watson and D. Sparkman (2007) *Introduction to Mass Spectrometry: Instrumentation, Applications, and Strategies for Data Interpretation*, 4th edn, Wiley, Chichester – A detailed introduction to the topic with many examples.

**Vibrational spectroscopy**

- J.A. McCleverty and T.J. Meyer, eds (2004) *Comprehensive Coordination Chemistry II*, Elsevier, Oxford – Volume 2 contains three articles covering Raman, FT-Raman and resonance Raman spectroscopies including applications in bioinorganic chemistry.
- K. Nakamoto (1997) *Infrared and Raman Spectra of Inorganic and Coordination Compounds*, 5th edn, Wiley, New York – Two volumes comprising an invaluable reference source for inorganic chemists.

**NMR spectroscopy**

- C. Brevard and P. Granger (1981) *Handbook of High Resolution Multinuclear NMR*, Wiley-Interscience, New York – A reference book listing nuclear properties, standard references, typical chemical shift ranges and coupling constants.
- R. Freeman (2003) *Magnetic Resonance in Chemistry and Medicine*, Oxford University Press, Oxford – An up-to-date treatment of high-resolution NMR spectroscopy, illustrating applications from discrete molecular to human body levels.
- C.E. Housecroft (1994) *Boranes and Metallaboranes: Structure, Bonding and Reactivity*, 2nd edn, Ellis Horwood, Hemel Hempstead – Chapter 2 includes an account of the interpretation of  $^{11}\text{B}$  and  $^1\text{H}$  NMR spectra of boranes and their derivatives.
- B.K. Hunter and J.K.M. Sanders (1993) *Modern NMR Spectroscopy: A Guide for Chemists*, 2nd edn, Oxford University Press, Oxford – An excellent, detailed and readable text.
- J.A. Iggo (1999) *NMR Spectroscopy in Inorganic Chemistry*, Oxford University Press, Oxford – A primer that introduces the theory of NMR spectroscopic techniques as well as their use in structure determination.

**Mössbauer spectroscopy**

- G.J. Long and F. Grandjean (2004) in *Comprehensive Coordination Chemistry II*, eds J.A. McCleverty and T.J. Meyer, Elsevier, Oxford, vol. 2, p. 269 – An introduction to Mössbauer spectroscopy with references to pertinent literature examples.
- A.G. Maddock (1997) *Mössbauer Spectroscopy: Principles and Applications*, Horwood Publishing, Chichester – A comprehensive account of the technique and its uses.

**Diffraction methods**

- P. Atkins and J. de Paula (2010) *Atkins' Physical Chemistry*, 9th edn, Oxford University Press, Oxford – Chapter 19 covers crystal lattices and diffraction methods.
- W. Clegg (1998) *Crystal Structure Determination*, Oxford University Press, Oxford – An excellent introductory text.
- W. Clegg (2004) in *Comprehensive Coordination Chemistry II*, eds J.A. McCleverty and T.J. Meyer, Elsevier, Oxford, vol. 2, p. 57 – A short review of X-ray diffraction methods.
- C. Hammond (2001) *The Basics of Crystallography and Diffraction*, 2nd edn, Oxford University Press, Oxford – A detailed treatment of crystal symmetry and diffraction methods.
- M.F.C. Ladd and R.A. Palmer (2003) *Structure Determination by X-ray Crystallography*, 4th edn, Kluwer/Plenum, New York – A detailed introduction to crystal symmetry, lattices and diffraction methods.
- A.G. Orpen (2002) *Acta Crystallogr., Sect. B*, vol. 58, p. 398 – A discussion of the applications of the Cambridge Structural Database to inorganic compounds.

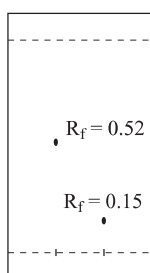
**Computational methods**

- L. Banci (2003) *Curr. Opin. Chem. Biol.*, vol. 7, p. 143 – A short review focusing on molecular dynamics simulations in metalloproteins (e.g. zinc enzymes, haem proteins and copper proteins).
- G.H. Grant and W.G. Richards (1995) *Computational Chemistry*, Oxford University Press, Oxford – An OUP Primer covering the basics of computational methods in chemistry.
- J.A. McCleverty and T.J. Meyer, eds (2004) *Comprehensive Coordination Chemistry II*, Elsevier, Oxford – Volume 2 contains a section 'Theoretical models, computational methods, and simulation' consisting of a series of articles covering computational methods including molecular mechanics, semi-empirical SCF MO methods, and density functional theory.

## PROBLEMS

[Additional problems on IR and electronic spectroscopies can be found in Chapters 3 and 20, respectively.]

- 4.1 The conversion of solar energy into chemical energy using artificial photosynthesis involves the photocatalytic conversion of  $\text{H}^+$  to  $\text{H}_2$ . Why is GC suitable for the detection and quantification of  $\text{H}_2$ ?
- 4.2 A test TLC plate (silica) using a 1:3 mixture of  $\text{CH}_3\text{CN}:\text{H}_2\text{O}$  as eluent shows that two compounds have  $R_f$  values of 0.52 and 0.15:



You plan to use column LC to separate a mixture of the two compounds. How can you attempt to ensure that their behaviour on the column will closely mimic that on the TLC plate?

- 4.3 What are the near UV and visible ranges in nm? In its UV-VIS spectrum,  $\text{Ru}_3(\text{CO})_{12}$  absorbs at 392 nm. Explain why, in a column chromatographic separation of this compound, visual detection is possible.
- 4.4 Why can a CHN analysis of a compound not distinguish between a monomer and dimer of the species? What technique would you use to confirm that a dimer was present?
- 4.5 The reaction of  $\text{NbCl}_4(\text{THF})_2$  with pyridine in the presence of a reducing agent gives  $\text{NbCl}_x(\text{py})_y$ , which contains 50.02% C, 4.20% H and 11.67% N. Determine the values of  $x$  and  $y$ .
- 4.6 During purification of 2,2'-bipyridine (see structure 4.5), the compound was accidentally exposed to a mineral acid. Elemental analysis gave the following results: C 62.35, H 4.71, N 14.54%. Suggest the identity of the isolated compound.
- 4.7 On being heated, the fullerene solvate  $\text{C}_{60} \cdot x\text{CHBr}_3$  loses solvent in a two-step process. The final weight loss is 41%. Account for these data and determine  $x$ .
- 4.8 When gypsum ( $\text{CaSO}_4 \cdot 2\text{H}_2\text{O}$ ) is heated to 433 K, it converts to the hemihydrate  $\text{CaSO}_4 \cdot \frac{1}{2}\text{H}_2\text{O}$ , and at 463 K, it forms  $\gamma\text{-CaSO}_4$ . Calculate the % weight changes at 433 and 463 K, and sketch what you expect to see in a TGA curve.
- 4.9 Birnessite,  $[\text{Na},\text{K}][\text{Mn}^{\text{IV}}\text{Mn}^{\text{III}}]\text{O}_4 \cdot x\text{H}_2\text{O}$ , is a mineral with a layered structure of the same type as  $\text{CdI}_2$

(see Fig. 6.23) comprising octahedral  $\text{MnO}_6$  units.  $\text{Na}^+$  and  $\text{K}^+$  ions and  $\text{H}_2\text{O}$  molecules are sited between the layers. The Na/K composition is variable. Analysis for Na is carried out using AAS. A 20 mg sample of birnessite is dissolved in concentrated  $\text{HCl}/\text{HNO}_3$  and the solution made up to  $200\text{ cm}^3$  in a volumetric flask. (a) Why is birnessite treated with acid? (b) Detail how you would proceed with the sodium analysis. (c) How would you determine the water content in the sample of birnessite?

- 4.10 The EI mass spectrum and structure of  $\text{Cr}(\text{CO})_6$  is shown in Fig. 4.36. Rationalize the peaks in the spectrum. Why is the EI technique suitable for recording the mass spectrum of  $\text{Cr}(\text{CO})_6$ ?
- 4.11 In the FAB mass spectrum of  $[\text{Pd}(\text{PPh}_3)_4]$  with NOBA matrix, the base peak appears at  $m/z$  279.1. The isotope pattern shows that Pd is absent from the ion. Suggest an identity for the ion. Why can a peak at  $m/z$  154.0 be ignored?
- 4.12 The EI mass spectrum of lead(II) acetate shows four peak envelopes, each with an isotope pattern characteristic of Pb. The most intense peak in each envelope appears at  $m/z$  326.0, 267.0, 224.0 and 208.0, respectively. (a) By using Appendix 5, sketch the pattern of each peak envelope. (b) Assign the peaks.
- 4.13 Four MeCN solutions were made up containing  $\text{AgNO}_3$  and  $\text{PPh}_3$  in molar ratios of 1 : 1, 1 : 2, 1 : 3 and 1 : 4, respectively. ESI mass spectra (positive mode) of the solutions were recorded, and the data are tabulated below. Account for the data, including

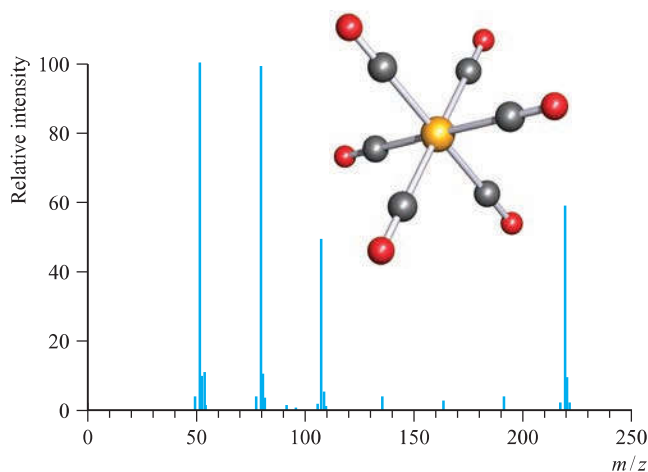


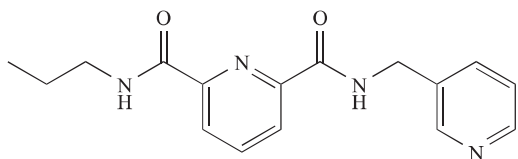
**Fig. 4.36** The EI mass spectrum and structure of  $\text{Cr}(\text{CO})_6$ . Colour code: Cr, yellow; C, grey; O, red. [Dr. P. Rösel and H. Nadig are acknowledged for the data.]

the differences between the spectra. Comment on the isotope patterns that you expect to see for each peak (see Appendix 5).

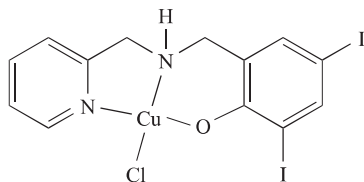
$m/z$	Relative intensities (%) for different ratios $\text{AgNO}_3 : \text{PPh}_3$			
	1 : 1	1 : 2	1 : 3	1 : 4
369	42	32	0	0
410	100	89	0	0
633	20	100	100	100
802	11	2	0	0
893	1	3	22	22
1064	2	4	0	0

[Data: L.S. Bonnington *et al.* (1999) *Inorg. Chim. Acta*, vol. 290, p. 213.]

- 4.14 The ESI mass spectrum (positive mode) of the ligand shown below exhibits two peaks at  $m/z$  299.2 (base peak) and 321.1. (a) What is a 'base peak'? (b) Suggest how the observed peaks arise. [Data: C.J. Sumby *et al.* (2009) *Tetrahedron*, vol. 65, p. 4681.]



- 4.15 The ESI mass spectrum (positive mode) of the complex shown below contained a peak envelope with  $m/z$  527.9 (100%), 528.9 (15%), 529.9 (46%), 530.9 (7%), 531.9 (0.5%). A group of peaks of low intensity and with spacings of  $m/z = 1$  was also observed around  $m/z$  994. (a) What is the oxidation state of Cu in the complex? (b) Assign the major peak and account for the isotope pattern. (c) Suggest how the minor peak arises. (Isotopes: see Appendix 5.)

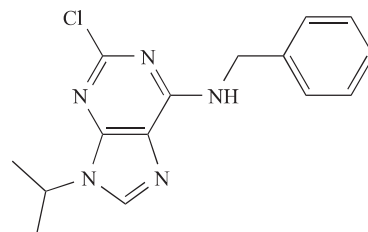


[Data: S.S. Hindo *et al.* (2009) *Eur. J. Med. Chem.*, vol. 44, p. 4353.]

- 4.16 Both positive and negative-ion ESI mass spectra of  $[\text{Me}_4\text{Sb}][\text{Ph}_2\text{SbCl}_4]$  were recorded. In one spectrum,

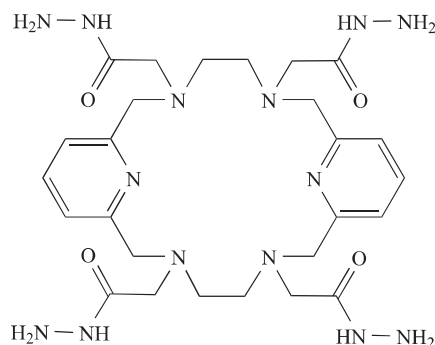
peaks at  $m/z$  181 (100%), 182 (4.5%), 183 (74.6%) and 184 (3.4%) were observed. The other mass spectrum revealed peaks at  $m/z$  415 (48.8%), 416 (6.4%), 417 (100%), 418 (13.1%), 419 (78.6%), 420 (10.2%), 421 (30.1%), 422 (3.9%) and 423 (5.7%). (a) Account for the results, stating which mass spectrum was recorded in positive and which in negative mode. (b) Draw the structures of the ions present in  $[\text{Me}_4\text{Sb}][\text{Ph}_2\text{SbCl}_4]$ . Does either of the ions possess isomers? If so, do the mass spectrometric data provide information about which isomer or isomers are present? (Isotopes: see Appendix 5.) [Data: H.J. Breunig *et al.* (2010) *J. Organomet. Chem.*, vol. 695, p. 1307.]

- 4.17 1.0 mmol of the ligand, L, shown below was reacted with 0.50 mmol of  $\text{PtCl}_2$ . The positive mode MALDI-TOF mass spectrum of the purified product was run in  $\alpha$ -cyano-4-hydroxycinnamic acid matrix. The most intense peaks in the peak envelopes in the mass spectrum were  $m/z$  891.1, 869.1, 833.2 and 302.1. Assign these peaks and suggest a formula for the product that is consistent with the data.



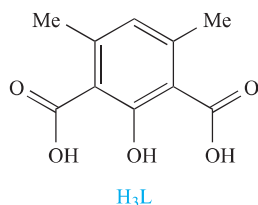
[Data: L. Szücs *et al.* (2008) *Polyhedron*, vol. 27, p. 2710.]

- 4.18 In the MALDI-TOF mass spectrum of the macrocyclic ligand shown below in 1,8,9-trihydroxyanthracene matrix, the dominant peaks are at  $m/z$  615.7 (base peak), 637.7. Assign the peaks.



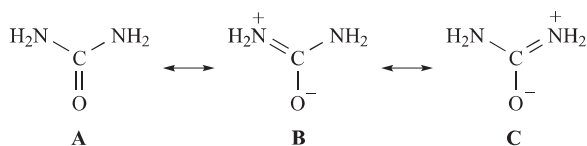
[Data: C. Nuñez *et al.* (2009) *Inorg. Chim. Acta*, vol. 362, p. 3454.]

- 4.19 Reaction of  $\text{H}_3\text{L}$  (drawn below) with  $\text{Cu}(\text{O}_2\text{CMe})_2 \cdot \text{H}_2\text{O}$  in MeOH with addition of pyridine (py) yields  $[\text{Cu}_4\text{L}_2(\text{O}_2\text{CMe})_2(\text{py})_4(\text{MeOH})_2]$ . Show that a MALDI-TOF mass spectrum with peak envelopes at  $m/z$  977 and 611 is consistent with this formulation.



[Data: J.D. Crane *et al.* (2004) *Inorg. Chem. Comm.*, vol. 7, p. 499.]

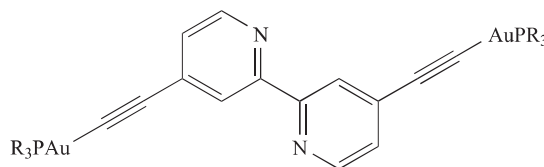
- 4.20 What is the rule of mutual exclusion? Give two examples of molecular species to which this rule applies.
- 4.21 The  $\nu_3$  vibrational wavenumber for  $[\text{BF}_4]^-$  comes at  $1070\text{ cm}^{-1}$ , whereas the corresponding band for  $[\text{BCl}_4]^-$ ,  $[\text{BBr}_4]^-$  and  $[\text{BI}_4]^-$  comes at 722, 620 and  $533\text{ cm}^{-1}$ , respectively. Rationalize this trend.
- 4.22 Vibrational wavenumbers for  $\text{K}[\text{N}_3]$  are 2041, 1344 and  $645\text{ cm}^{-1}$ . Draw the structure of the  $[\text{N}_3]^-$  ion and sketch the three vibrational modes. Which are IR active?
- 4.23 Resonance structures for urea are represented below:



The IR spectrum of free urea has absorptions at 3500 and  $3350\text{ cm}^{-1}$  ( $\nu(\text{NH}_2)$ ),  $1683\text{ cm}^{-1}$  ( $\nu(\text{CO})$ ) and  $1471\text{ cm}^{-1}$  ( $\nu(\text{CN})$ ). Urea can bond to metal ions through either an *N*- or *O*-donor atom. When urea bonds through the O atom, the contribution from resonance form A decreases. In the IR spectrum of  $[\text{Pt}(\text{urea})_6]\text{Cl}_2$ , bands at 3390, 3290, 3130, 3030, 1725 and  $1395\text{ cm}^{-1}$  are assigned to the vibrational modes of metal-bound urea. Suggest why these data suggest the formation of Pt–N rather than Pt–O bonds.

- 4.24 The IR spectrum of  $\text{Li}_3[\text{PO}_4]$  shows absorptions at 1034 and  $591\text{ cm}^{-1}$ . There are no bands below the  $400\text{ cm}^{-1}$  cutoff of the IR spectrometer. Why are these data consistent with the  $[\text{PO}_4]^{3-}$  ion being tetrahedral rather than square planar?

- 4.25 The UV-VIS spectrum of a  $\text{CH}_3\text{CN}$  solution ( $2.0 \times 10^{-5}\text{ mol dm}^{-3}$ ) of an iron(II) complex is:  $\lambda_{\text{max}}(\epsilon) = 245 (48\ 200)$ ,  $276 (74\ 100)$ ,  $284 (81\ 700)$ ,  $324 (45\ 100)$ ,  $569\text{ nm} (25\ 000\text{ dm}^3\text{ mol}^{-1}\text{ cm}^{-1})$ . A quartz cuvette with path length 1 cm was used for the measurement. (a) Explain why the compound is coloured. What colour do you expect the compound to be? (b) Which is the lowest energy absorption? Rationalize your answer. (c) The initial data were recorded as a plot of absorbance against wavelength. What was the value of  $A_{\text{max}}$  for the band at 245 nm?
- 4.26 The UV-VIS spectrum of a  $\text{CH}_2\text{Cl}_2$  solution of the gold(I) compound shown below with  $\text{R} = \text{Ph}$  is:  $\lambda_{\text{max}}(\epsilon) = 239 (92\ 500)$ ,  $269 (67\ 000)$ ,  $286 (72\ 000)$ ,  $303 (28\ 000)$ ,  $315\text{ nm} (21\ 000\text{ dm}^3\text{ mol}^{-1}\text{ cm}^{-1})$ .



[Data: E.C. Constable *et al.* (2009) *Eur. J. Inorg. Chem.*, p. 4710.]

- (a)  $\pi^* \leftarrow \pi$  transitions contribute to the observed spectrum. How do these arise? (b) Is the compound coloured? (c) You are asked to compare the UV-VIS spectra of a series of these compounds with different R substituents. Why should you compare plots of  $\epsilon$  against  $\lambda$  rather than  $A$  against  $\lambda$ ?
- 4.27 Two isomers, **A** and **B**, of a complex can be distinguished because the UV-VIS spectrum of **B** is blue shifted with respect to that of **A**. Explain what this means. What is another term used for a blue shift?

In problems 4.28 to 4.51, refer to Table 4.3 for isotopic abundances where needed.

- 4.28 Why is a coupling constant measured in Hz and is not recorded as a chemical shift difference?
- 4.29 Long-range couplings are often observed between  $^{31}\text{P}$  and  $^{19}\text{F}$  nuclei, between  $^{31}\text{P}$  and  $^1\text{H}$  nuclei, but not between remote non-equivalent  $^1\text{H}$  nuclei. What does this tell you about the relative magnitudes of values of  $J_{\text{PF}}$ ,  $J_{\text{PH}}$  and  $J_{\text{HH}}$  for the respective pairs of nuclei when they are directly attached?
- 4.30 Rationalize the fact that the  $^{13}\text{C}$  NMR spectrum of  $\text{CF}_3\text{CO}_2\text{H}$  consists of two binomial quartets with coupling constants of 44 and 284 Hz respectively.
- 4.31 How might you use  $^{31}\text{P}$  NMR spectroscopy to distinguish between  $\text{Ph}_2\text{PH}$  and  $\text{Ph}_3\text{P}$ ?

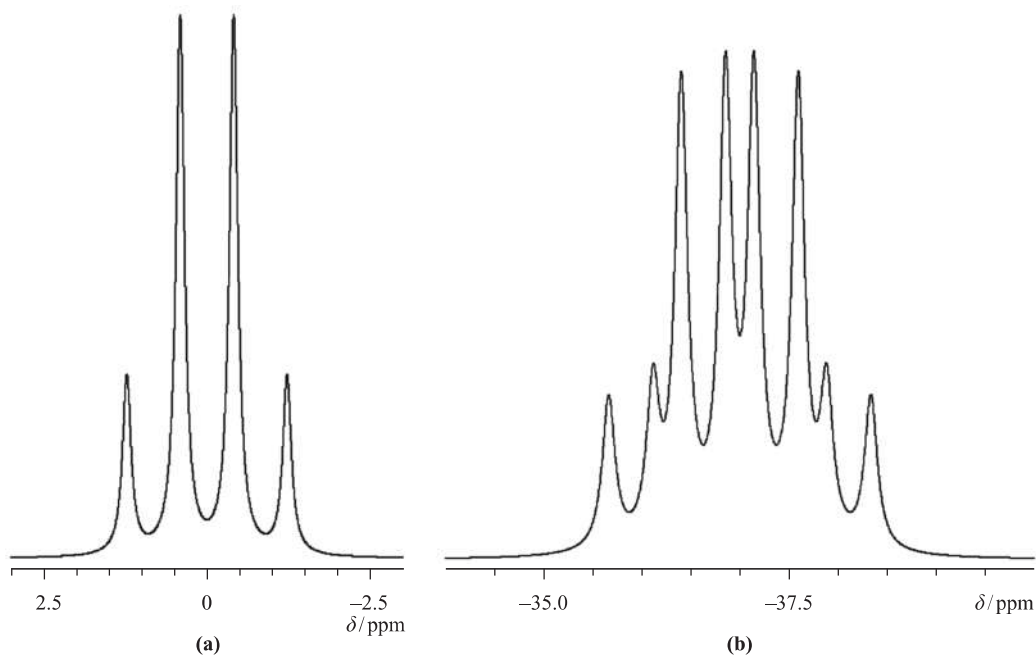
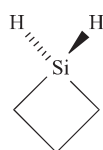


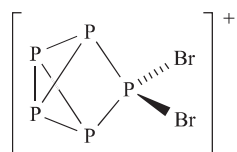
Fig. 4.37 Figure for problem 4.34.

- 4.32 The  $^{31}\text{P}$  NMR spectrum of  $\text{PMe}_3$  consists of a binomial decet ( $J$  2.7 Hz). (a) Account for this observation. (b) Predict the nature of the  $^1\text{H}$  NMR spectrum of  $\text{PMe}_3$ .
- 4.33 The  $^{29}\text{Si}$  NMR spectrum of compound **4.15** shows a triplet with a coupling constant of 194 Hz. (a) Rationalize these data and (b) predict the nature of the signal in the  $^1\text{H}$  NMR spectrum of **4.15** that is assigned to the silicon-bound protons. [ $^{29}\text{Si}$ : 4.7% abundant;  $I = \frac{1}{2}$ ]



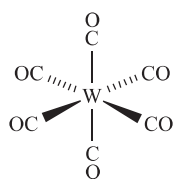
(4.15)

- 4.34 Figure 4.37 shows the  $^{11}\text{B}$  NMR spectra of (a)  $\text{THF}\cdot\text{BH}_3$  (**4.16**) and (b)  $\text{PhMe}_2\text{P}\cdot\text{BH}_3$ . Interpret the observed coupling patterns and mark on the figure where you would measure relevant coupling constants.
- 
- (4.16)
- 4.35 (a) Predict the structure of  $\text{SF}_4$  using the VSEPR model. (b) Account for the fact that at 298 K and in solution the  $^{19}\text{F}$  NMR spectrum of  $\text{SF}_4$  exhibits a singlet but that at 175 K, two equal-intensity triplets are observed.
- 4.36 The  $^{19}\text{F}$  NMR spectrum of each of the following molecules exhibits one signal. For which species is this observation consistent with a static molecular structure as predicted by the VSEPR model: (a)  $\text{SiF}_4$ ; (b)  $\text{PF}_5$ ; (c)  $\text{SF}_6$ ; (d)  $\text{SOF}_2$ ; (e)  $\text{CF}_4$ ?
- 4.37 Outline the mechanism of Berry pseudo-rotation, giving two examples of molecules that undergo this process.
- 4.38 Is it correct to interpret the phrase 'static solution structure' as meaning necessarily rigid? Use the following molecules to exemplify your answer:  $\text{PMe}_3$ ;  $\text{OPMe}_3$ ;  $\text{PPh}_3$ ;  $\text{SiMe}_4$ .
- 4.39 Account for the fact that the  $^{29}\text{Si}$  NMR spectrum of a mixture of  $\text{SiCl}_4$  and  $\text{SiBr}_4$  that has been standing for 40 h contains five singlets which include those assigned to  $\text{SiCl}_4$  ( $\delta$  -19 ppm) and  $\text{SiBr}_4$  ( $\delta$  -90 ppm).
- 4.40 The structure of  $[\text{P}_5\text{Br}_2]^+$  is shown in diagram **4.17**. Account for the fact that the  $^{31}\text{P}$  NMR spectrum of this cation at 203 K consists of a doublet of triplets ( $J$  321 Hz, 149 Hz), a triplet of triplets ( $J$  321 Hz, 26 Hz) and a triplet of doublets ( $J$  149 Hz, 26 Hz).



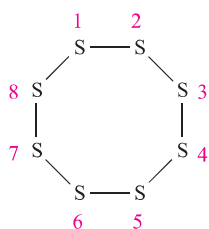
(4.17)

- 4.41 Tungsten hexacarbonyl (**4.18**) contains six equivalent CO ligands. With reference to Table 4.3, suggest what you would expect to observe in the  $^{13}\text{C}$  NMR spectrum of a  $^{13}\text{C}$ -enriched sample of  $\text{W}(\text{CO})_6$ .



(4.18)

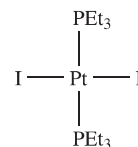
- 4.42 The compounds  $\text{Se}_n\text{S}_{8-n}$  with  $n = 1-5$  are structurally similar to  $\text{S}_8$ . Structure **4.19** shows a representation of the  $\text{S}_8$  ring (it is actually non-planar) and the atom numbering scheme; all the S atoms are equivalent. Using this as a guide, draw the structures of  $\text{SeS}_7$ ,  $1,2\text{-Se}_2\text{S}_6$ ,  $1,3\text{-Se}_2\text{S}_6$ ,  $1,2,3\text{-Se}_3\text{S}_5$ ,  $1,2,4\text{-Se}_3\text{S}_5$ ,  $1,2,5\text{-Se}_3\text{S}_5$  and  $1,2,3,4\text{-Se}_4\text{S}_4$ . How many signals would you expect to observe in the  $^{77}\text{Se}$  ( $I = \frac{1}{2}$ , 7.6%) NMR spectrum of each compound?



(4.19)

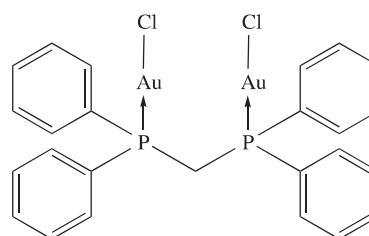
- 4.43 Explain why the  $^{19}\text{F}$  NMR spectrum of  $\text{BFCl}_2$  consists of a 1:1:1:1 quartet. What would you expect to observe in the  $^{19}\text{F}$  NMR spectrum of  $\text{BF}_2\text{Cl}$ ?
- 4.44 Rationalize the fact that at 173 K,  $^1\text{H}$  NMR spectroscopy shows that  $\text{SbMe}_5$  possesses only one type of Me group.
- 4.45 MeCN solutions of  $\text{NbCl}_5$  and HF contain a mixture of octahedral  $[\text{NbF}_6]^-$ ,  $[\text{NbF}_5\text{Cl}]^-$ ,  $[\text{NbF}_4\text{Cl}_2]^-$ ,  $[\text{NbF}_3\text{Cl}_3]^-$  and  $[\text{NbF}_2\text{Cl}_4]^-$ . Predict the number and coupling patterns of the signals in the  $^{19}\text{F}$  NMR spectrum of each separate component in this mixture, taking into account possible isomers. (Assume static structures and no coupling to  $^{93}\text{Nb}$ .)
- 4.46 (a) Explain why the  $^{19}\text{F}$  NMR spectrum of  $[\text{PF}_6]^-$  appears as a doublet.

- (b) The  $^{31}\text{P}\{^1\text{H}\}$  NMR spectrum of *trans*- $[\text{PtI}_2(\text{PEt}_3)_2]$  (**4.20**) shows a three-line pattern, the lines in which have relative integrals of  $\approx 1 : 4 : 1$ . What is the origin of this pattern?



(4.20)

- 4.47 (a) In the  $^1\text{H}$  NMR spectrum of compound **4.21**, there is a triplet at  $\delta$  3.60 ppm ( $J$  10.4 Hz). Assign the signal and explain the origin of the coupling. What would you observe in the  $^{31}\text{P}\{^1\text{H}\}$  NMR spectrum of compound **4.21**?



(4.21)

- (b) Figure 4.38 shows the solid state structure of a phosphorus-containing cation. The  $^{31}\text{P}$  NMR spectrum of a  $\text{CDCl}_3$  solution of the  $[\text{CF}_3\text{SO}_3]^-$  salt was recorded. How many signals (ignore spin-spin

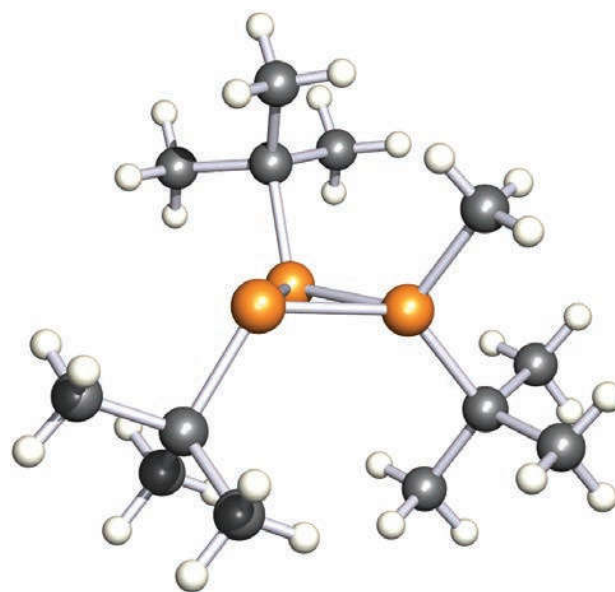
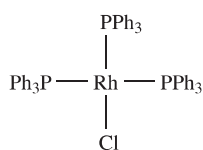


**Fig. 4.38** The structure of the  $[(\text{PCMe}_3)_3\text{Me}]^+$  cation in the salt  $[(\text{PCMe}_3)_3\text{Me}][\text{CF}_3\text{SO}_3]$  determined by X-ray diffraction [N. Burford *et al.* (2005) *Angew. Chem. Int. Ed.*, vol. 44, p. 6196]. Colour code: P, orange; C, grey; H, white.



coupling) would you expect to see in the spectrum, assuming that the solid state structure is retained in solution?

- 4.48 The  $^{19}\text{F}$  NMR spectrum of the octahedral ion  $[\text{PF}_5\text{Me}]^-$  shows two signals ( $\delta -45.8$  and  $-57.6$  ppm). Why are *two* signals observed? From these signals, three coupling constants can be measured:  $J_{\text{PF}} = 829$  Hz,  $J_{\text{PF}} = 680$  Hz and  $J_{\text{FF}} = 35$  Hz. Explain the origins of these coupling constants.
- 4.49 The  $^{31}\text{P}\{^1\text{H}\}$  NMR spectrum of a  $\text{CDCl}_3$  solution of the square planar rhodium(I) complex **4.22** exhibits a doublet of doublets ( $J$  38 Hz, 145 Hz) and a doublet of triplets ( $J$  38 Hz, 190 Hz). Rationalize these data. [*Hint*: look at Table 4.3.]



(4.22)

- 4.50  $\text{NaBH}_4$  contains the tetrahedral  $[\text{BH}_4]^-$  ion. Although  $\text{NaBH}_4$  hydrolyses slowly in water, it is possible to obtain a clean  $^1\text{H}$  NMR spectrum of the compound in  $\text{D}_2\text{O}$ . Naturally occurring boron consists of two isotopes:  $^{11}\text{B}$ , 80.1%,  $I = \frac{3}{2}$ , and  $^{10}\text{B}$ , 19.9%,  $I = 3$ . Assuming that a sharp, well-resolved spectrum is obtained, sketch the expected 400 MHz  $^1\text{H}$  NMR spectrum (including a scale) if the signal for the protons occurs at  $\delta -0.2$  ppm, and the values of  $J_{^{11}\text{B}^1\text{H}} = 80.5$  Hz and  $J_{^{10}\text{B}^1\text{H}} = 27.1$  Hz. How would the spectrum differ if it were recorded at 100 MHz?
- 4.51 (a) Predict what you would expect to see in the  $^{15}\text{N}$  NMR spectrum of the isotopically labelled compound *cis*- $[\text{Pt}(^{15}\text{NH}_3)_2\text{Cl}_2]$ . (b) The observed coupling constants for this compound are  $J_{^{15}\text{N}^1\text{H}} = 74$  Hz and  $J_{^{15}\text{N}^{95}\text{Pt}} = 303$  Hz. Using your predicted spectrum as a starting point, explain why the observed spectrum is an *apparent* octet.
- 4.52 (a) If Na has the ground state electronic configuration of  $[\text{Ne}]3s^1$ , why is  $\text{NaCl}$  EPR silent? (b) Sketch an EPR spectrum for an isotropic system in which an electron interacts with a  $^{14}\text{N}$  ( $I = 1$ ) nucleus.
- 4.53 Vanadium has two isotopes ( $^{50}\text{V}$ , 0.25%;  $^{51}\text{V}$ , 99.75%). The EPR spectrum of an aqueous solution of  $[\text{VO}(\text{OH}_2)_5]^{2+}$  shows an 8-line pattern, and  $g$ -values of  $g_{zz} = 1.932$ ,  $g_{xx} = 1.979$  and  $g_{yy} = 1.979$  were determined. What can you deduce from the data?
- 4.54 Figure 4.39 shows the single crystal EPR spectrum arising from  $\text{Cu}^{2+}$  doped into  $\text{CaCd}(\text{O}_2\text{CMe})_4 \cdot 6\text{H}_2\text{O}$  for one orientation of the crystal relative to the external magnetic field. The spectrum illustrates the

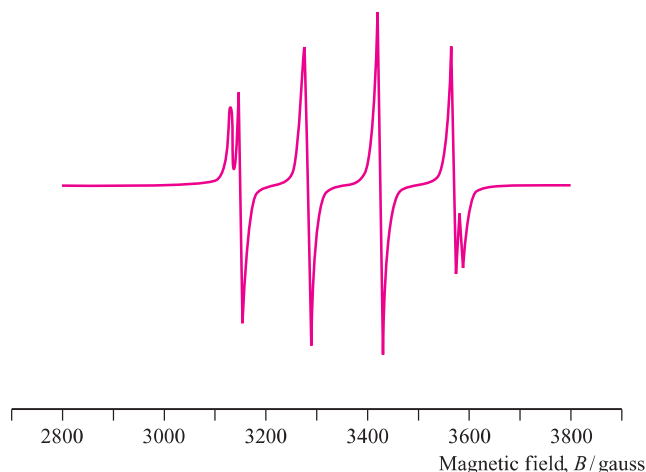
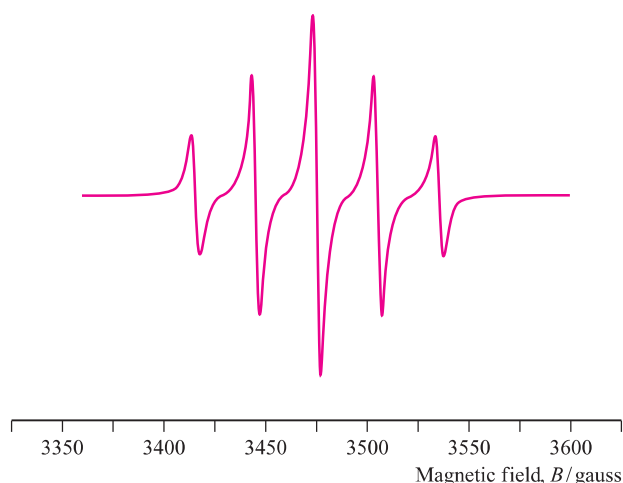


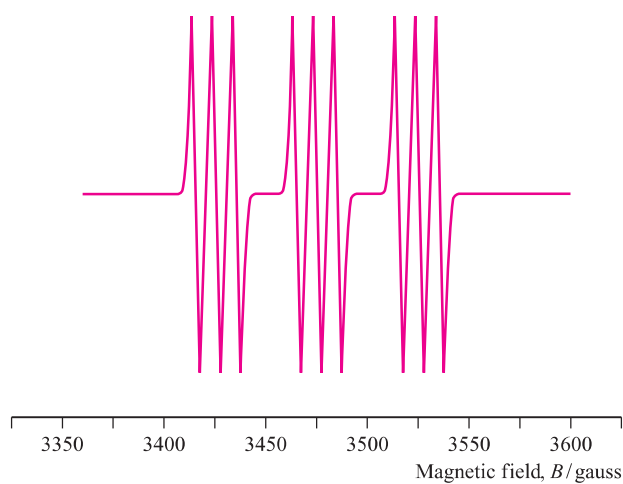
**Fig. 4.39** The single crystal EPR spectrum of  $\text{Cu}^{2+}$  doped- $\text{CaCd}(\text{O}_2\text{CMe})_4 \cdot 6\text{H}_2\text{O}$ . [Simulated by Dr. C. Palivan, University of Basel.]

presence of both isotopes of Cu ( $^{63}\text{Cu}$  and  $^{65}\text{Cu}$ , natural abundances 69.2% and 30.8%, respectively, both  $I = \frac{3}{2}$ ). (a) How many peaks do you expect to observe for each isotope? (b) Explain why the intensities of the central peaks in Fig. 4.39 are higher than those of the outer peaks. (c) The hyperfine coupling constant  $A(^{65}\text{Cu})$  is 1.07 times higher than  $A(^{63}\text{Cu})$ . Which signals in Fig. 4.39 arise from each isotope? Calculate the value of  $A$  (in G) for each isotope. (d) The EPR spectrum in Fig. 4.39 was measured as 9.75 GHz. Calculate the gyromagnetic factor of the copper(II) paramagnetic species.

- 4.55 Figure 4.40 shows the EPR spectra for two isotropic systems in which the unpaired electron interacts with two  $^{14}\text{N}$  nuclei ( $I = 1$ ). (a) Use Fig. 4.40a to calculate the gyromagnetic factor of the paramagnetic species if the spectrum was measured at 9.75 GHz. (b) Which EPR spectrum in Fig. 4.40 indicates the interaction of the unpaired electron with two equivalent nitrogen nuclei? (c) Calculate the values of the hyperfine coupling constants for both cases in Fig. 4.40.
- 4.56 Predict what you expect to observe in the EPR spectrum of a species in which an unpaired electron interacts with one  $^{14}\text{N}$  nucleus ( $I = 1$ ) and one  $^1\text{H}$  nucleus ( $I = \frac{1}{2}$ ) if the hyperfine coupling constants are (a)  $A(^{14}\text{N}) = A(^1\text{H}) = 30$  G; (b)  $A(^{14}\text{N}) = 30$  G,  $A(^1\text{H}) = 10$  G.
- 4.57 Figure 4.41 shows the 9.214 GHz EPR spectrum arising from the two sites of  $\text{Co}^{2+}$  ( $^{59}\text{Co}$ , 100% abundant,  $I = \frac{7}{2}$ ) doped into magnesium acetate. The sites differ slightly in their effective hyperfine coupling constants, and more significantly in their  $g$ -values. (a) Calculate the  $g$ -values for the two sites.



(a)



(b)

**Fig. 4.40** EPR spectra for problem 4.55. [Simulated by Dr. C. Palivan, University of Basel.]

(b) Explain why the central peak is more intense than the peaks appearing at higher magnetic field. (c) What would happen if the differences in  $g$ -values of the two sites is smaller than is observed in Fig. 4.41?

4.58 Suggest a suitable technique for investigating the presence of  $\text{Fe}^{2+}$  and/or  $\text{Fe}^{3+}$  ions in clays, and for distinguishing between tetrahedrally and octahedrally sited Fe centres. Give reasons for your choice.

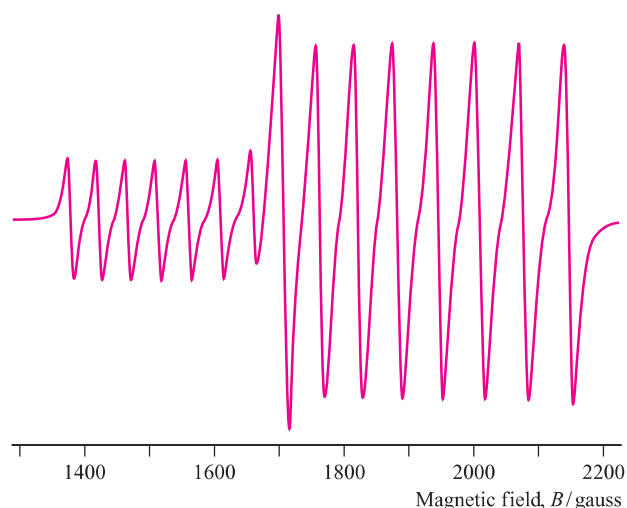


**Fig. 4.41** EPR spectrum for problem 4.57. [Simulated by Dr. C. Palivan, University of Basel.]

4.59 (a) Explain why the location of H atoms by X-ray diffraction is difficult. (b) What technique (and why) is used for the accurate determination of H atom positions in a structure? Comment on any limitations of this method.

4.60 What are the features that distinguish X-ray quality single crystals, a polycrystalline solid and an amorphous solid?

4.61 By referring to Section 10.6, suggest how the following solid state structures (i.e. the organization of the molecules in the solid state) may be affected by hydrogen bonding: (a)  $\text{PhB}(\text{OH})_2$ , (b)  $\text{H}_2\text{SO}_4$ , (c)  $\text{MeCO}_2\text{H}$ .

4.62 Comment on ways in which you can ensure that the X-ray crystal structure of a compound that you have prepared is representative of the bulk sample of the compound.

4.63 Molecular structures determined by X-ray diffraction are often represented in the form of ORTEP diagrams showing thermal ellipsoids for non-hydrogen atoms. (a) What do you understand by a *thermal ellipsoid*? (b) Why are H atoms usually represented isotropically?

## OVERVIEW PROBLEMS

4.64 Suggest a suitable experimental technique for each of the following problems.

(a) Single crystal X-ray diffraction data show that a compound crystallizes as a dihydrate. How could you show that the bulk sample was anhydrous?

(b) The single crystal structure of a compound has been determined, and you wish to prepare the same polymorph in bulk in a series of syntheses over a period of several weeks. How can you ensure that the products fulfil this aim?

- (c) Changing the conditions under which a compound **X** crystallizes leads to two batches of crystals with melting points of 97 and 99 °C, respectively. How can you show that the compounds are polymorphs?
- 4.65 (a) The IR spectrum of naturally occurring CO shows an absorption at  $2170\text{ cm}^{-1}$  assigned to the molecular vibrational mode. If the sample is enriched in  $^{13}\text{C}$ , what change do you expect to see in the IR spectrum?
- (b) The IR spectra of salts of  $[\text{Fe}(\text{CO})_6]^{2+}$  and  $[\text{Fe}(\text{CO})_4]^{2-}$ , respectively show absorptions at 2204 and  $1788\text{ cm}^{-1}$  assigned to carbonyl vibrational modes. What do these tell you about the strengths of the carbon–oxygen bonds in the complexes compared to that in free CO?
- (c)  $[\text{Fe}(\text{CO})_4]^{2-}$  and  $\text{Fe}(\text{CO})_5$  have  $T_d$  and  $D_{3h}$  symmetries respectively. What do you expect to observe in the room temperature  $^{13}\text{C}$  NMR spectra of  $\text{Na}_2[\text{Fe}(\text{CO})_4]$  and  $\text{Fe}(\text{CO})_5$ ? Rationalize your answer.
- 4.66 You have prepared the complex  $[\text{Ru}(\text{py})_6][\text{BF}_4]_2$  (py = pyridine). (a) What information can you obtain from the elemental analysis? (b) How would you confirm the presence of the  $[\text{BF}_4]^-$  ion? (c) How would you confirm that all the pyridine ligands were in the same environment in solution? (d) How would you confirm the presence of an octahedral  $[\text{Ru}(\text{py})_6]^{2+}$  ion in the solid state? (e) What would you expect to see in the ESI mass spectrum of  $[\text{Ru}(\text{py})_6][\text{BF}_4]_2$ ?
- 4.67 The question of whether you have synthesized a monomeric (**X**) or dimeric (**X**<sub>2</sub>) species can be solved in a number of ways. (a) Will elemental analysis help you? (b) The compound contains an organic unit that can be probed by  $^1\text{H}$  NMR spectroscopy. Will this technique distinguish between monomer and dimer? (c) What information could you gain from mass spectrometry? (d) A single crystal X-ray diffraction study at 223 K shows the presence of the dimer **X**<sub>2</sub>? Does this mean that monomeric **X** never forms?
- 4.68 NMR spectroscopy is considered to be one of the most powerful, routine analytical tools for the characterization of new compounds. Comment on the validity of this statement.
- 4.69 A student has prepared a sample of  $[\text{Zn}(\text{en})_3]\text{Cl}_2$  (en =  $\text{H}_2\text{NCH}_2\text{CH}_2\text{NH}_2$ ) but is worried that the complex appears blue when  $[\text{Zn}(\text{en})_3]\text{Cl}_2$  should be colourless. The student wonders if she picked up a bottle of nickel(II) chloride instead of zinc(II) chloride. The experimental CHN analysis for the complex is C 23.00, H 7.71, N 26.92%. (a) Do the elemental analytical data distinguish between  $[\text{Zn}(\text{en})_3]\text{Cl}_2$  and  $[\text{Ni}(\text{en})_3]\text{Cl}_2$ ? Comment on your answer. (b) How would mass spectrometry help you to distinguish between the two compounds? (c) By referring to Chapter 20, suggest why  $^1\text{H}$  NMR spectroscopy might be useful in distinguishing between  $[\text{Zn}(\text{en})_3]\text{Cl}_2$  and  $[\text{Ni}(\text{en})_3]\text{Cl}_2$ . (d) A single crystal X-ray diffraction study was carried out and confirms the presence of  $[\text{M}(\text{en})_3]\text{Cl}_2$ . Can this technique unambiguously assign M to Zn or Ni? (e) Explain why AAS could be used to confirm the identity of the metal.

## INORGANIC CHEMISTRY MATTERS

- 4.70 Portable mass spectrometers are now available for monitoring gaseous emissions from volcanoes. Analyses after the eruption of the Turrialba Volcano in Costa Rica in January 2010 showed the presence of  $[\text{M}]^+$  ions (i.e. atomic ions and non-fragmented molecular ions) at  $m/z$  64, 44, 40, 34, 32, 28 and 18. Mass spectra recorded before the eruption confirmed that the peak at  $m/z$  64 was missing, and the peak at  $m/z$  34 was substantially diminished. (a) To what do you assign the peaks at  $m/z$  64 and 34? (b) Bearing in mind the composition of the Earth's atmosphere, what molecular ion interferes with the detection of the volcanic emission observed at  $m/z$  34? (c) Volcanic gases mix with the surrounding air. Suggest what atmospheric gases give rise to the ions at  $m/z$  40, 32 and 28. (d) Sampling of the volcanic plume peak before and after the eruption reveals that the molecular ion with  $m/z$  18 is present on both occasions, but in greater amounts after the eruption. Identify this ion. (e) Helium forms under the Earth's crust and is released during volcanic activity. Mass spectrometric ground monitoring of vents (fumaroles) in the Turrialba crater showed 20 ppm levels of He being released. What  $m/z$  value characterizes helium emission and what is the formula of the corresponding ion?
- [Data: J.A. Diaz *et al.* (2010) *Int. J. Mass. Spec.*, vol. 295, p. 105.]

4.71 Ultramarines are bright blue pigments based on a zeolite (sodalite) that hosts the *colour centres*  $[S_2]^-$  and  $[S_3]^-$ . Ultramarines include lapis lazuli and have been in use for over 5500 years. The UV-VIS spectrum of  $[S_2]^-$  exhibits a broad band centred at 370 nm, while  $[S_3]^-$  absorbs at 595 nm. (a) Draw Lewis structures for  $[S_2]^-$  and  $[S_3]^-$ . What shape is the  $[S_3]^-$  ion? (b) Why can EPR spectroscopy be used to study these ions? Suggest a reason why both

ions behave isotropically even at low temperatures. (c) Explain why an ultramarine containing only  $[S_3]^-$  colour centres appears violet-blue in colour. (d) Why does  $[S_2]^-$  contribute to the colour of ultramarine pigments even though  $\lambda_{\max}$  is 370 nm, i.e. in the UV region? (e) In synthetic ultramarines, the ratio of  $[S_3]^- : [S_2]^-$  can be altered to produce pigments ranging from violet-blue through blues to green. Account for this.